自旋電子學 -----
從2007年諾貝爾物理獎巨磁阻現象談起
Spintronics materials and device
---- a quest from the Giant Magnetoresistance Effect, Nobel prize in Physics, 2007

Point Contact Andreev Reflection,
Current Perpendicular to Plane resistance, Spin transfer torque in magnetic nanostructures, and spin pumping effect

Shang-Fan Lee (李尚凡)

S. Y. Huang (黃斯衍), C. Yu (于 淳),
T. W. Chiang (江典蔚), L. K. Lin (林呂圭), L. J. Chang (張良君), Faris B.
Y. C. Chiu (邱昱哲), Y. L. Chen(陳彥霖), Y. H. Chiu (邱亦欣)
Institute of Physics, Academia Sinica

J. J. Liang (梁君致)
Dept. of Physics, Fu Jen University

D. S. Hung(洪東興)
Dept. of Info. Telecom. Eng.
Ming Chuan University

Financial support from National Science Council and Academia Sinica

Spintronics :

Electronics with electron spin as an extra degree of freedom
Generate, inject, process, and detect spin currents

- **Generation: ferromagnetic materials, spin Hall effect, spin pumping effect etc.**

- **Injection: interfaces, heterogeneous structures, tunnel junctions**

- **Process: spin transfer torque**

- **Detection: Giant Magnetoresistance, Tunneling MR**

科學月刊 **38**, 898 (2007).
物理雙月刊 **30**, 116 (2008).
科學人 **87**, 82 (2009).

2007 Nobel prize in Physics

2007年諾貝爾物理獎得主 左 亞伯・費爾(Albert Fert)
與右彼得・葛倫貝格(Peter Grünberg)

(圖片資料來源：Copyright © Nobel Web AB 2007/ Photo: Hans Mehlin)

鐵磁性元素：鐵 Fe, 鈷 Co, 鎳 Ni, 釓 Gd, 鏑 Dy,
錳 Mn, 鈀 Pd ??

Elements with ferromagnetic properties

合金, alloys

錳氧化物 MnOx

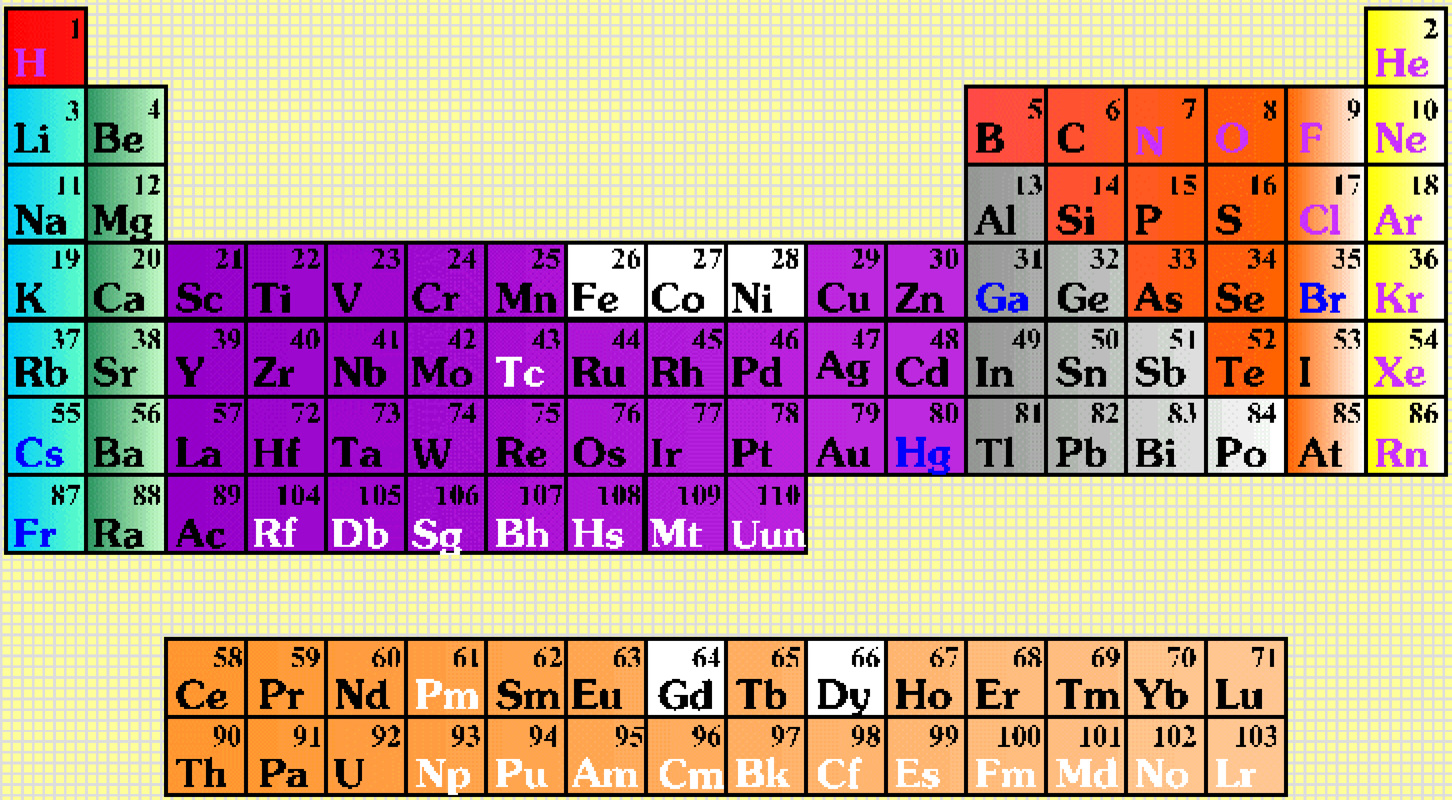

Solar system

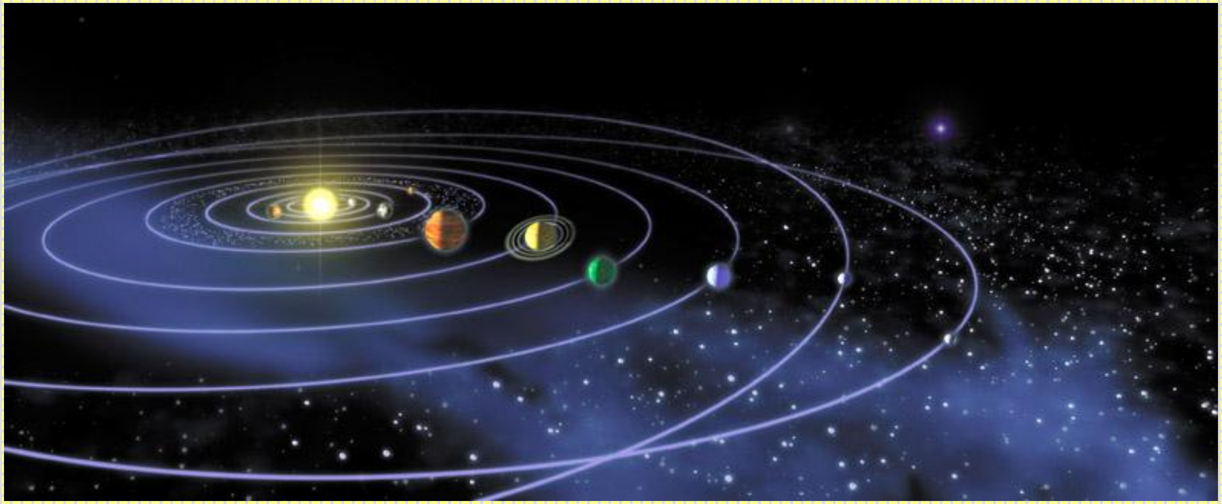

s, p electron orbital

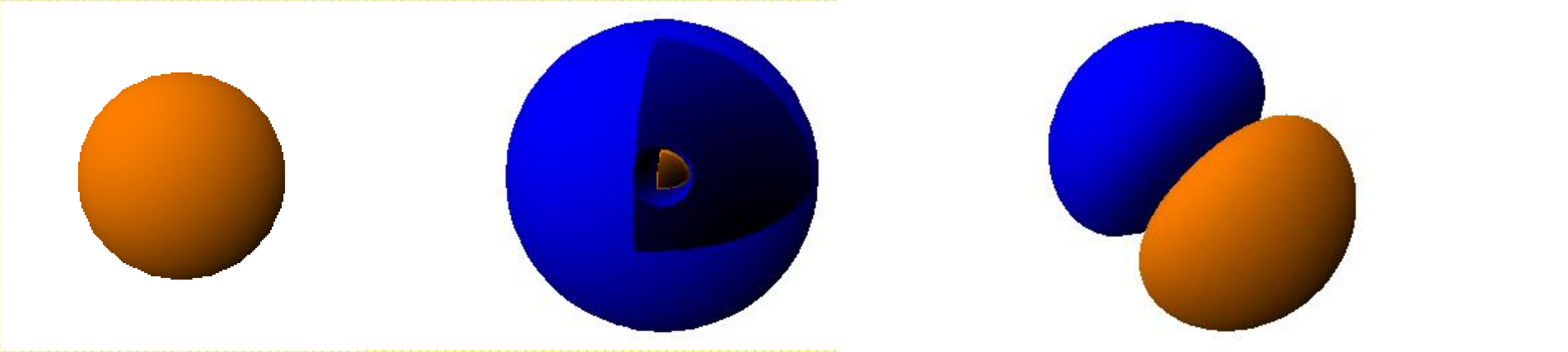

Orbital viewer

Platonic solid

From Wikipedia

In geometry, a Platonic solid is a convex polyhedron that is regular, in the sense of a regular polygon. Specifically, the faces of a Platonic solid are congruent regular polygons, with the same number of faces meeting at each vertex; thus, all its edges are congruent, as are its vertices and angles.

There are precisely five Platonic solids (shown below):

The name of each figure is derived from its number of faces: respectively 4, 6, 8, 12, and 20.

The aesthetic beauty and symmetry of the Platonic solids have made them a favorite subject of geometers for thousands of years. They are named for the ancient Greek philosopher Plato who theorized that the classical elements were constructed from the regular solids.

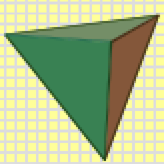	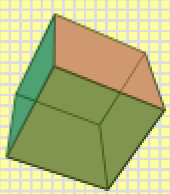	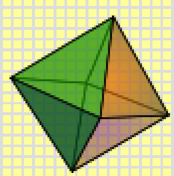	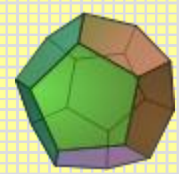	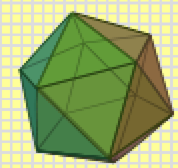
Tetrahedron	Cube hexahedron	Octahedron	Dodecahedron	Icosahedron

3d transition metals:

Mn atom has 5 d ↑ electrons
Bulk Mn is NOT magnetic.

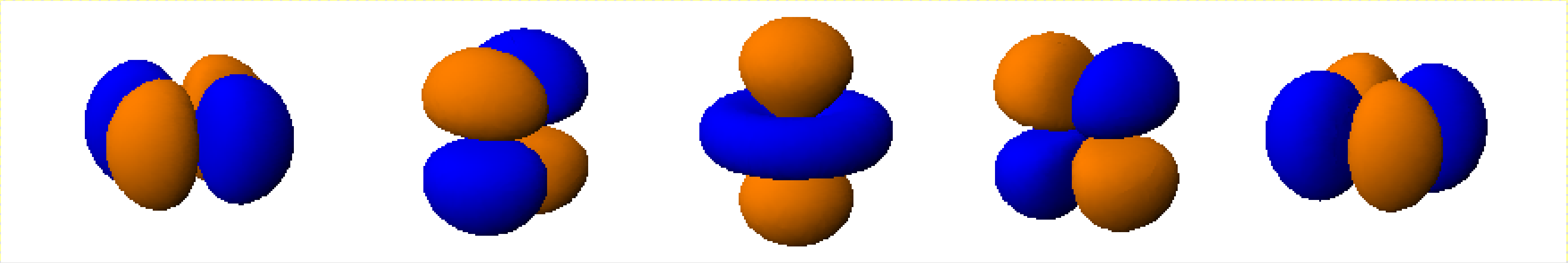

3d electron distribution in real space

Co atom has 5 d ↑electrons and 2 d ↓ electrons
Bulk Co is magnetic.

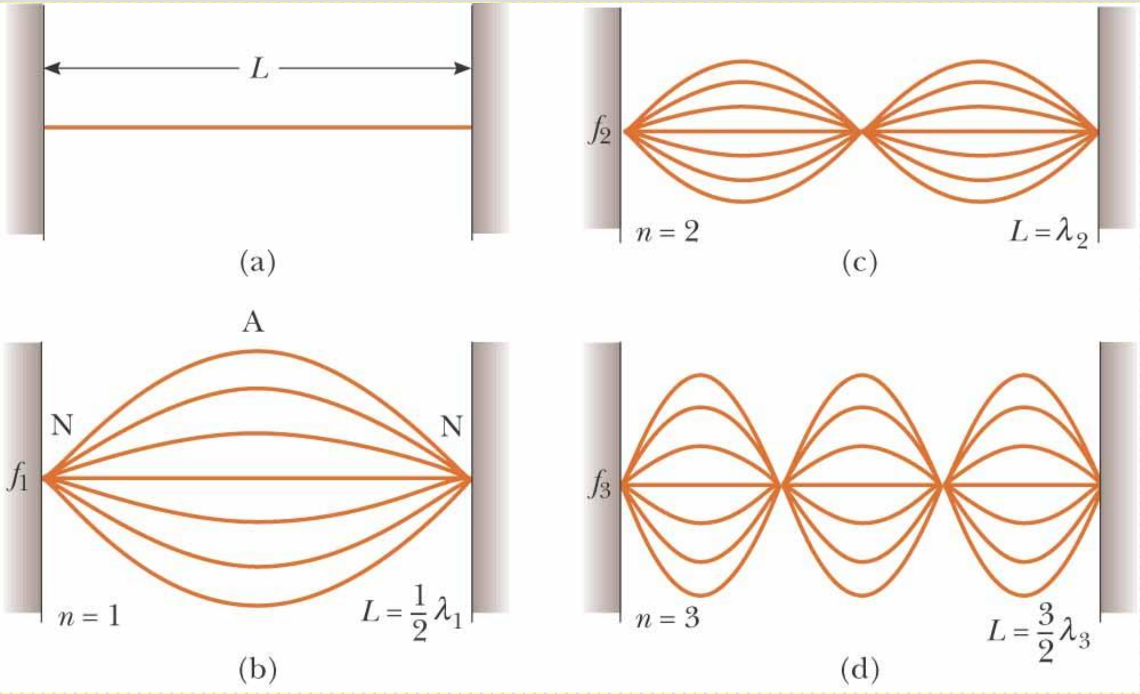

One-dimensional resonance

Two-dimensional resonance

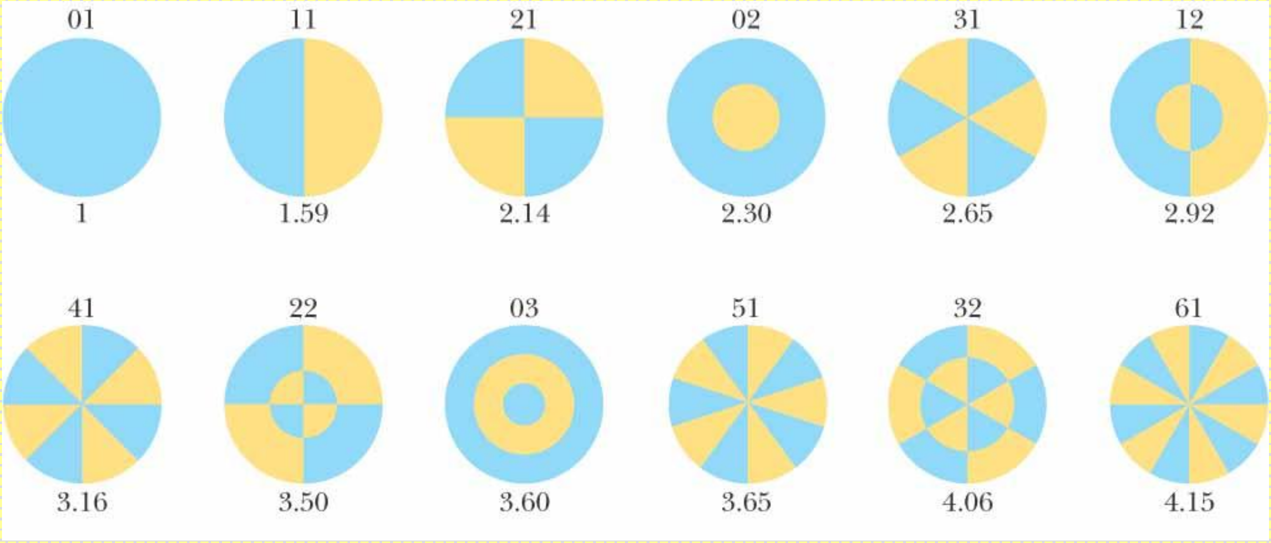

Stoner criterion for ferromagnetism:

$I\,N(E_F) > 1$, I is the Stoner exchange parameter and $N(E_F)$ is the density of states at the Fermi energy.

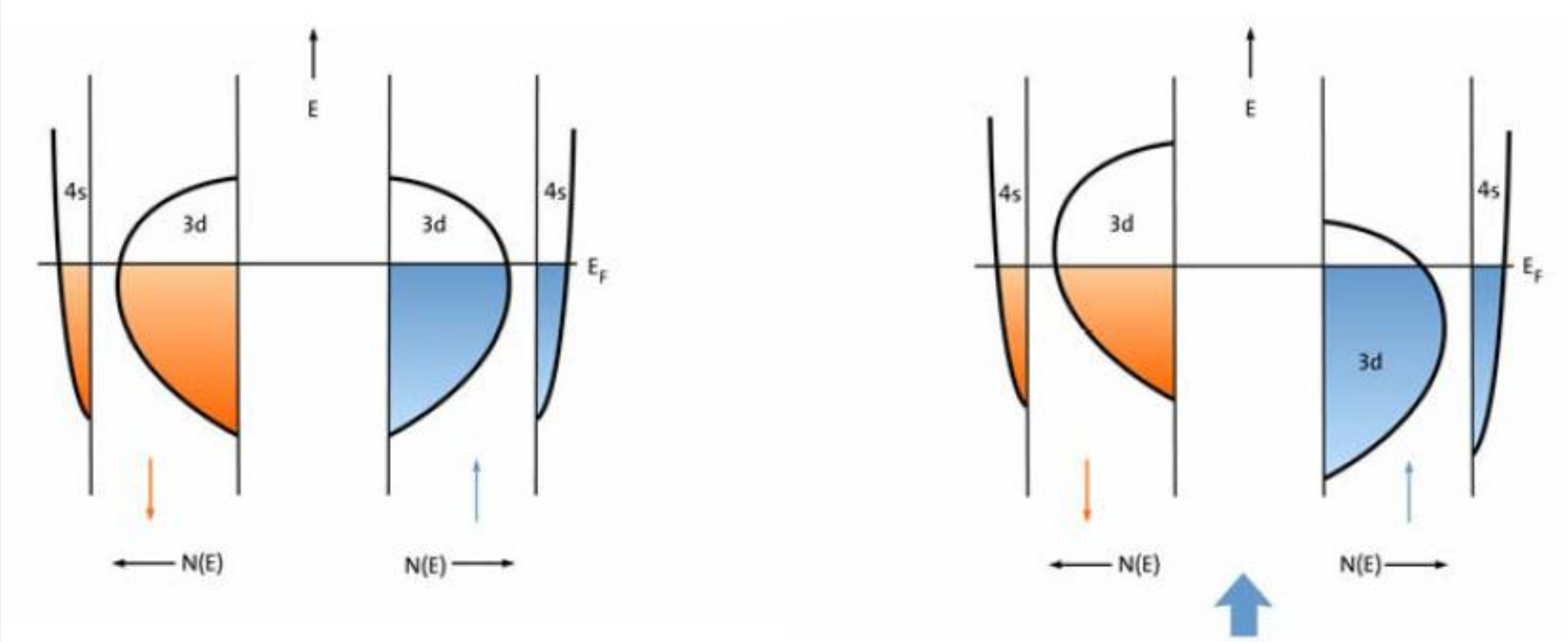

For the non-magnetic state there are identical density of states for the two spins.

For a ferromagnetic state, N↑ > N↓. The polarization is indicated by the thick blue arrow.

Schematic plot for the energy band structure of 3d transition metals.

Spin-dependent conduction in Ferromagnetic metals (Two-current model)

First suggested by Mott (1936)

Experimentally confirmed by I. A. Campbell and A. Fert (~1970)

At low temperature

$$\rho = \frac{\rho_\uparrow \rho_\downarrow}{\rho_\uparrow + \rho_\downarrow}$$

At high temperature

$$\rho = \frac{\rho_\uparrow \rho_\downarrow + \rho_{\uparrow\downarrow}(\rho_\uparrow + \rho_\downarrow)}{\rho_\uparrow + \rho_\downarrow + 4\rho_{\uparrow\downarrow}}$$

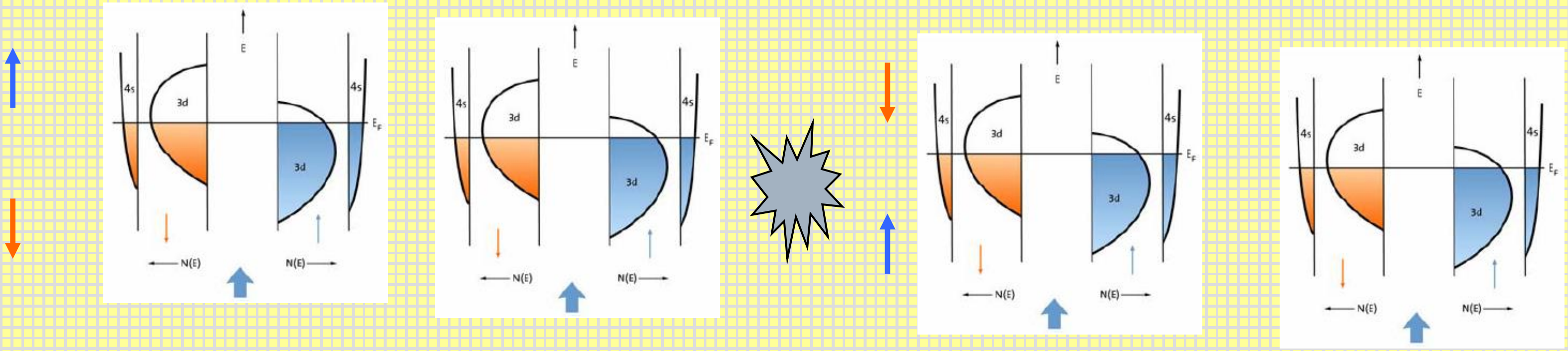

Spin mixing effect equalizes two currents

Magnetic coupling in multilayers

- **Long-range incommensurate magnetic order in a Dy-Y multilayer**

  M. B. Salamon, Shantanu Sinha, J. J. Rhyne, J. E. Cunningham, Ross W. Erwin, Julie Borchers, and C. P. Flynn, Phys. Rev. Lett. 56, 259 - 262 (1986)

- **Observation of a Magnetic Antiphase Domain Structure with Long-Range Order in a Synthetic Gd-Y Superlattice**

  C. F. Majkrzak, J. W. Cable, J. Kwo, M. Hong, D. B. McWhan, Y. Yafet, and J. V. Waszczak,C. Vettier, Phys. Rev. Lett. 56, 2700 - 2703 (1986)

- **Layered Magnetic Structures: Evidence for Antiferromagnetic Coupling of Fe Layers across Cr Interlayers**

  P. Grünberg, R. Schreiber, Y. Pang, M. B. Brodsky, and H. Sowers, Phys. Rev. Lett. 57, 2442 - 2445 (1986)

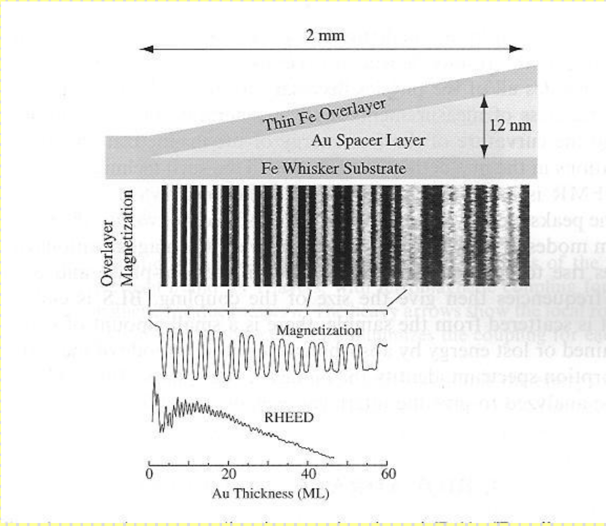

Coupling in wedge-shaped

Fe/Cr/Fe

Fe/Au/Fe

Fe/Ag/Fe

J. Unguris, R. J. Celotta, and D. T. Pierce

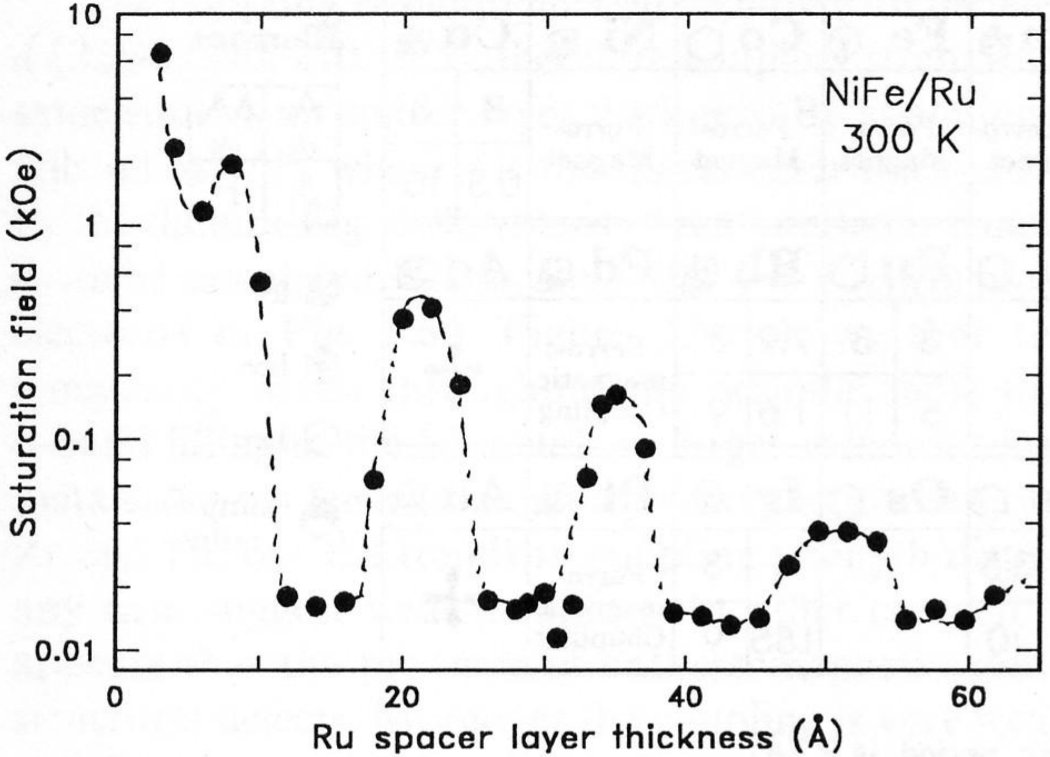

Fig. 2.58. Dependence of saturation field on Ru spacer layer thickness for several series of $Ni_{81}Fe_{19}$/Ru multilayers with structure, 100 Å Ru/[30 Å $Ni_{81}Fe_{19}$/Ru(t_{Ru})]$_{20}$, where the topmost Ru layer thickness is adjusted to be $\simeq$25 Å for all samples

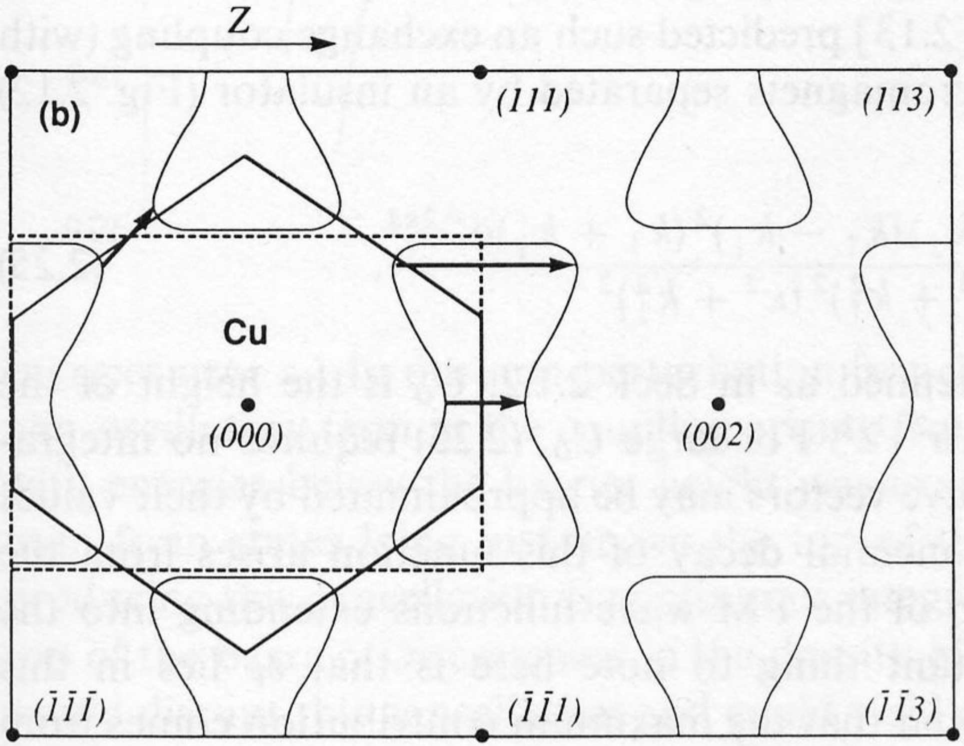

Fig. 2.11. Fermi surface of Cu in the (1 0 0) plane in the extended zone scheme. Arrows indicate values of $2(k_F - G)$ for reciprocal lattice vectors G which can give rise to oscillations with periods greater than π/k_F

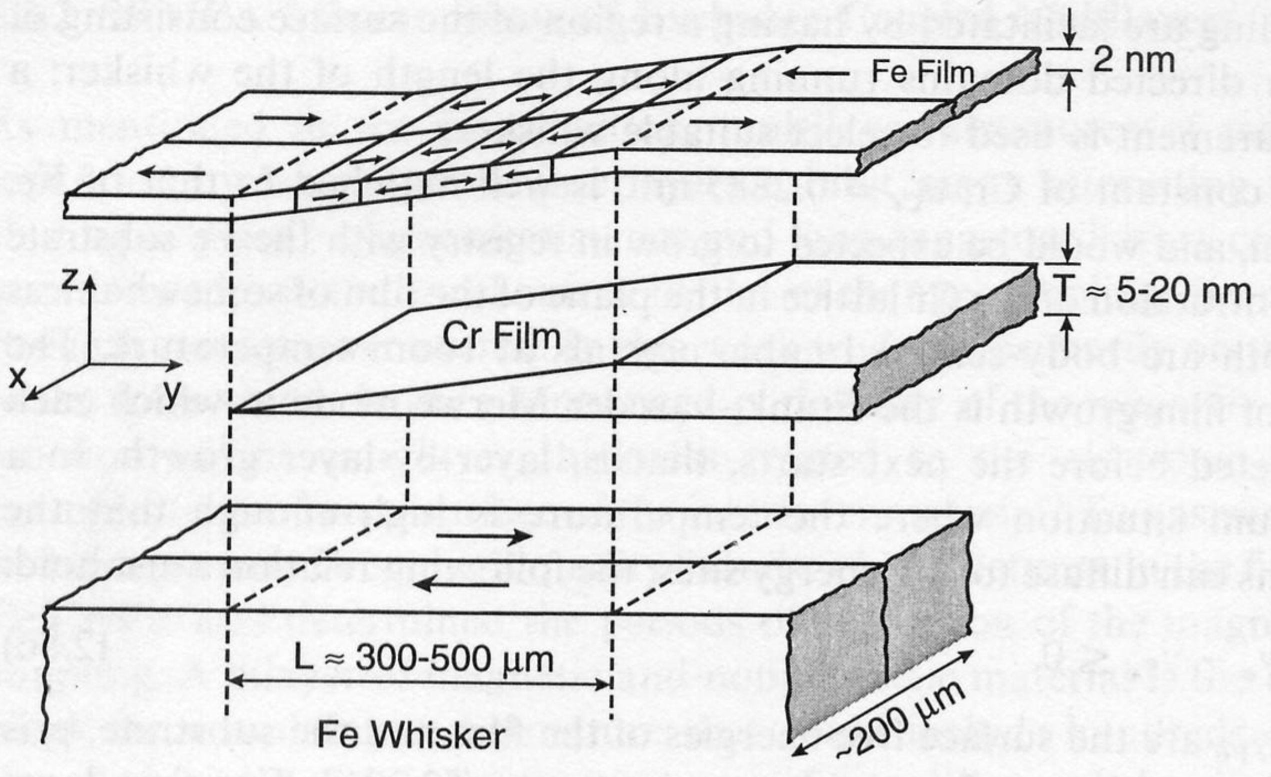

Fig. 2.41. A schematic expanded view of the sample structure showing the Fe(0 0 1) single-crystal whisker substrate, the evaporated Cr wedge, and the Fe overlayer. The arrows in the Fe show the magnetization direction in each domain. The *z*-scale is expanded approximately 5000 times. (From [2.206])

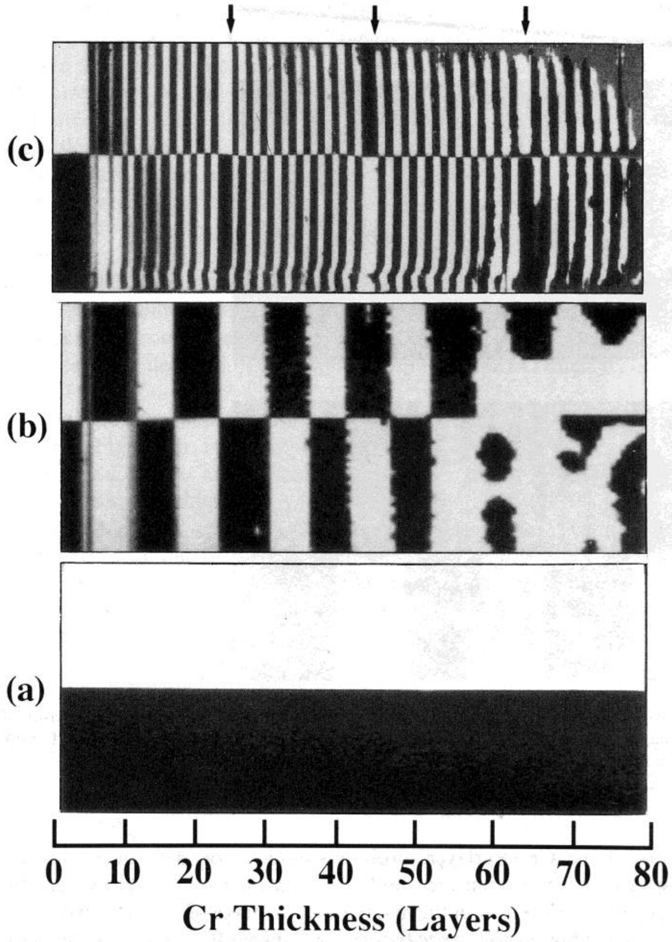

Fig. 2.43. SEMPA image of the magnetization M_y (axes as in Fig. 2.41) showing domains in (**a**) the clean Fe whisker, (**b**) the Fe layer covering the Cr spacer layer evaporated at 30 °C, and (**c**) the Fe layer covering a Cr spacer evaporated on the Fe whisker held at 350 °C. The scale at the bottom shows the increase in the thickness of the Cr wedge in (**b**) and (**c**). The arrows at the top of (**c**) indicate the Cr thicknesses where there are phase slips. The region of the whisker imaged is about 0.5 mm long

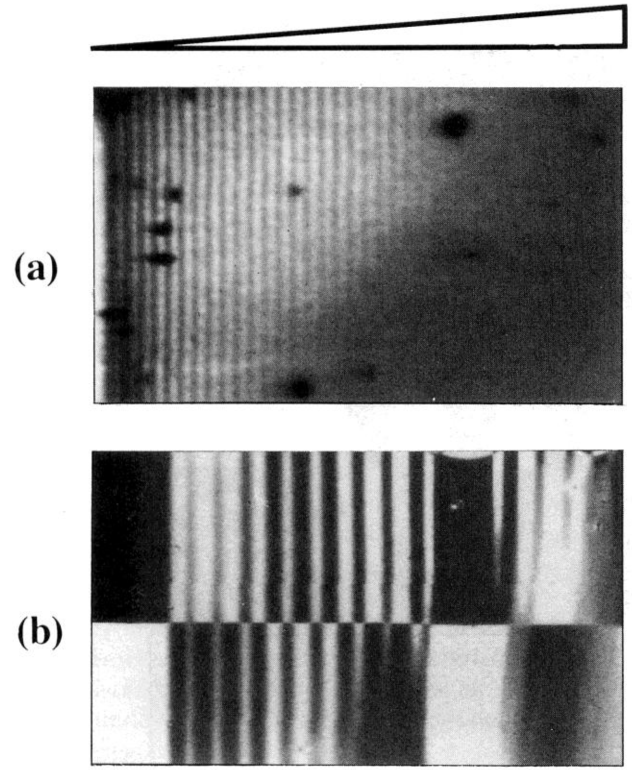

Fig. 2.44. The effect of roughness on the inertlayer exchange coupling is shown by a comparison of (**a**) the oscillations of the RHEED intensity along the bare Cr wedge with (**b**) the SEMPA magnetization image over the same part of the wedge

Aliasing

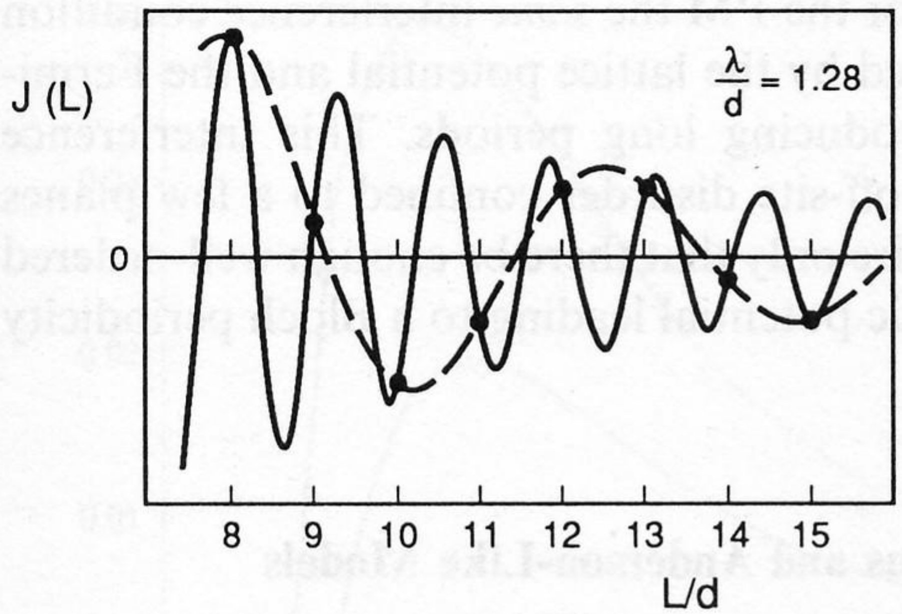

Fig. 2.10. RKKY-like oscillating exchange coupling with period λ (solid line) showing the longer period oscillation (dashed line) obtained by sampling the function only at integral values of the spacing, *a*, between atomic planes, i.e. "aliasing". From [2.21]

Different aspect of Magnetoresistance
Anisotropic MR (異向磁阻)
Giant MR (巨磁阻– CPP, CIP)
Tunneling MR (穿隧磁阻)

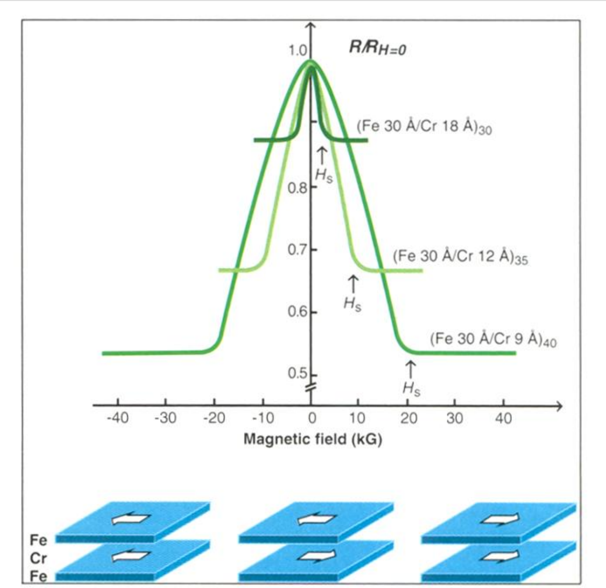

Discovery of Giant MR -- Two-current model combines with magnetic coupling in multilayers

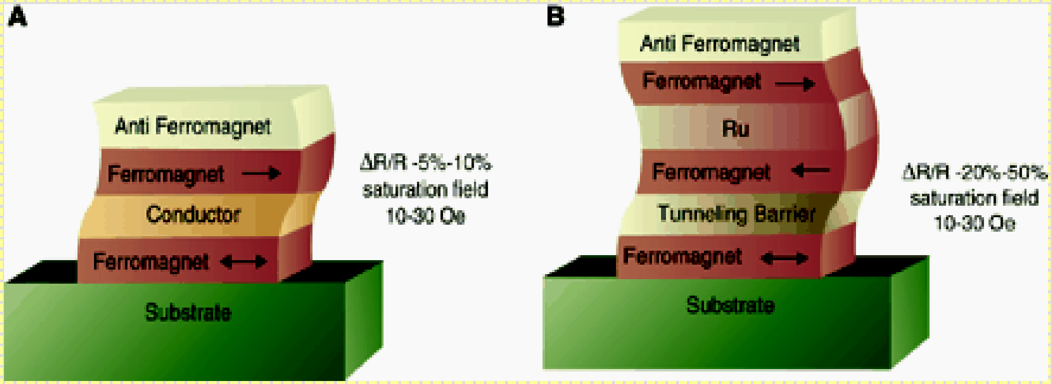

Spin-dependent transport structures. (A) Spin valve. (B) Magnetic tunnel junction. (from Science)

Schematic illustration of GMR

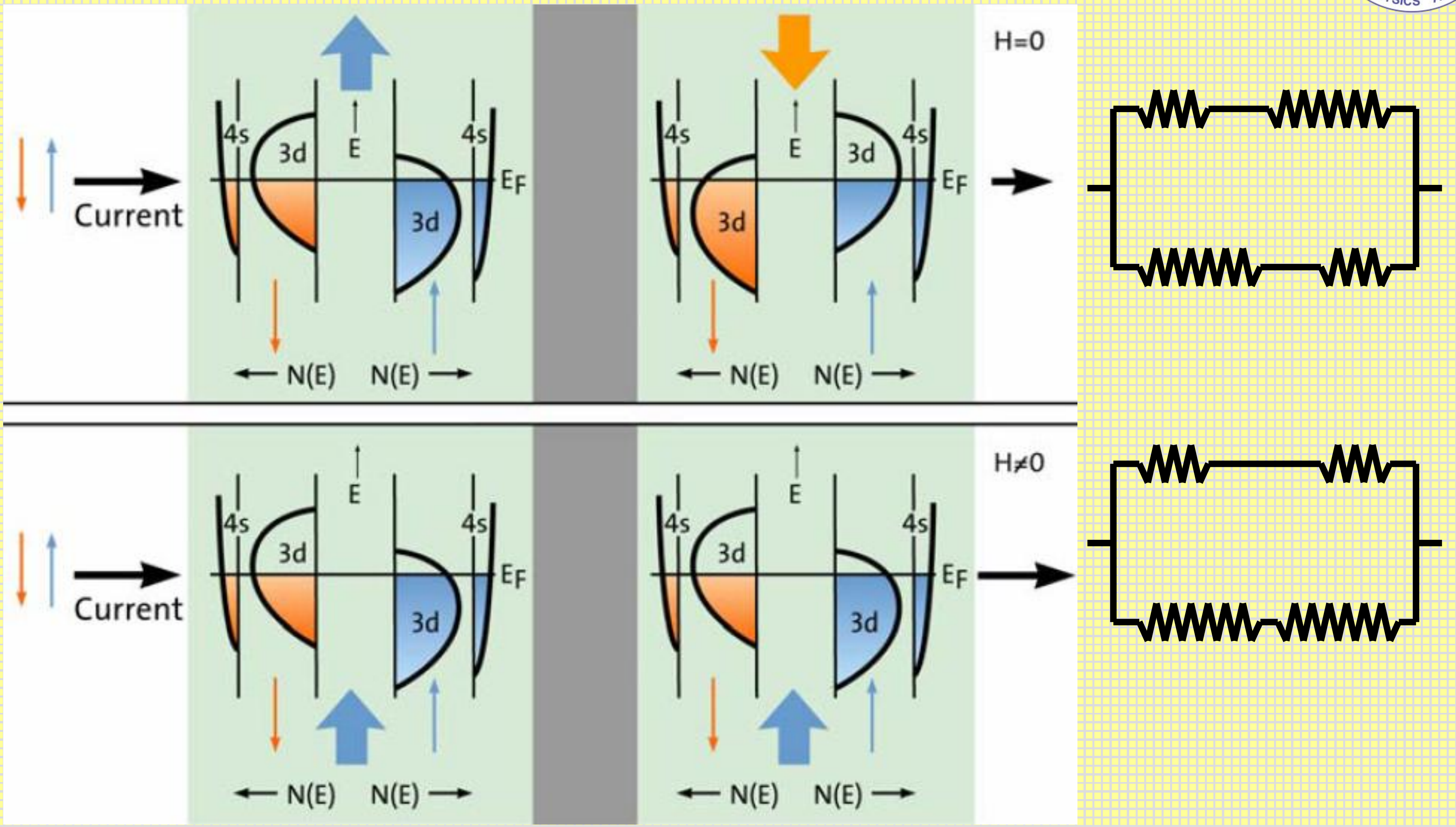

"short circuit effect" of one spin channel results in small resistance in parallel configuration

Electron potential landscape in a F/N multilayer

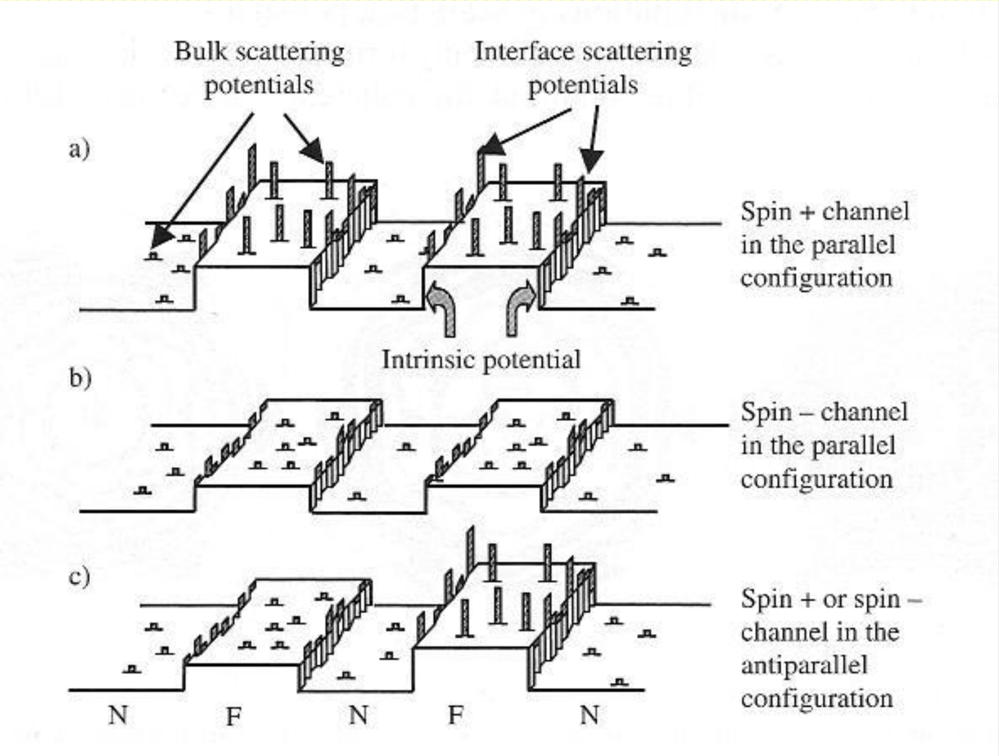

Intrinsic potential +
Scattering potentials due to

- **Impurities**
- **Vacancies**
- **Lattice mismatches**
- **……**

•Can we distinguish the interface effect from the bulk effect?

Transport geometry

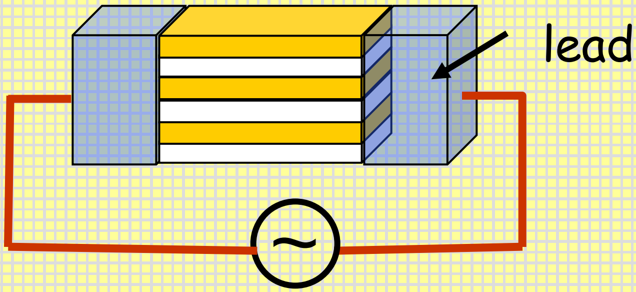

CIP geometry

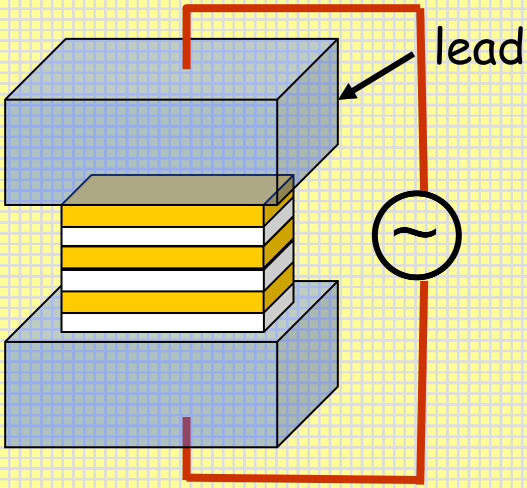

CPP geometry

- CIP resistance can be measured easily, CPP resistance needs special techniques.
- From CPP resistance in metallic multilayers, one can measure interface resistances, spin diffusion lengths, and polarization in ferromagnetic materials, etc.

Valet and Fert model of CPP-GMR

Based on the Boltzmann equation

A semi-classical model with spin taken into consideration

$$j_{+(-)} = \frac{1}{e\rho_{+(-)}} \frac{\partial \mu_{+(-)}}{\partial x}$$

$$j_+ + j_- = j_e$$

$$\frac{\partial (j_+ - j_-)}{\partial x} = \frac{2eN(E_F)\Delta\mu}{\tau_{sf}}$$

$$\frac{\partial^2 \mu_{+(-)}}{\partial z^2} = \frac{\mu_{+(-)}}{l_{sf}^2} \qquad l_{sf}^F = \left[\lambda_{sf}^F / 3(\lambda_\uparrow^{-1} + \lambda_\downarrow^{-1})\right]^{1/2}, \quad l_{sf}^N = \left[\lambda_{sf}^N \lambda / 6\right]^{1/2}$$

Spin accumulation at the interface is important
Spin diffusion length, instead of mean free path, is the dominant physical length scale

The Definition of Spin Polarization

Spin polarization (自旋極化率): $P_N = \dfrac{N_\uparrow - N_\downarrow}{N_\uparrow + N_\downarrow}$

P = 0 | 0 < P < 1 | P = 1

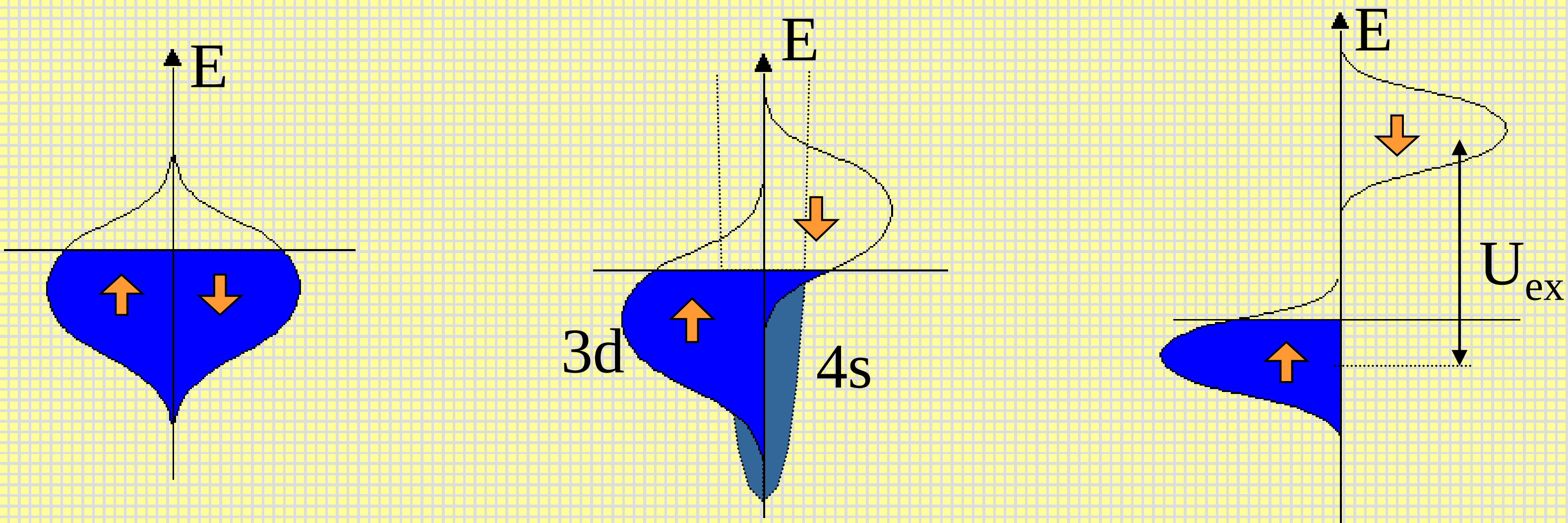

normal metal | metallic ferromagnet | half-metallic ferromagnet

Spin polarization of current: $P = \dfrac{I_\uparrow - I_\downarrow}{I_\uparrow + I_\downarrow}$ Ballistic or diffusive

Mazin, PRL **87**, 1427 (1999)

How to Determine the Spin Polarization

Spin-polarized photoemission

$$P = \frac{N_\uparrow - N_\downarrow}{N_\uparrow + N_\downarrow}$$

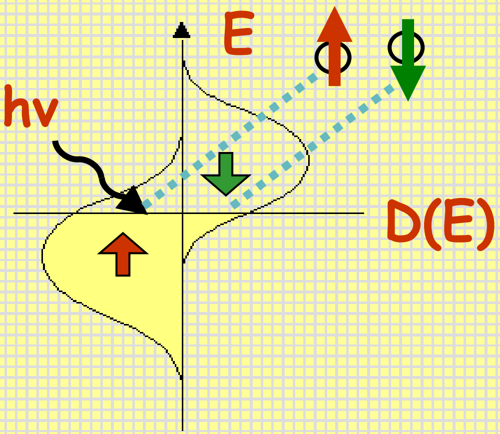

Spin-LED

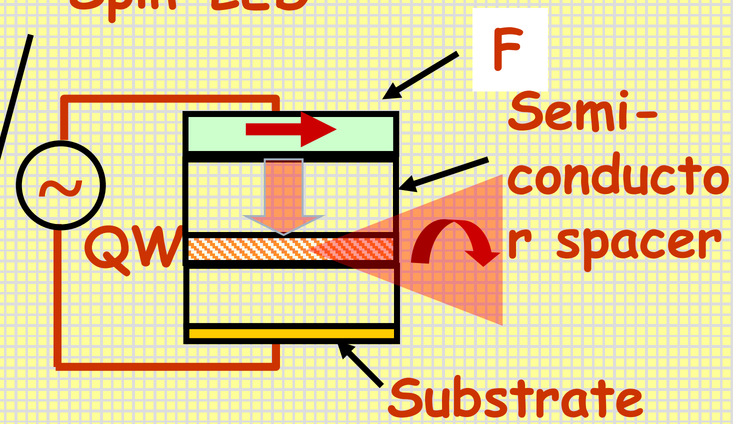

Efficiency of spin injection. Effects of the interface and spacer are included.

Spin-polarized tunneling

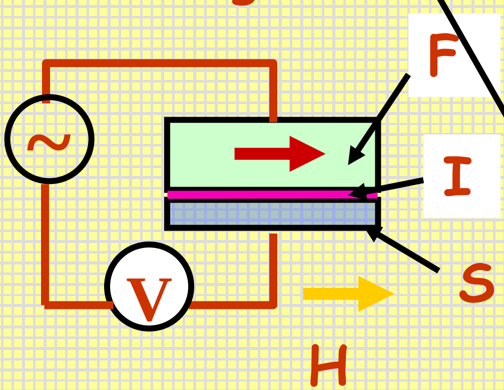

$$P = \frac{N_\uparrow \upsilon_{f\uparrow} - N_\downarrow \upsilon_{f\downarrow}}{N_\uparrow \upsilon_{f\uparrow} + N_\downarrow \upsilon_{f\downarrow}}$$

Point-contact Andreev reflection

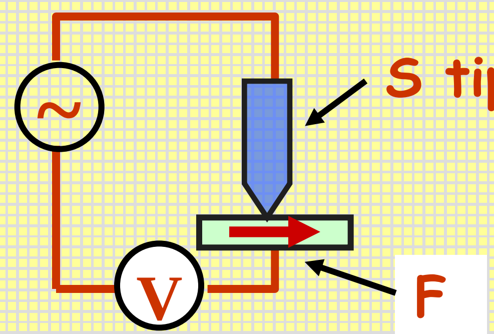

P is barrier dependent and junction dependent

Andreev Reflection : A Probe of Spin Polarization

Andreev reflection:
A conversion of normal current to supercurrent occuring at a metallic N/S interface.

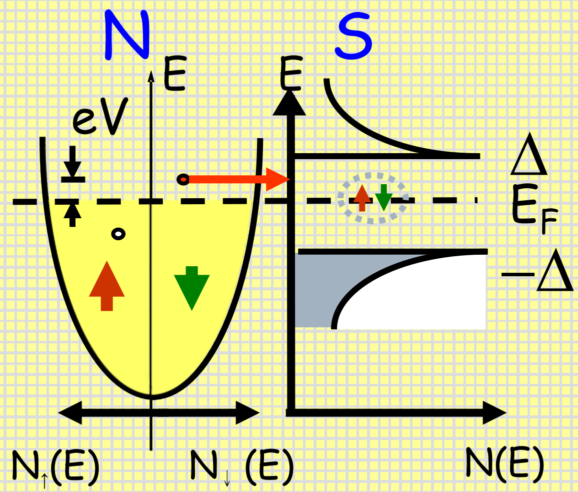

When N is ferromagnetic, only part of the electrons are paired.

The suppression of Andreev reflection due to spin polarization serves as a probe of the degree of spin polarization.

✓ Spin Polarization Determined by PCAR Measurement

	Fe	Co	Ni	CrO_2	LSMO
P	0.43±0.03	0.45±0.02	0.37±0.01	0.96±0.01	0.78±0.02 0.83±0.02

($La_{0.7}Sr_{0.3}MnO_3$)
($La_{0.6}Sr_{0.4}MnO_3$)

✓ Dilute magnetic semiconductor (Ga,Mn)As

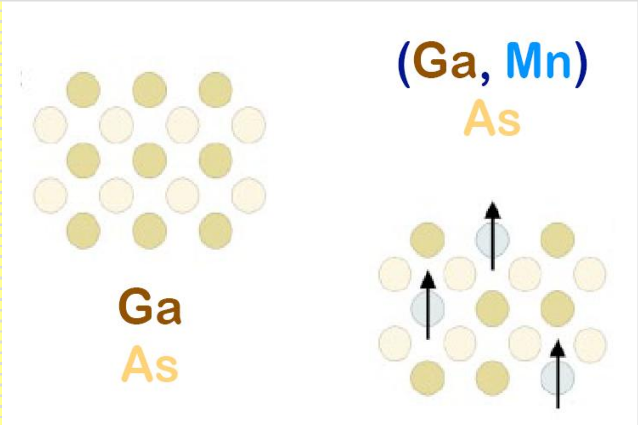

The exchange interaction below T_c comes from substitutional Mn S=5/2 and hole spins.

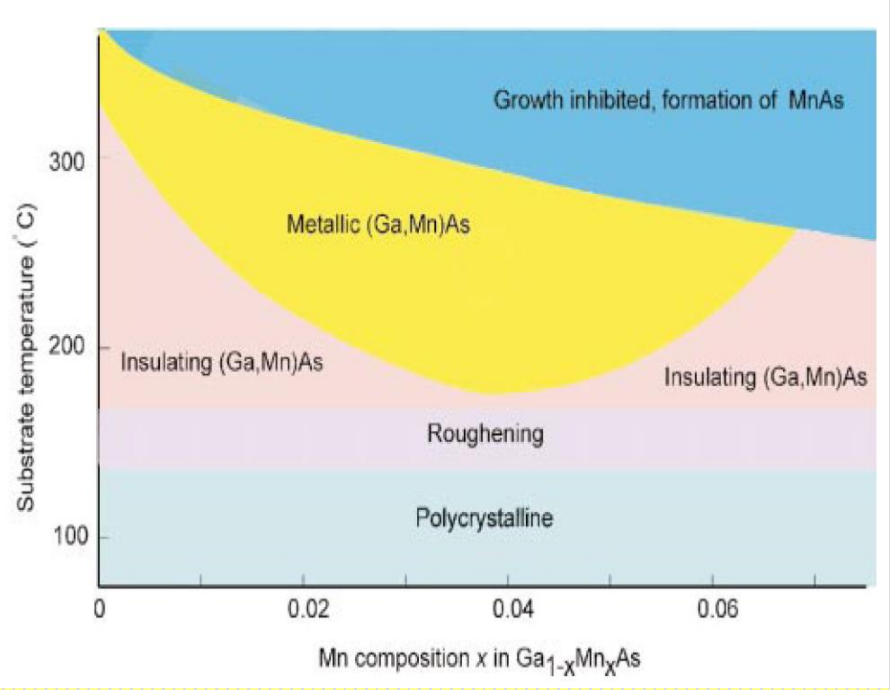

Tip-Sample Approach: Differential Screw

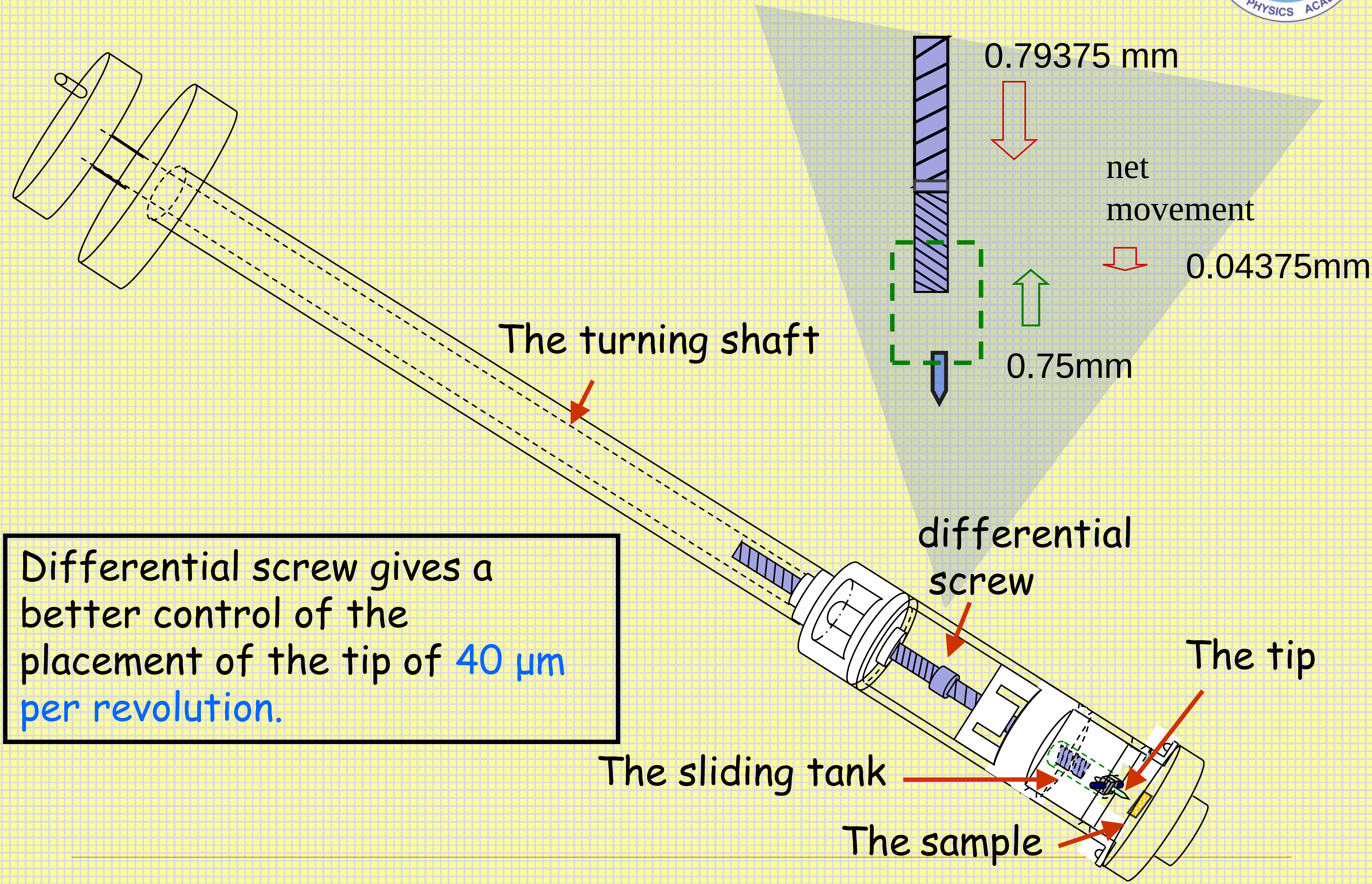

Differential screw gives a better control of the placement of the tip of 40 μm per revolution.

P=0.76, Z=0.00, Δ=1.09 meV, χ =4.8

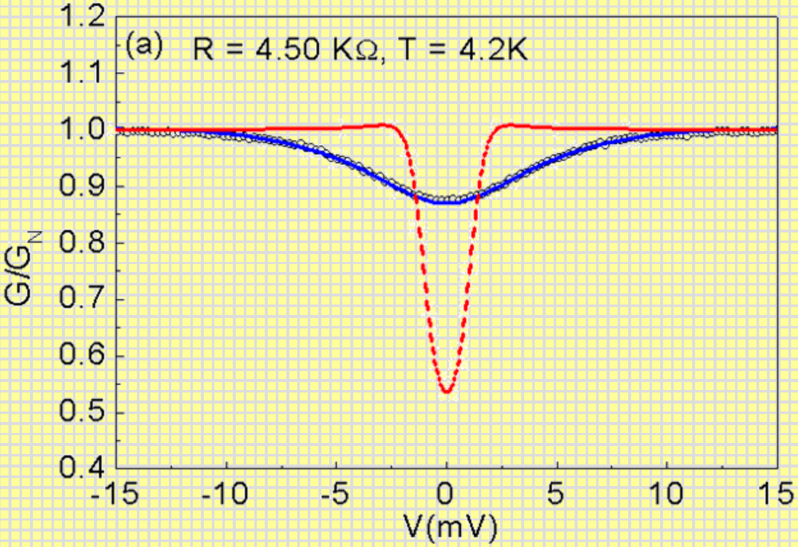

P=0.74, Z=0.04, Δ=0.85 meV, χ =4.0

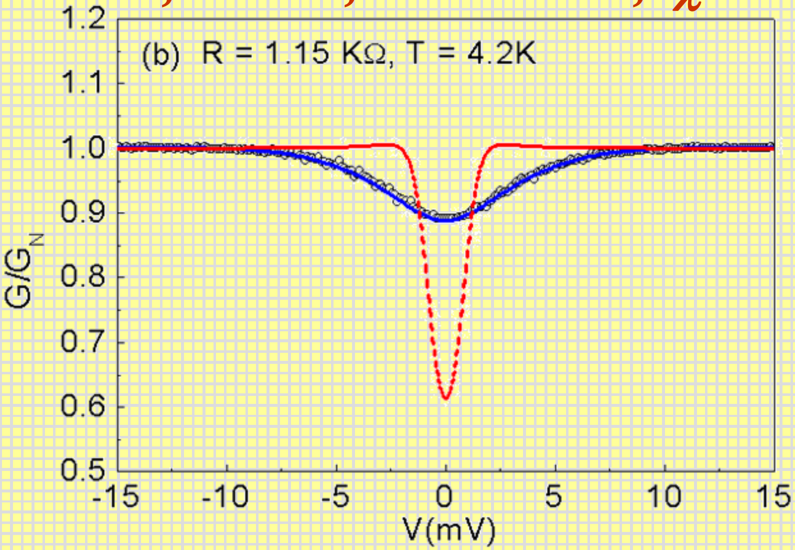

Black open circles with spreading resistance fits (blue solid lines) and the extracted PCAR spectra (red dashed line) after removing the contribution of spreading resistances in

(a) as-grown GaMnAs *P=0.76*

(b) annealed GaMnAs *P=0.74*

Point contact Andreev reflection

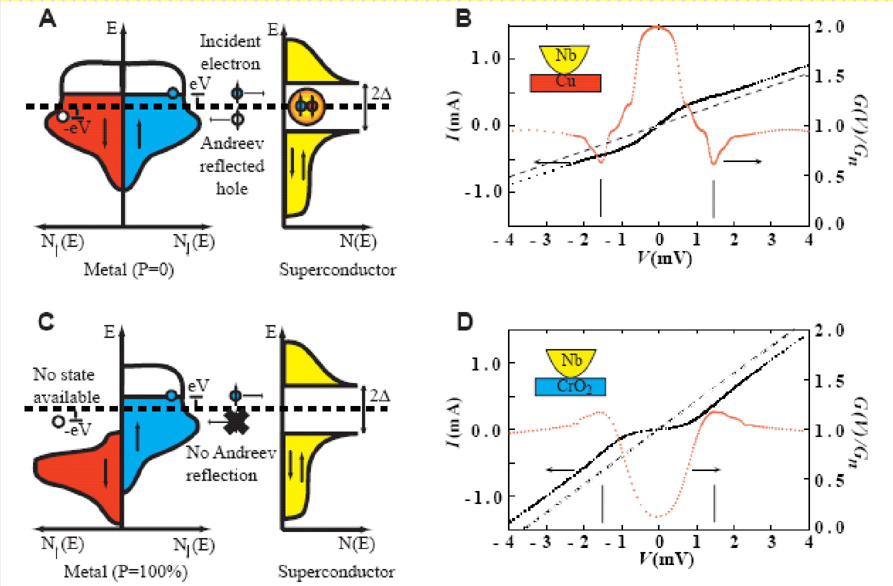

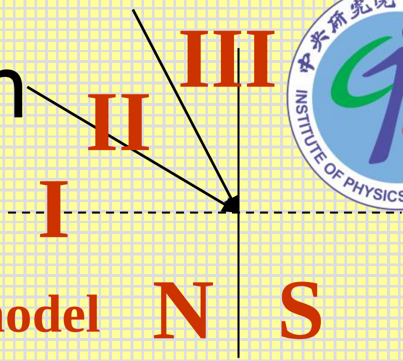

Our new BTK model

$$\frac{G_{NS}}{G_{NN}} = \int F(P, Z1, Z2, Z3, \Delta, E)\, f'(E - eV)\, dE$$

$$z = z1 + z2(a^*a)_{II} + z3(c^*c - d^*d)_{III}$$

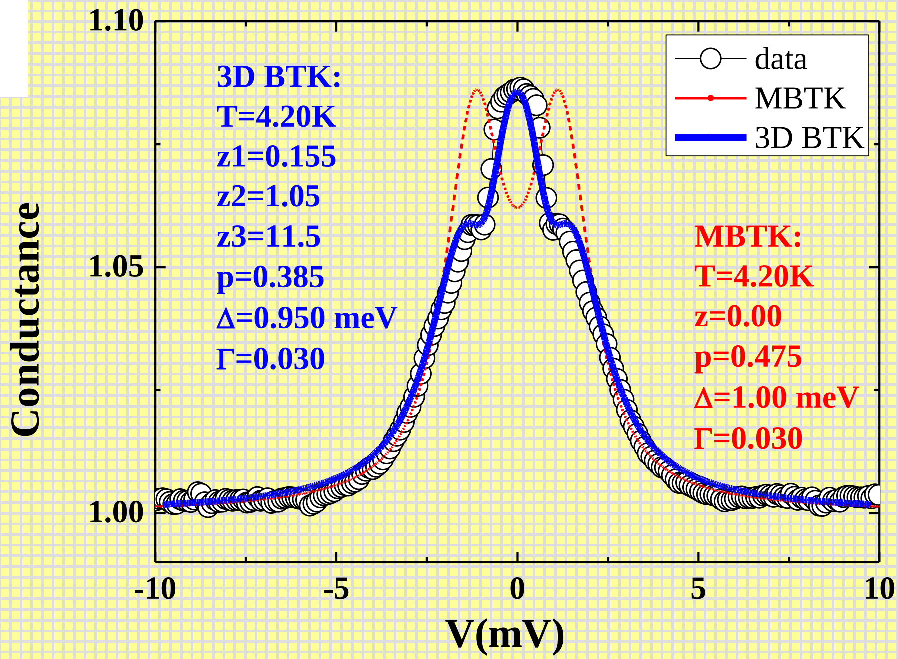

Modified BTK theory

$$\frac{G_{NS}}{G_{NN}} = \int F(P, Z, \Delta, E)\, f'(E - eV)\, dE$$

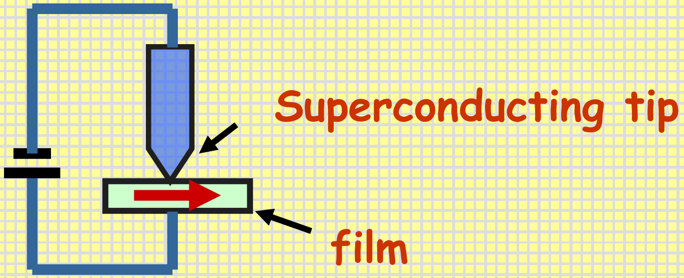

R.J. Soulen, J.M. Broussard, B. Nadgorny, T. Ambrose, Science 282, 85(1998)

Magnetic Nano-structures

Single Magnetic Domain Wall Resistance
Phase diagram of magnetization reversals
Edge roughness effect on domain wall mobility
Current driven magnetization reversals

Possible applications:

- Magnetic sensors, Reading heads
- Magnetic RAM
- Logic operation

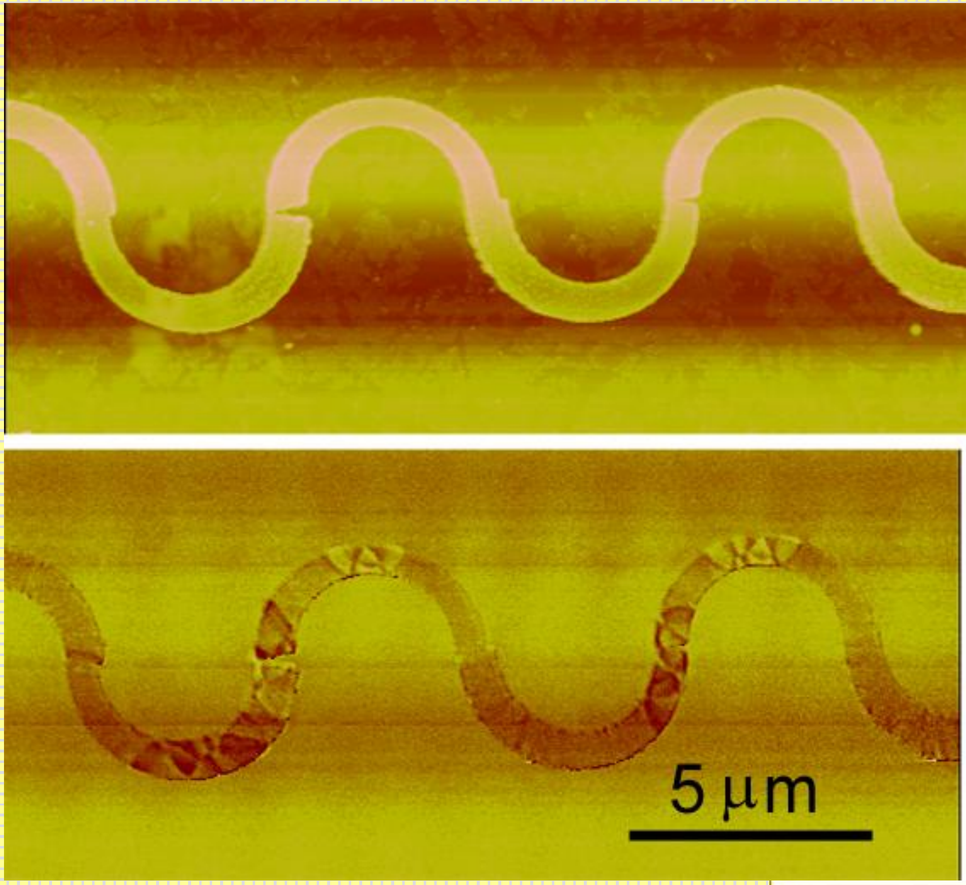

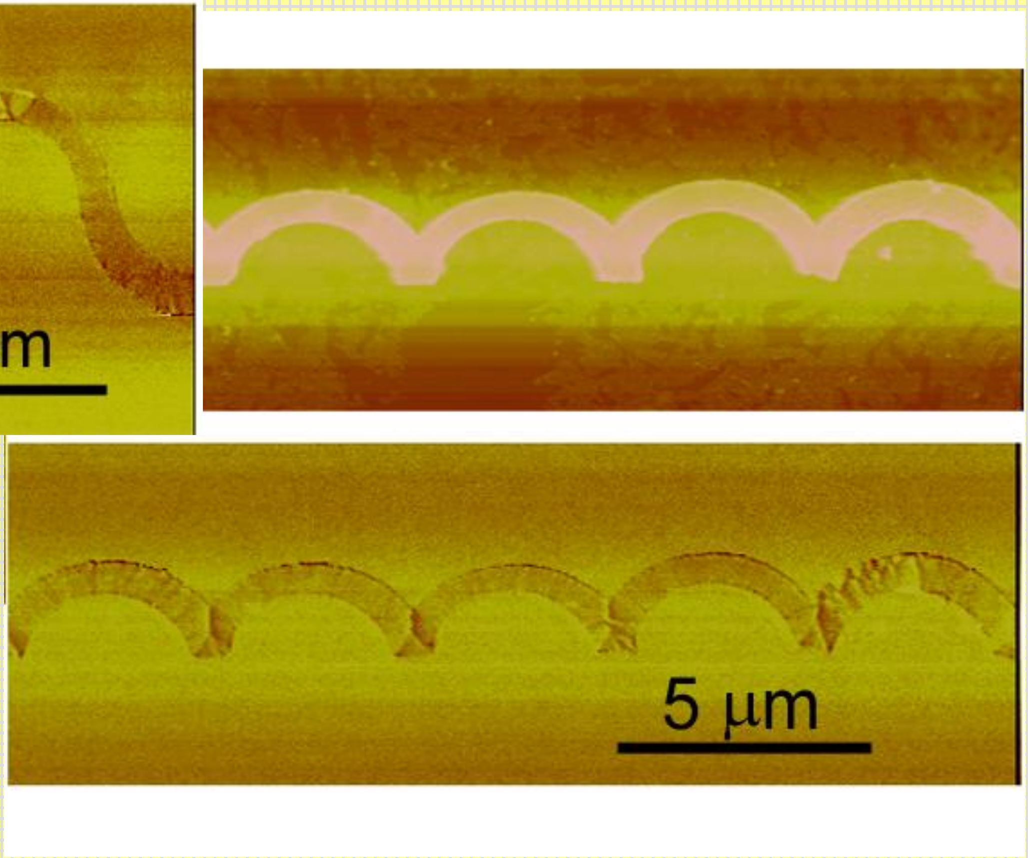

Atomic Force Microscope (AFM)
Magnetic Force Microscope (MFM)
images

Single Magnetic Domain Wall Resistance

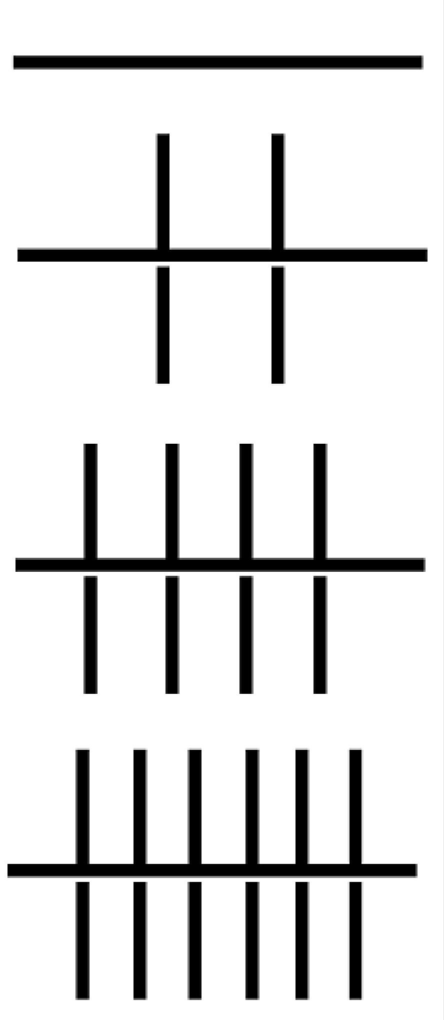

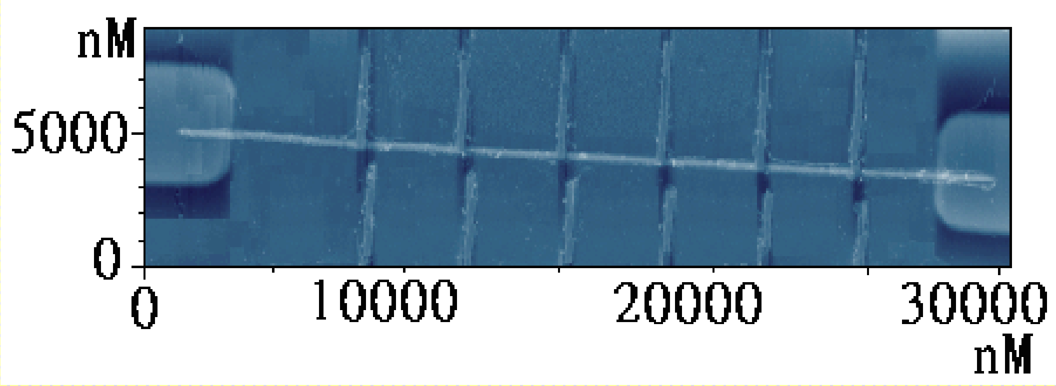

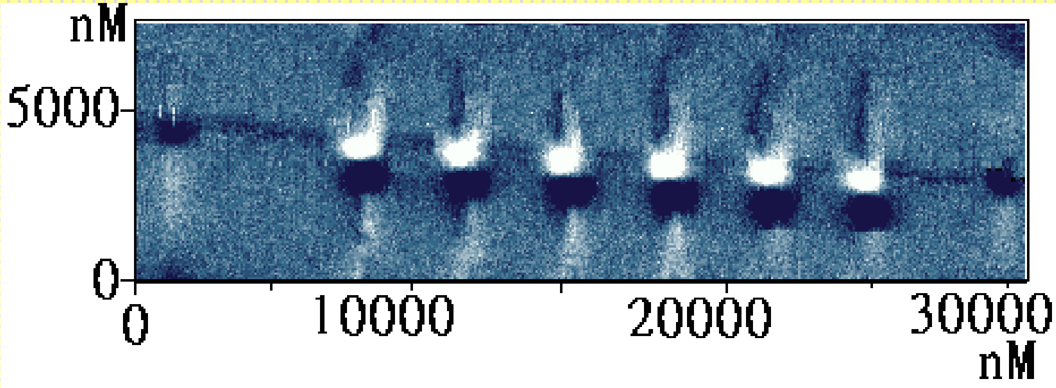

Phase diagram of magnetization reversals

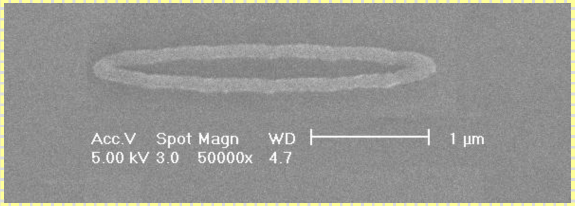

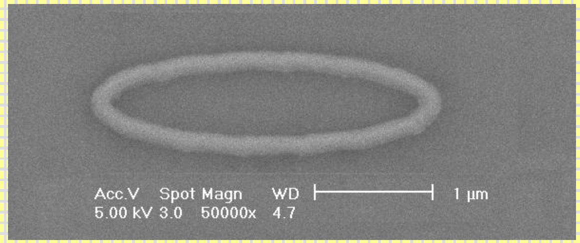

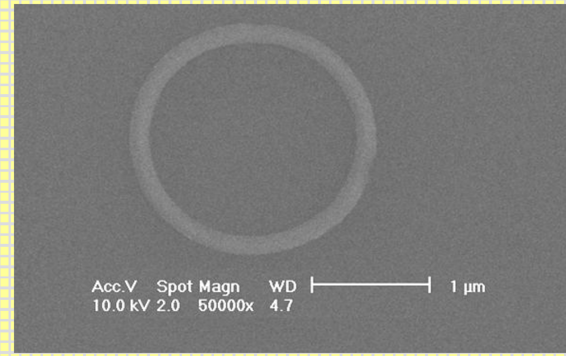

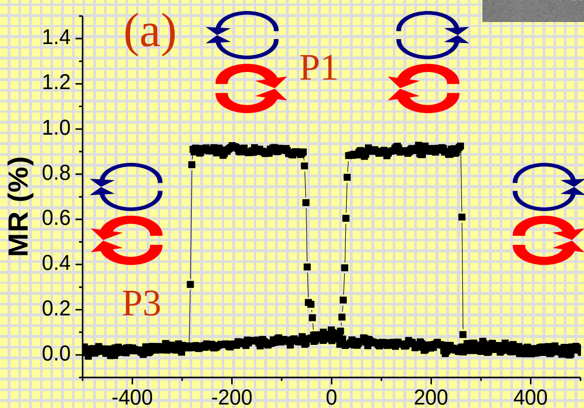

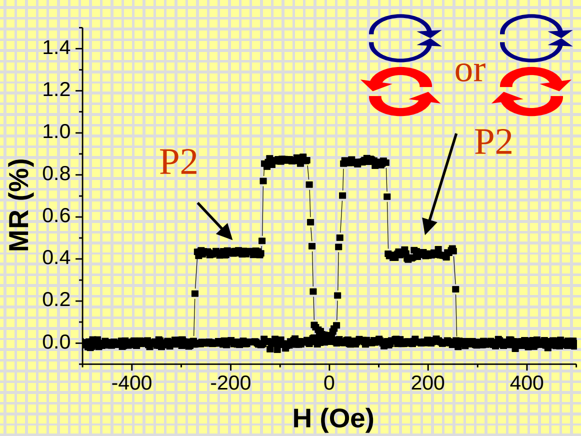

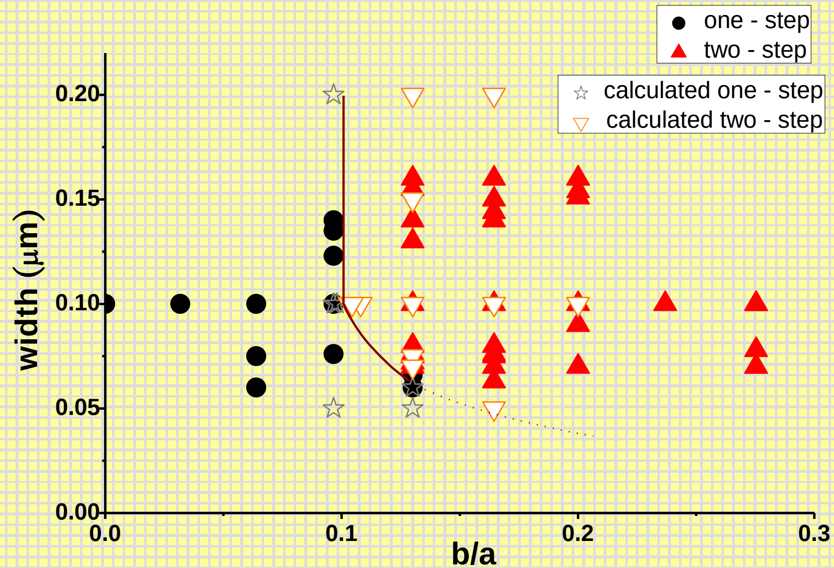

Magnetization reversal characteristics in NiFe elliptical ring arrays

The magnetization reversal processes of single layer nanoscale elliptical ring arrays are examined. For various aspect ratios and thicknesses, transition between single-step and double-step magnetization reversals was measured to form phase diagrams.

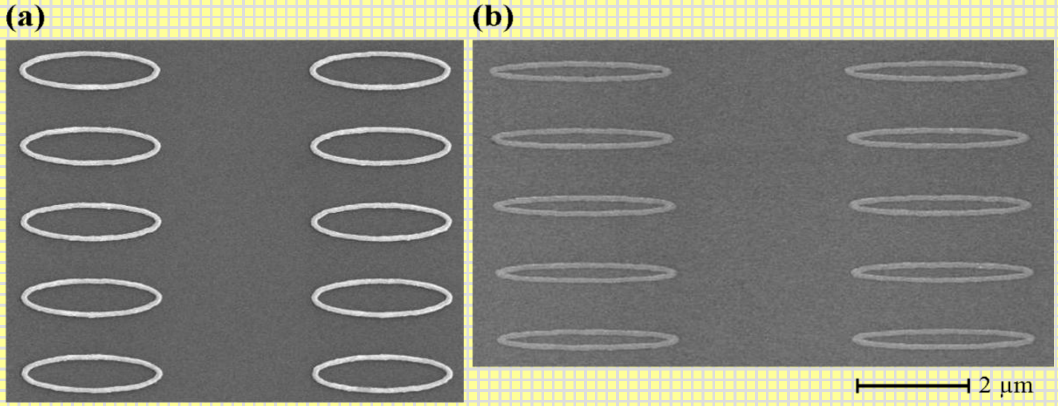

Scanning electron microscope images of selected samples (a) aspect ratio r=3.3 and (b) r=8 arrays of elliptical rings. The edge-to-edge distance in the long axis direction is fixed at 3 μm.

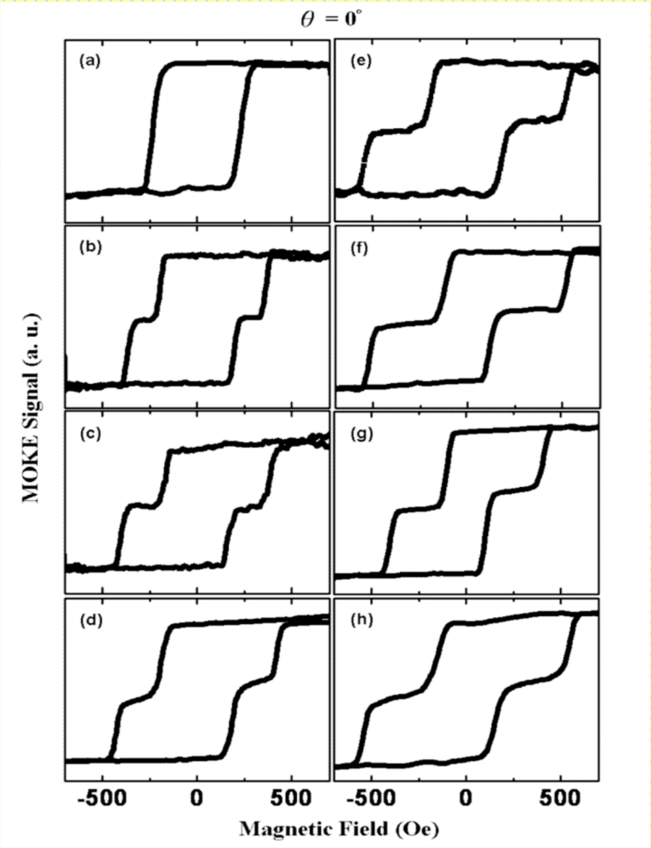

Figure 2. [(a)-(h)] The MOKE signals for 20 nm NiFe elliptical rings arrays of fixed width 100 nm and circumference 6.3μm for applied field parallel to the long axis of varied aspect ratios.

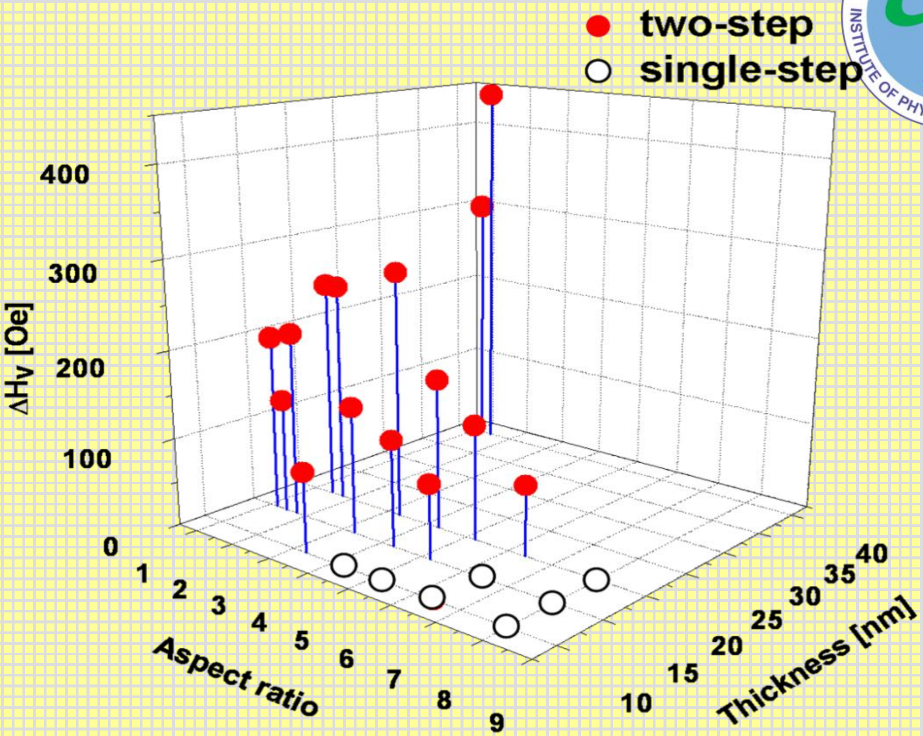

Figure 3. Phase diagram of elliptical ring reversal behavior and the field range of the vortex state ΔHv as functions of the aspect ratio r and thickness t for the applied field parallel to the long axis. The solid and open circles represent two-step and single-step switching, respectively.

Edge roughness effect on domain wall mobility

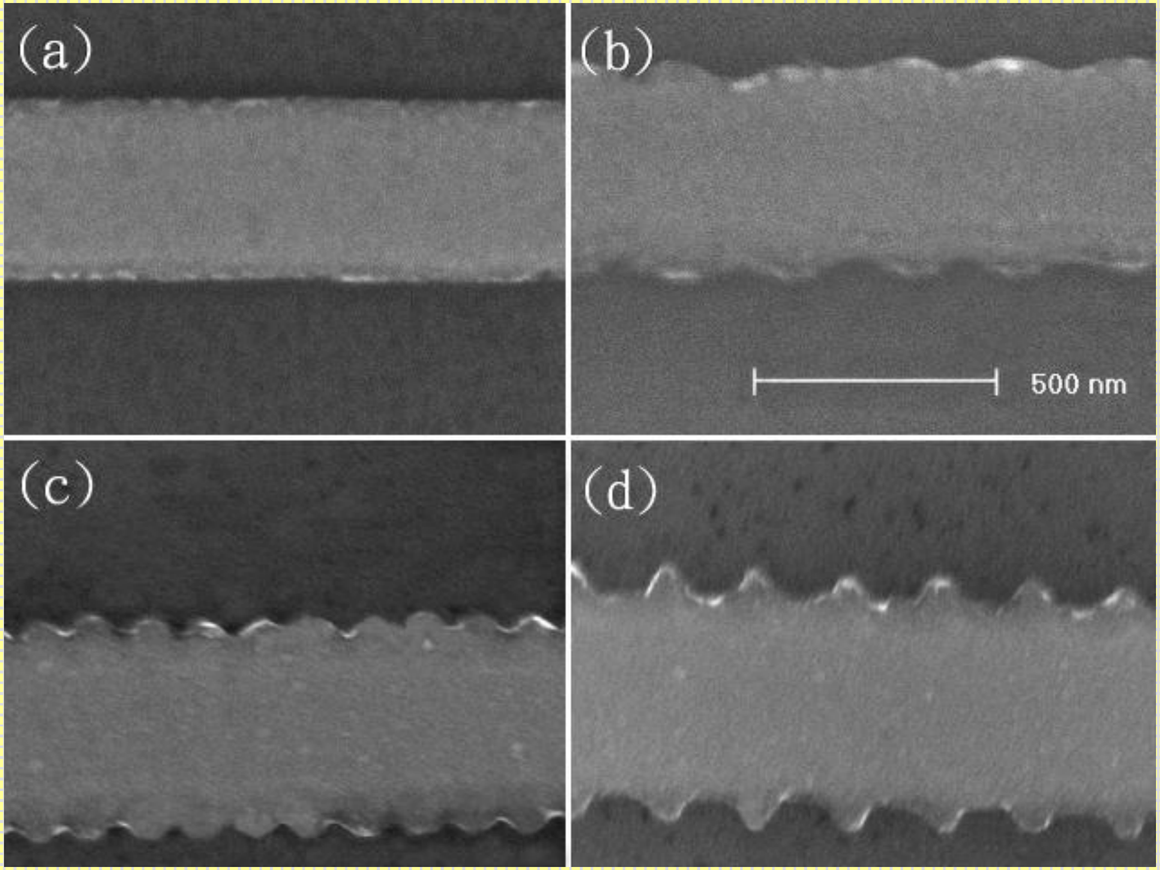

Spin transfer Torque

(tranport of magnetization by an electrical curent)

- **fundamentals**

- **switching of magnetization by spin transfer torque applications (STT-RAM, reprogrammable devices)**

- **microwave oscillations by spin transfer and applications to telecommunications**

Magnetic switching

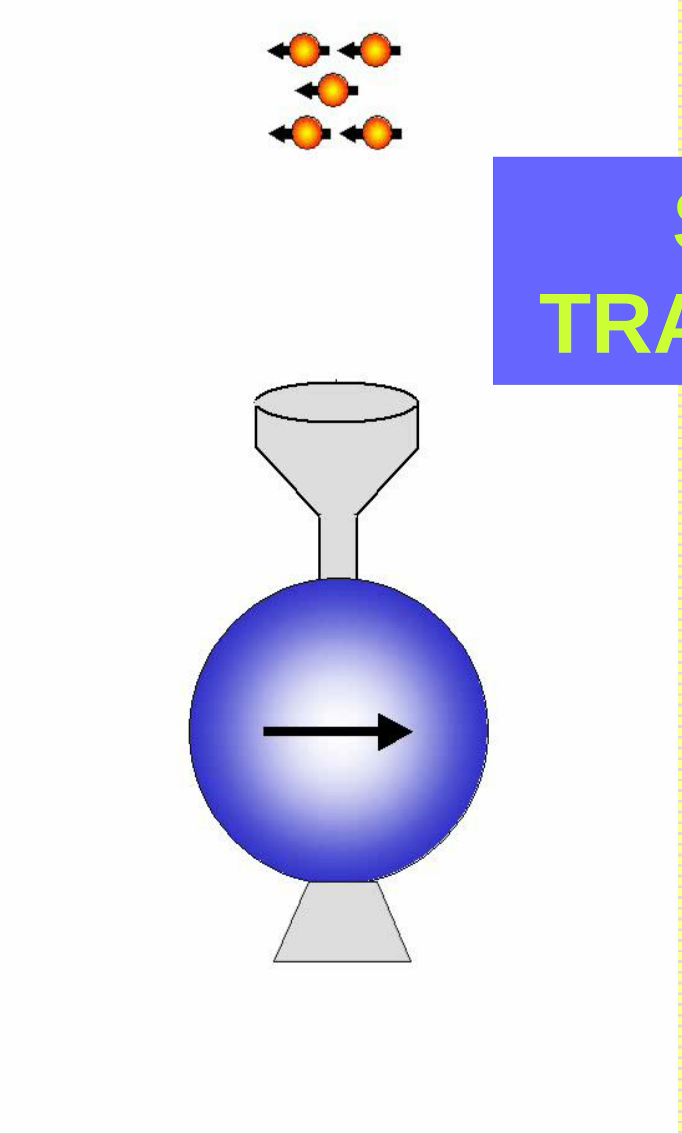

Generation of microwave oscillations

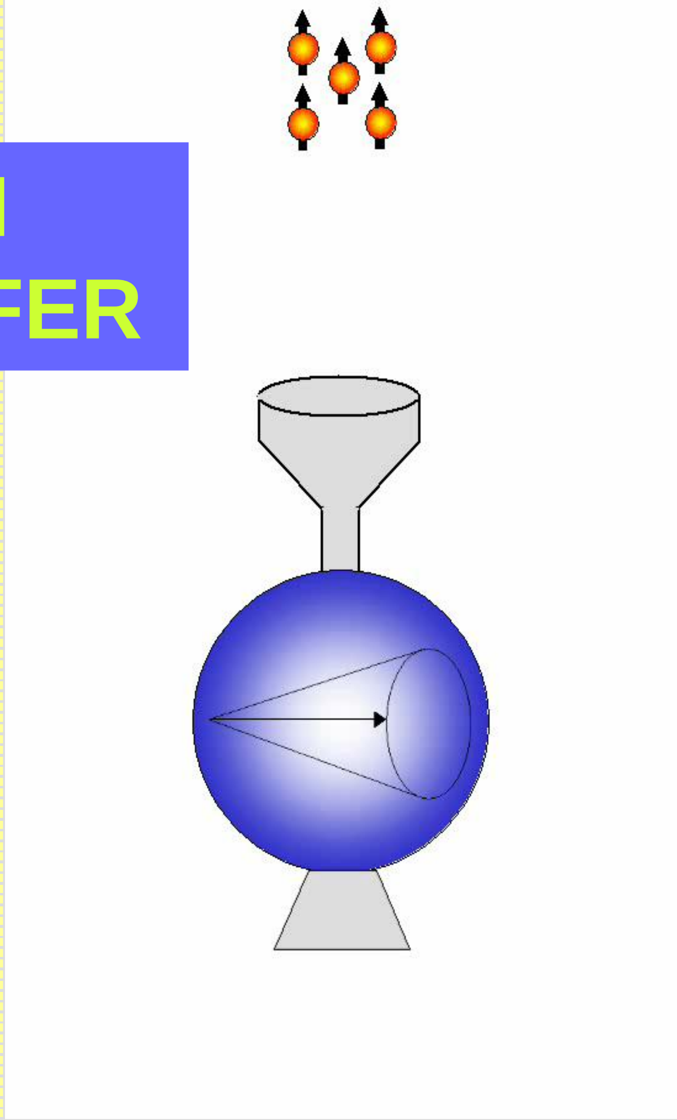

SPIN TRANSFER

Concept of spin transfer (Slonczewski 1996)

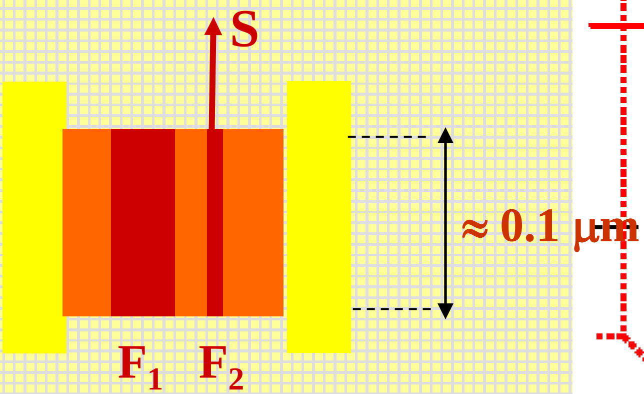

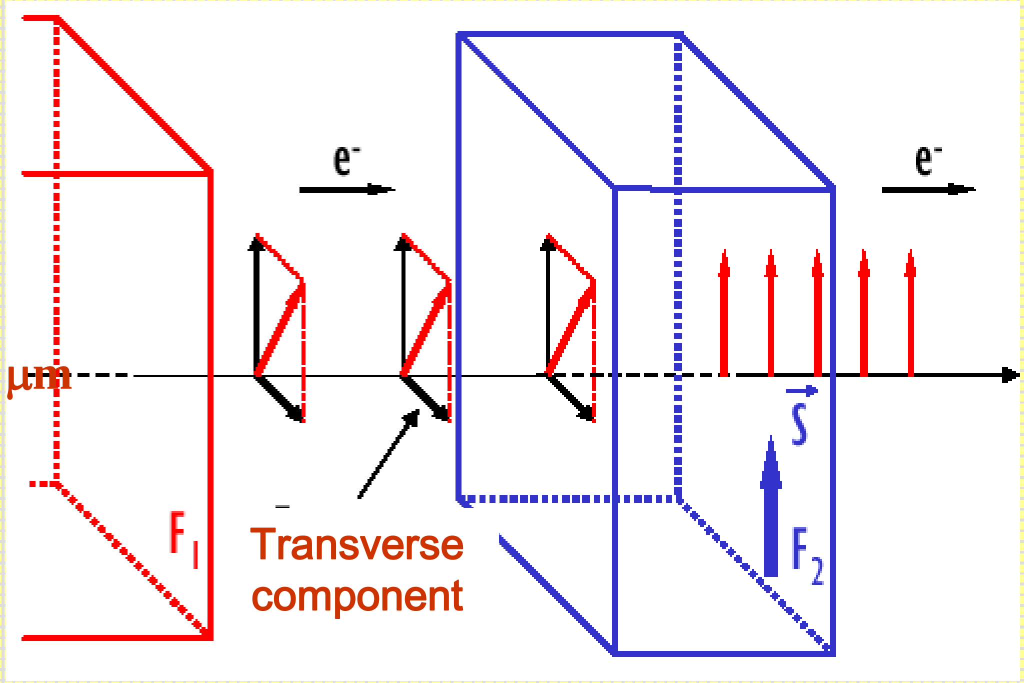

The transverse spin component is lost by the conduction electrons, but is actually transferred to the global SPIN $\vec{S}$ of the layer $\longrightarrow$ rotation of $\vec{S}$

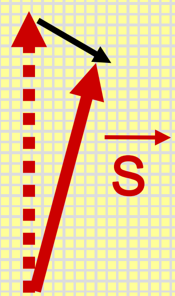

$$\dot{\boldsymbol{S}}_{1,2} = (I_e g/e)\hat{\boldsymbol{s}}_{1,2} \times (\hat{\boldsymbol{s}}_1 \times \hat{\boldsymbol{s}}_2)$$

Current-induced magnetization reversal by the spin-transfer torque can be understood in terms of collision of particles with material-dependent angular momentum transfer efficiencies.

Spin transfer torque

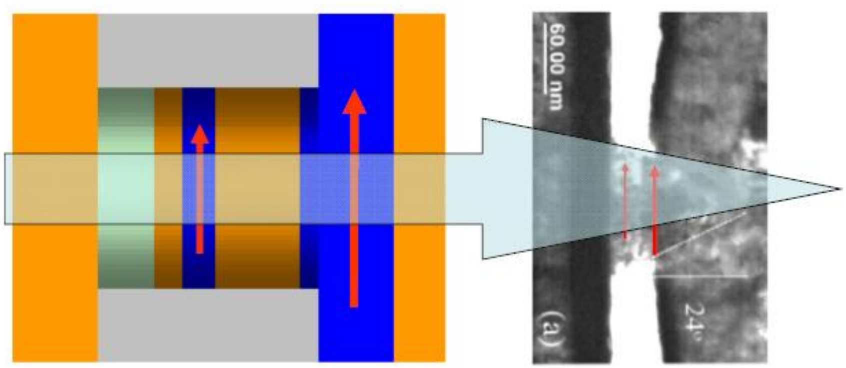

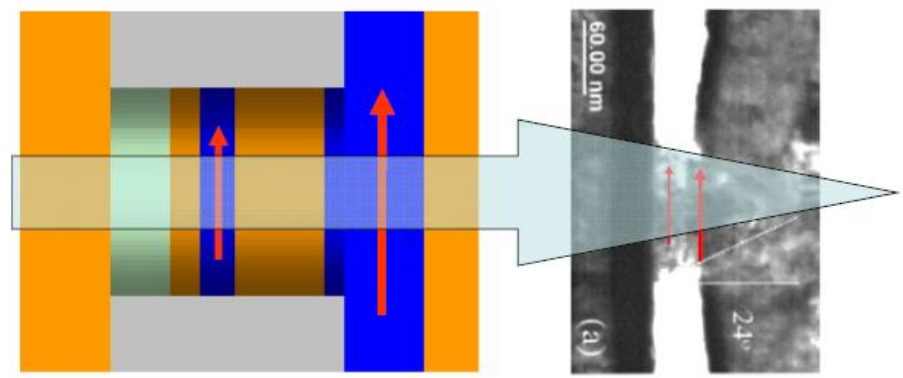

Trilayered pillar or tunnel junction

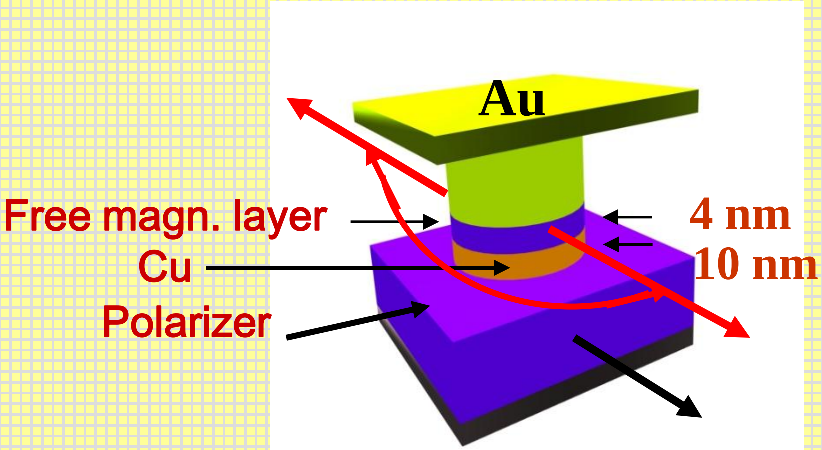

Metallic pillar ≈ 50x150 nm²

Tunnel junction ≈ 50x170 nm²

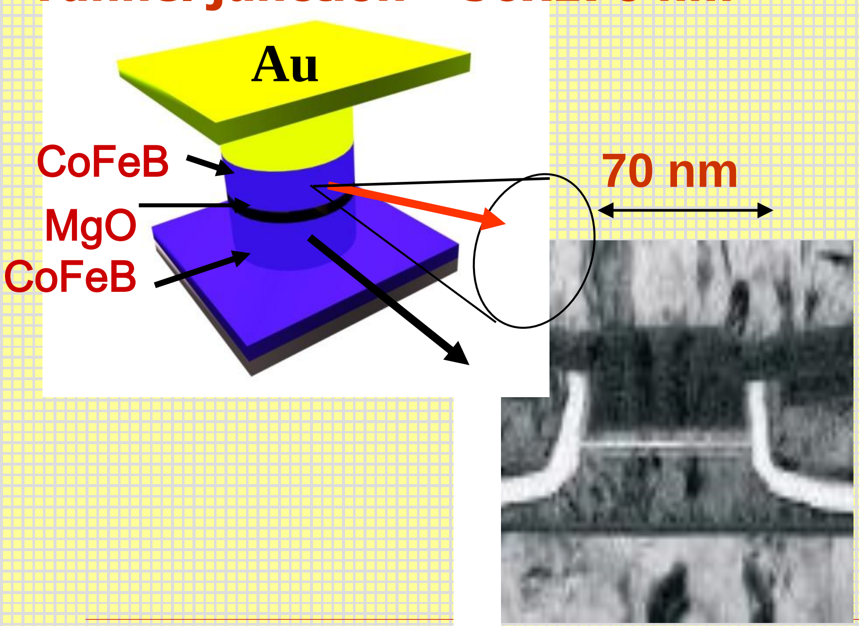

Two regimes of spin transfer

1) Magnetization switching by spin transfer

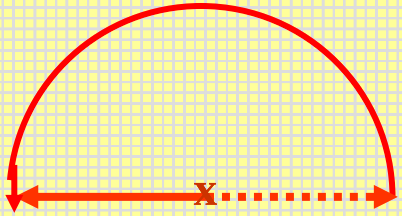

Zero or low field

Applications: writing a memory, etc

2) Sustained precession of the magnetization of the free layer and generation of radio-frequency oscillations

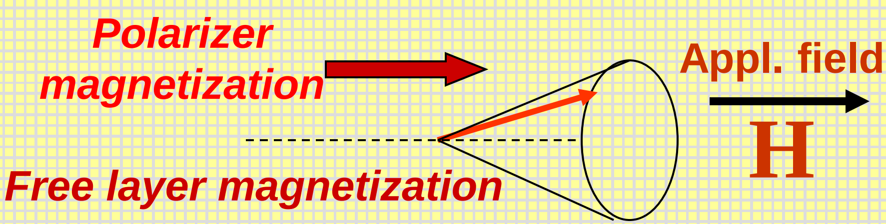

Applications: spin transfer nano-oscillators (NSTOs) for communications (telephone, radio, radar)

Applications of magnetic switching by spin transfer

Switching of reprogrammable devices (example: STT-RAM)

To replace M-RAM (switching by external magnetic field : *nonlocal, risk of « cross-talk » limiting integration, too large currents)*

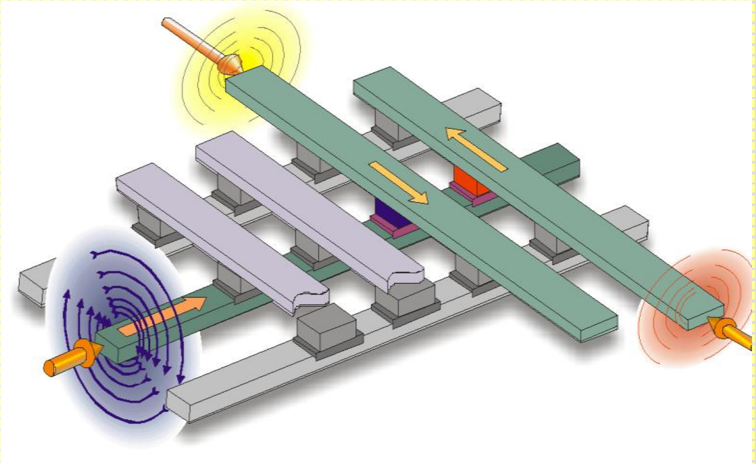

STT-RAM :«Electronic» reversal by spin transfer from an electrical current

Current pulse

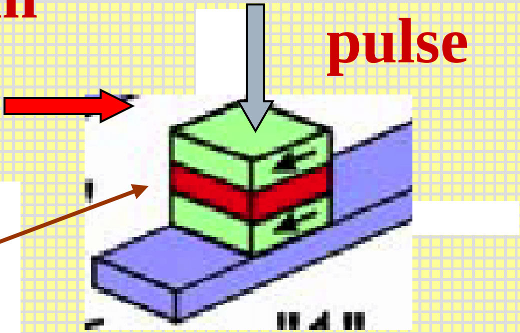

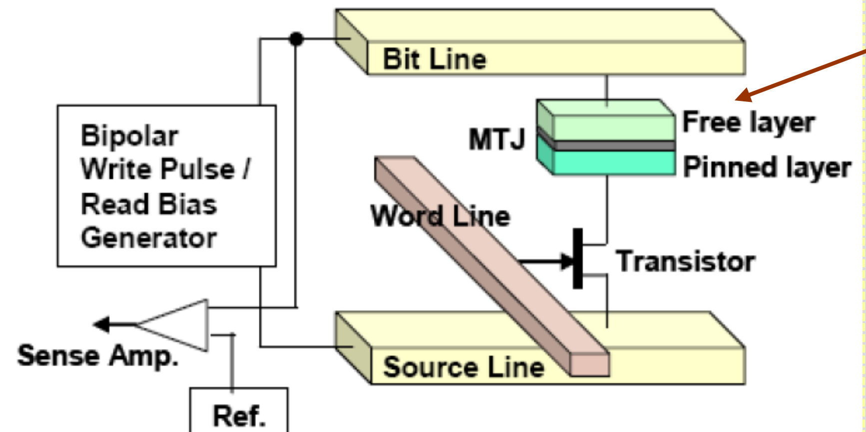

Source : SpinRAM SONY, IEEE 2005

Regime of steady precession for tunnel junctions

Tunnel junction ≈ 50x170 nm²

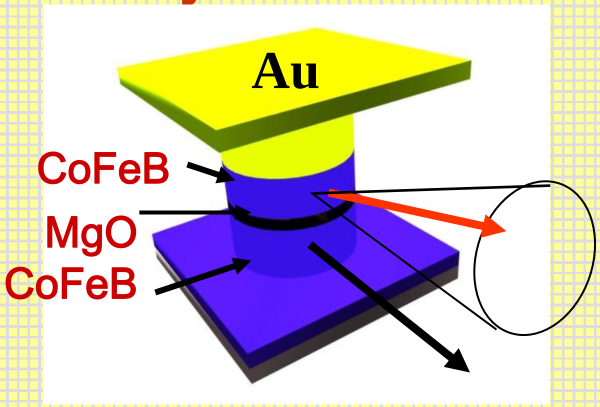

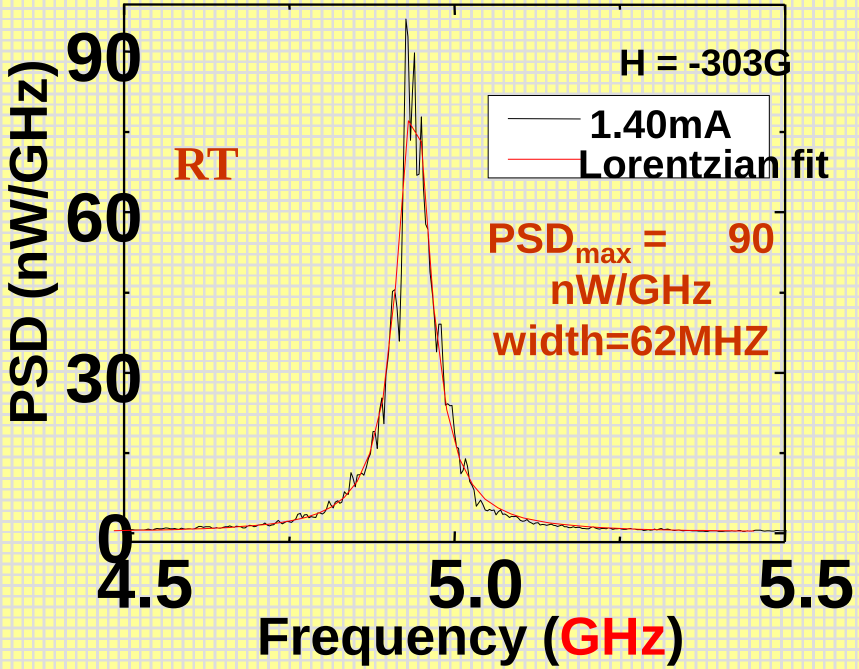

CoFeB/MgO/CoFeB junction (J.Grollier, AF et al 2008, collaboration S. Yuasa et al, AIST)

Regime of sustained vortex motion

Magnetic vortex creation and excitation

$2\,r \approx 10$ nm

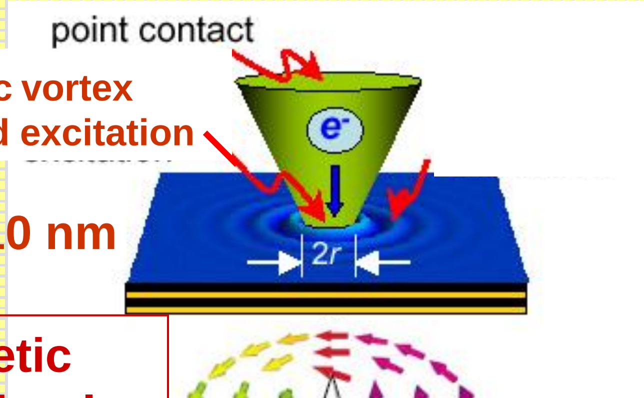

Magnetic vortex (circular magnetic configuration)

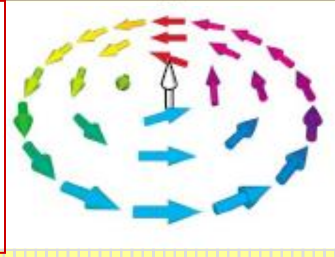

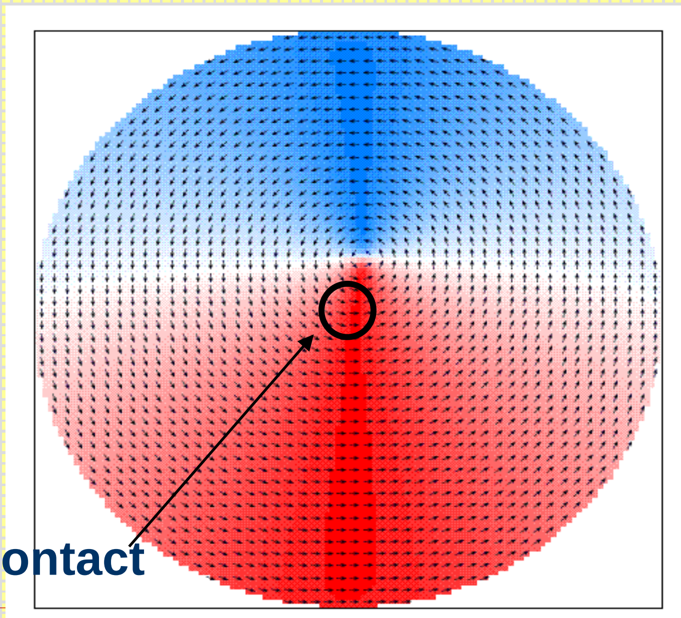

Nanocontact

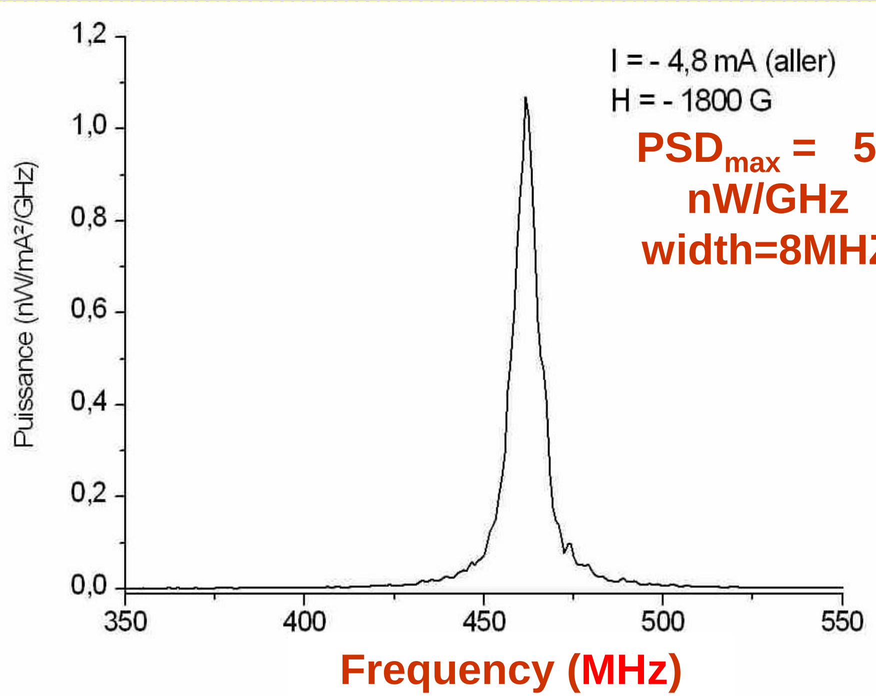

PSD_{max} = 50 nW/GHz

width=8MHZ

Low frequency vortex excitation in Py/Au/Co nanocontacts (CNRS/Thales, A.Ruotolo et al, 2008)

Spin Transfer Oscillators (STOs)

(telecommunications, radar, chip to chip communication…)

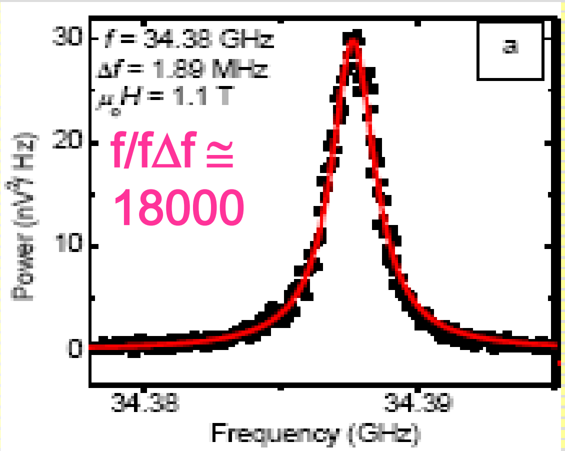

Advantages:

-direct oscillation in the microwave range (0.5-40 GHz)

-agility: control of frequency by dc current amplitude

- high quality factor

- small size (≈ 0.1μm) (on-chip integration, chip to chip com., microwave assisted writiing in HDD)

-Needed improvements

-- Increase of power by synchronization of a large number N of STOs (x N^2)

-Optimization of the emission linewidth

Programmable AND (OR) logic element operated by spin torque transfer

Area : 200*600 nm^2

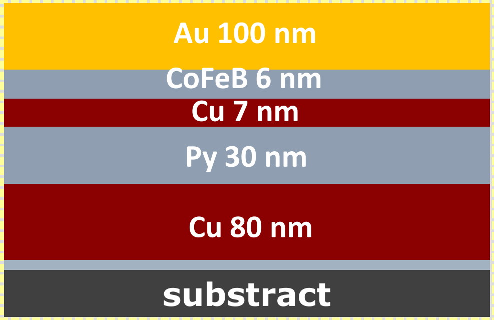

Layer structure

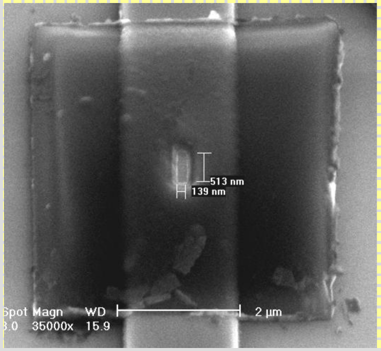

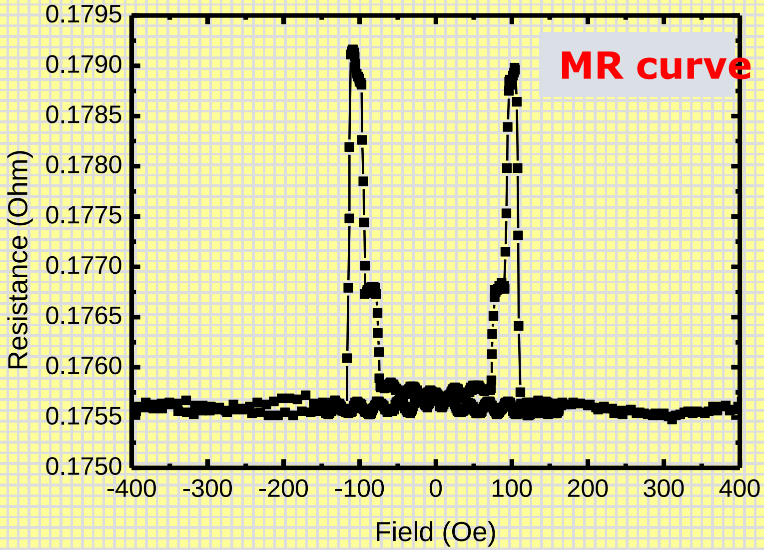

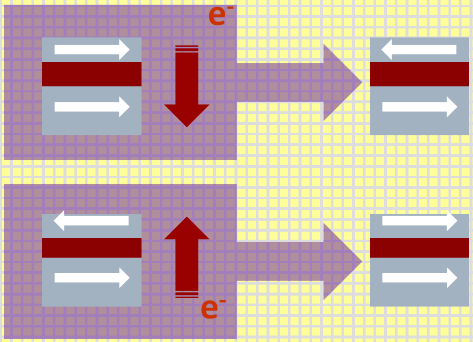

Current driven

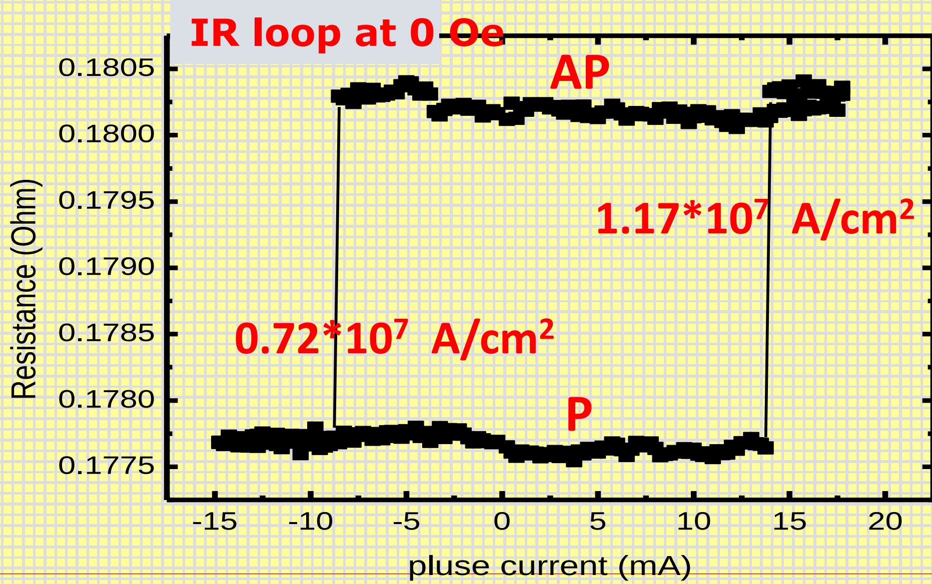

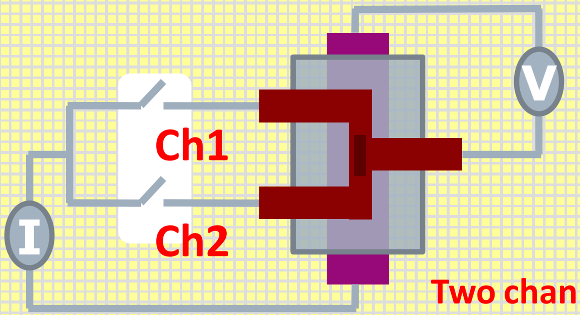

Two channels input

$I_{P\rightarrow AP} = 14$ mA, $I_{AP\rightarrow P} = -8.7$ mA

Input signal 1 ($I_{P\rightarrow AP}/2 < I = 8$ mA $< I_{P\rightarrow AP}$)

Input signal 0 ($I = 0$ mA)

Refresh current ($I = -11$ mA $> I_{AP\rightarrow P}$)

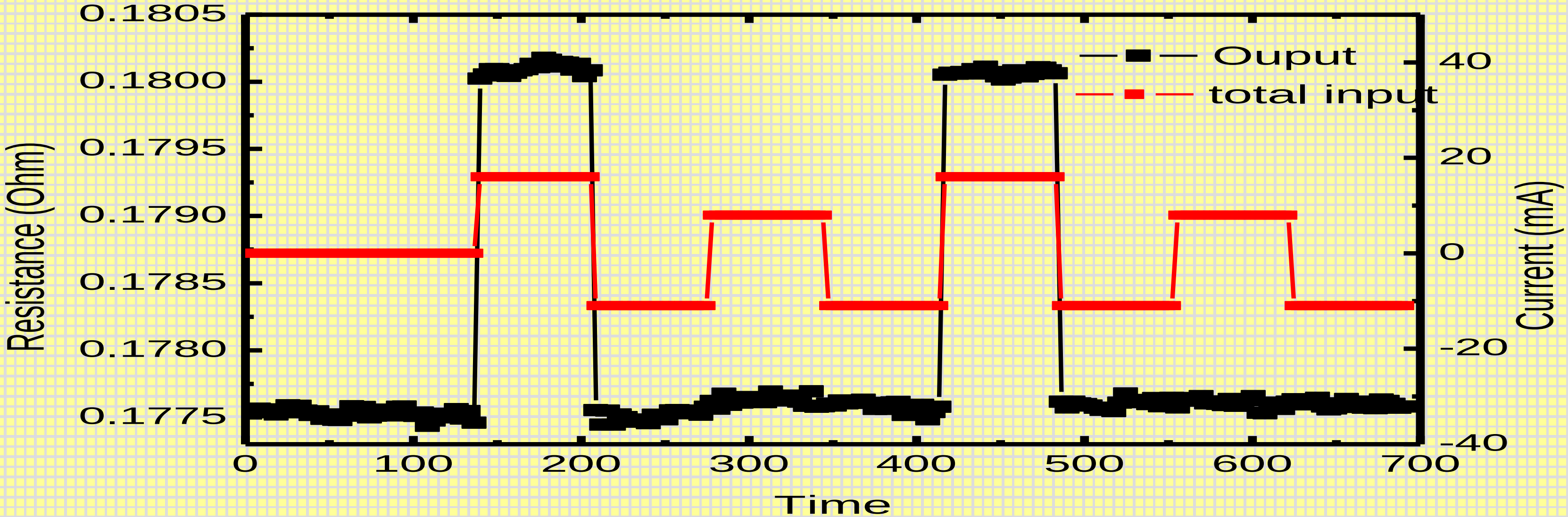

	input	refresh	input	refresh	input	refresh	input	refresh	input	refresh
Ch 1 (mA)	**0** (0)	(-11)	**1** (8)	(-11)	**0** (0)	(-11)	**1** (8)	(-11)	**1** (8)	(-11)
Ch 2 (mA)	**0** (0)	(0)	**1** (8)	(0)	**1** (8)	(0)	**1** (8)	(0)	**0** (0)	(0)
State	**L**		**H**		**L**		**H**		**L**	

Another spin transfer effect: displacement of a wall between magnetic domains

Domain wall

Magnetic film

Magnetization to the right →

← Magnetization to the left

Domain walls in a magnetic nano-stripe for the massive memories of tomorrow ?

(IBM project, replacement of hard discs ?)

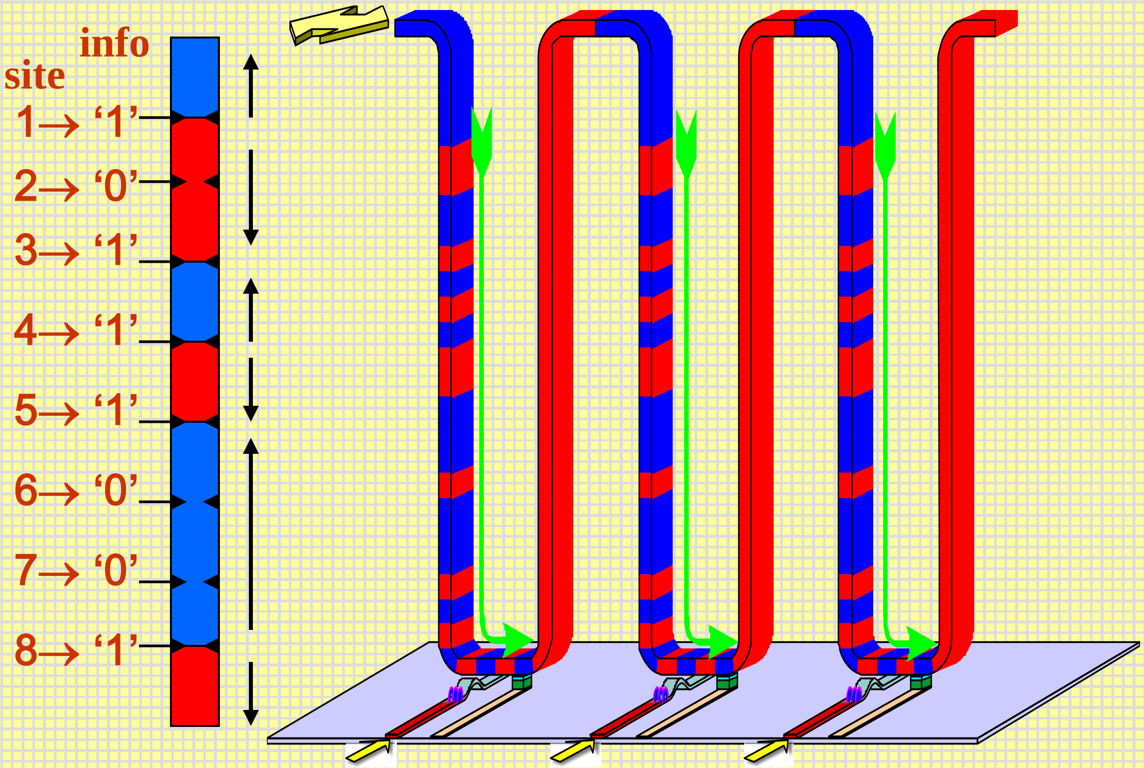

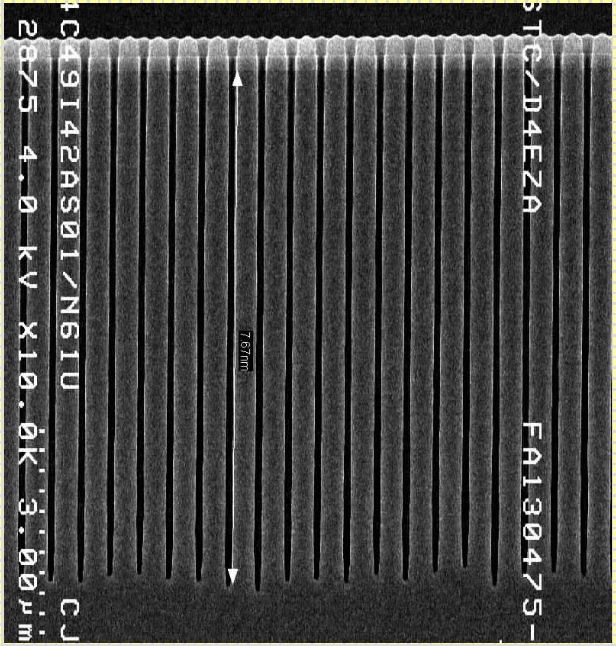

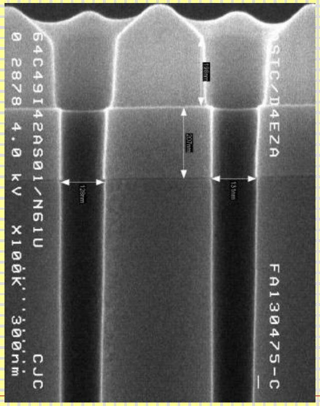

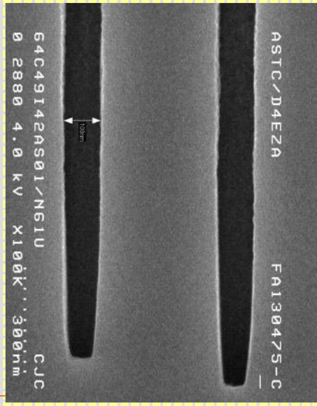

The information is stored by domain walls located on periodic notches:
No wall = "0", Wall = "1"

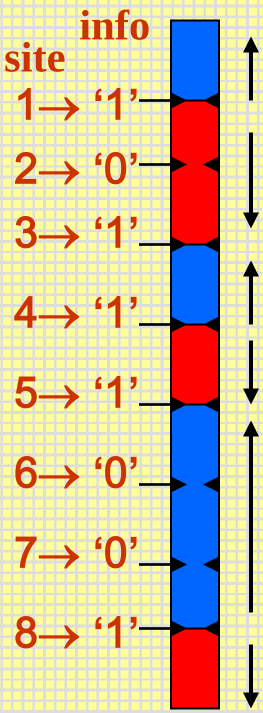

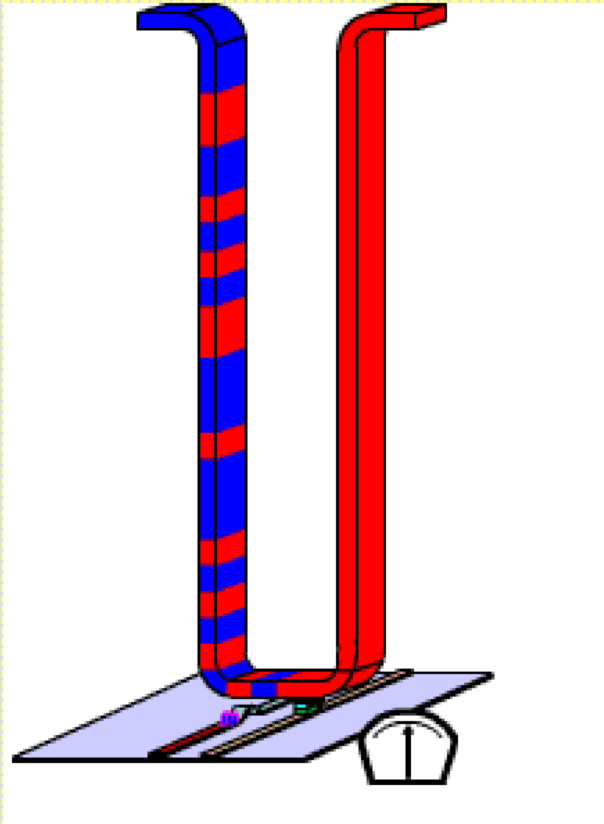

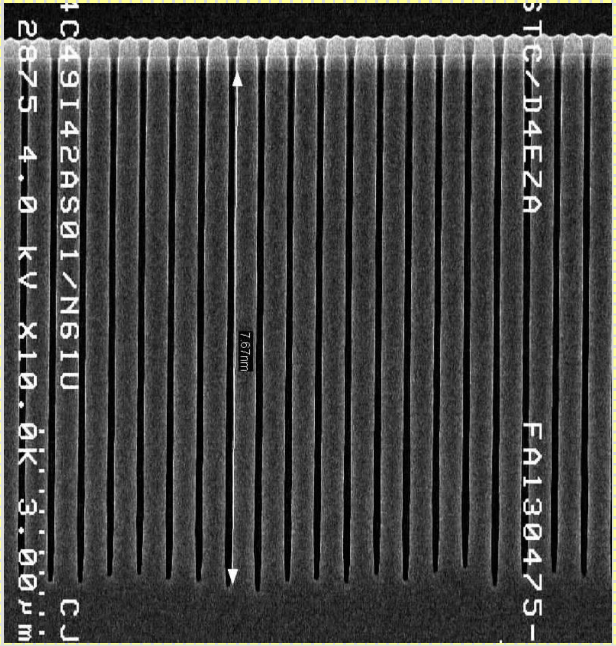

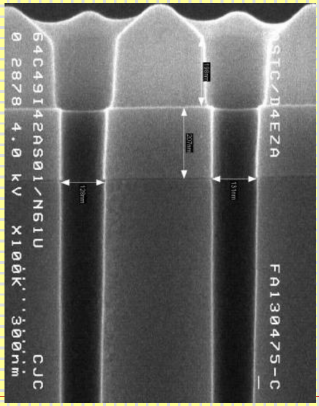

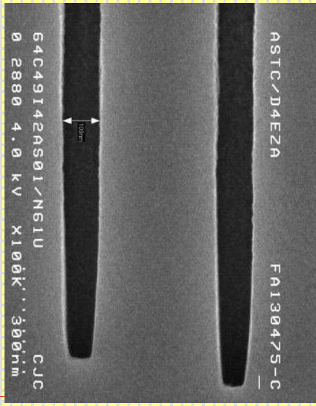

The information is stored by domain walls located on periodic notches: No wall = “0”, Wall = “1”

Edge Roughness effect on the magnetization reversal process of spin valve submicron wires

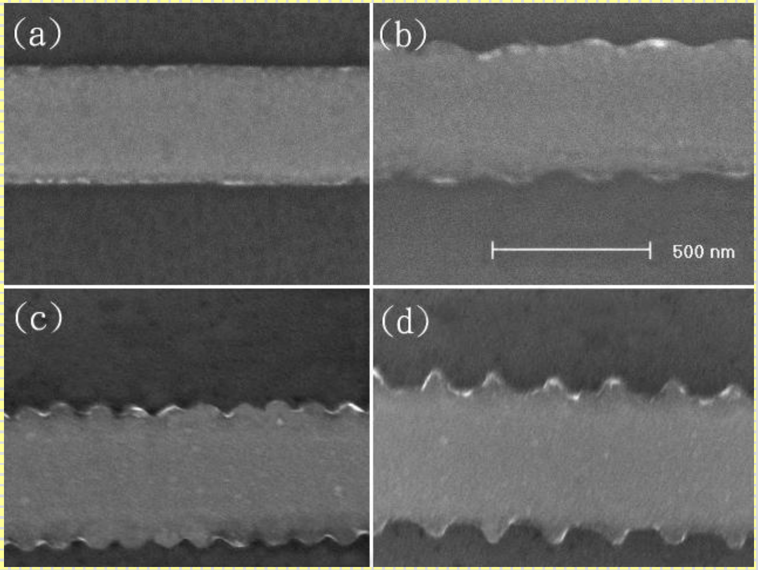

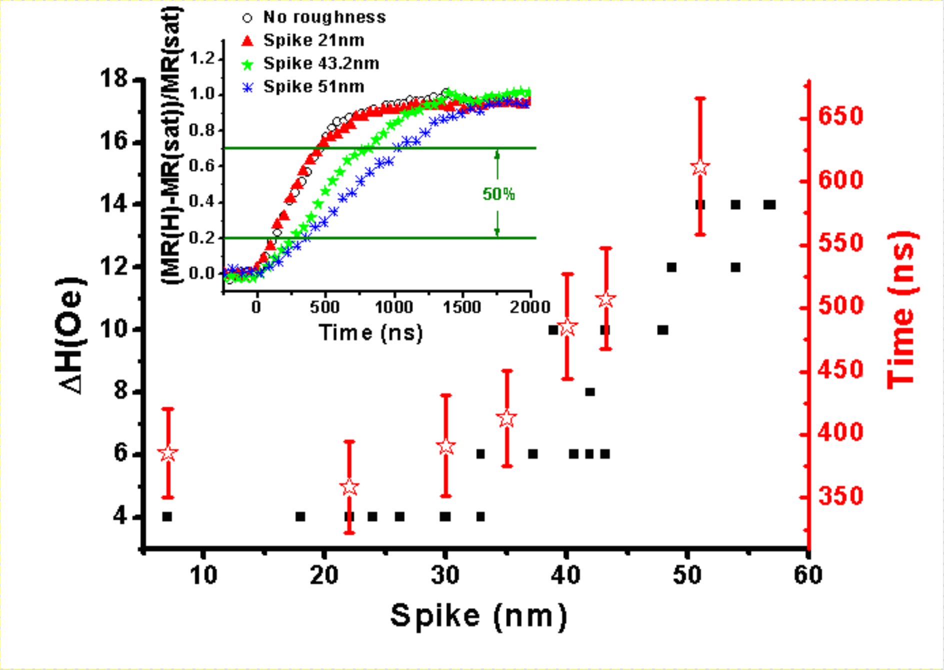

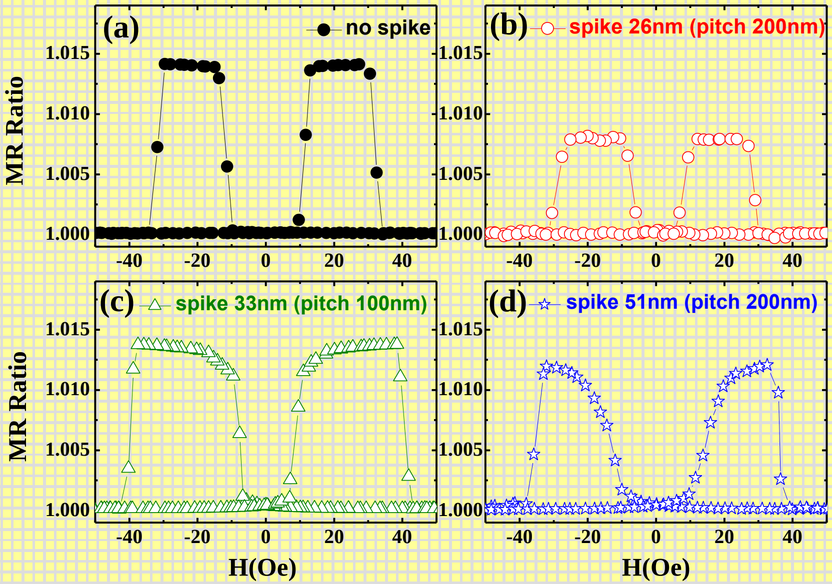

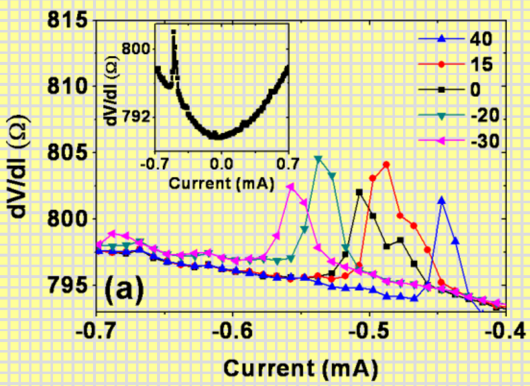

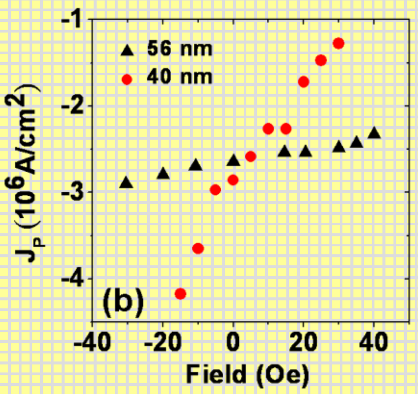

Non-local measurement

- Spin diffusion length
- Hanle effect
- Spin Hall effect & Inverse Spin Hall effect

Spin Pumping (spin battery)

- Pure spin current
- Spin Hall effect & Inverse Spin Hall effect

Spin Hall Effect: Electron flow generates transverse spin current

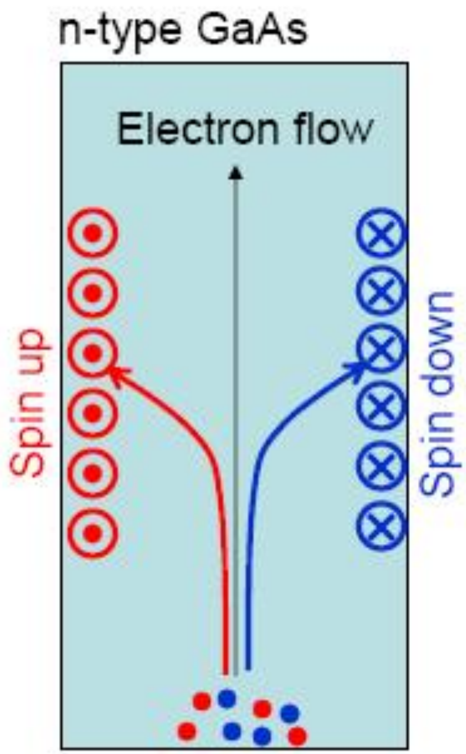

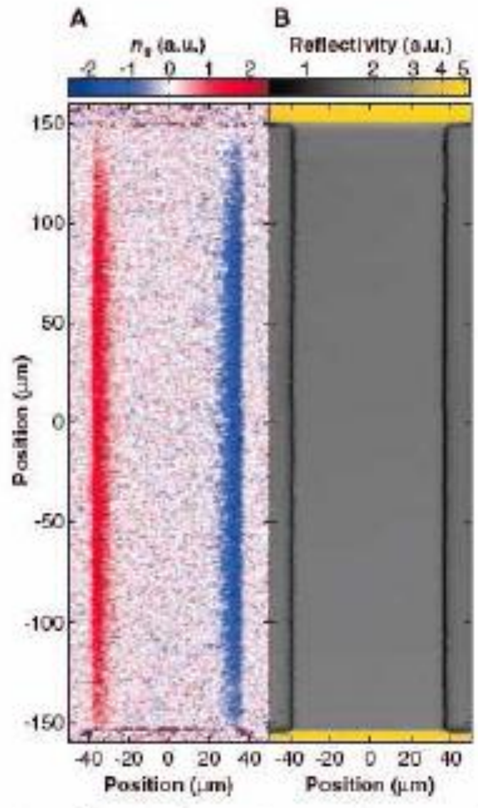

SHE observed
in GaAs
using Kerr effect
to measure spin

Kato et.al. (Awschalom),
Science 306, 1910 (2004)

Now observed at room temperature in ZnSe

The extrinsic SHE is due to asymmetry in electron scattering for up and down spins. – spin dependent probability difference in the electron trajectories
The Intrinsic SHE is due to topological band structures

Pure Spin Currents: The Johnson Transistor

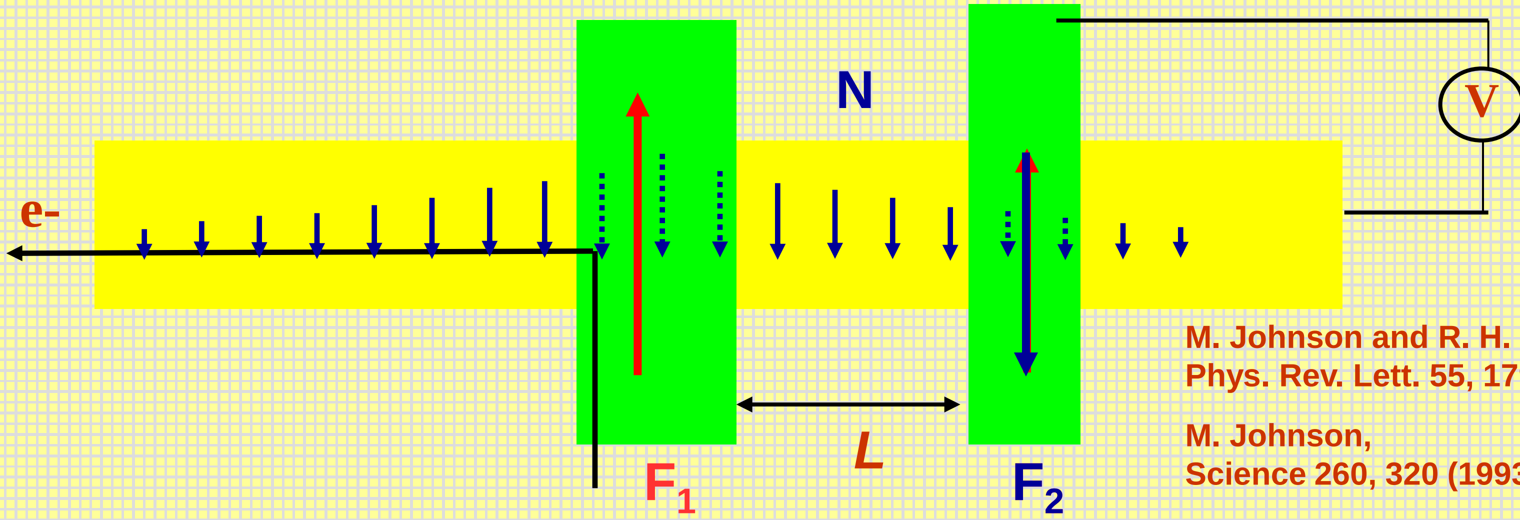

M. Johnson and R. H. Silsbee, Phys. Rev. Lett. 55, 1790 (1985)

M. Johnson, Science 260, 320 (1993)

First Experimental Demonstrations

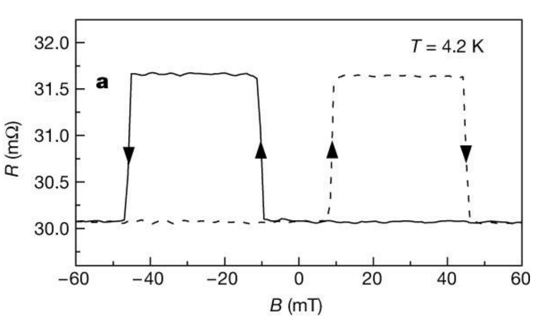

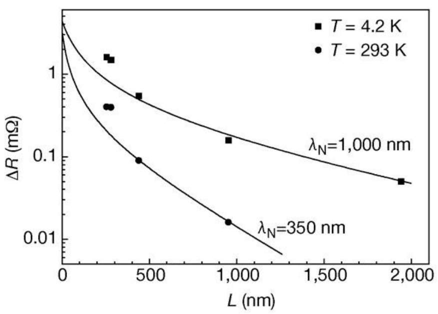

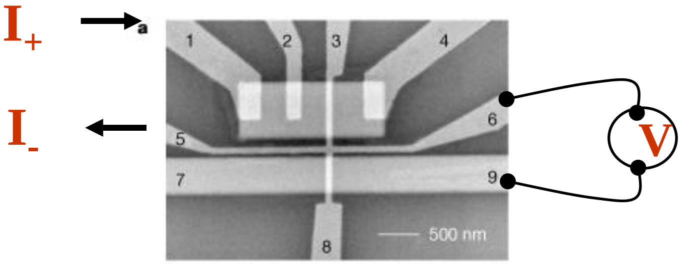

Cu film: λ_s = 1 μm (4.2 K)

Jedema *et al.*, Nature 410, 345 (2001)

Spin Hall Angle

$$\gamma = \frac{\sigma_{SH}}{\sigma_c}$$

σ_{SH} ← **spin Hall conductivity**

σ_c ← **charge conductivity**

stronger spin orbit interaction → **larger** γ

Goal:

- **experiments to quantify** γ

Importance:

- **understanding the effect of SO coupling on electron transport**
- **recognizing materials for spintronics applications**

Spin Pumping

-- dynamic behavior in F/N bilayers

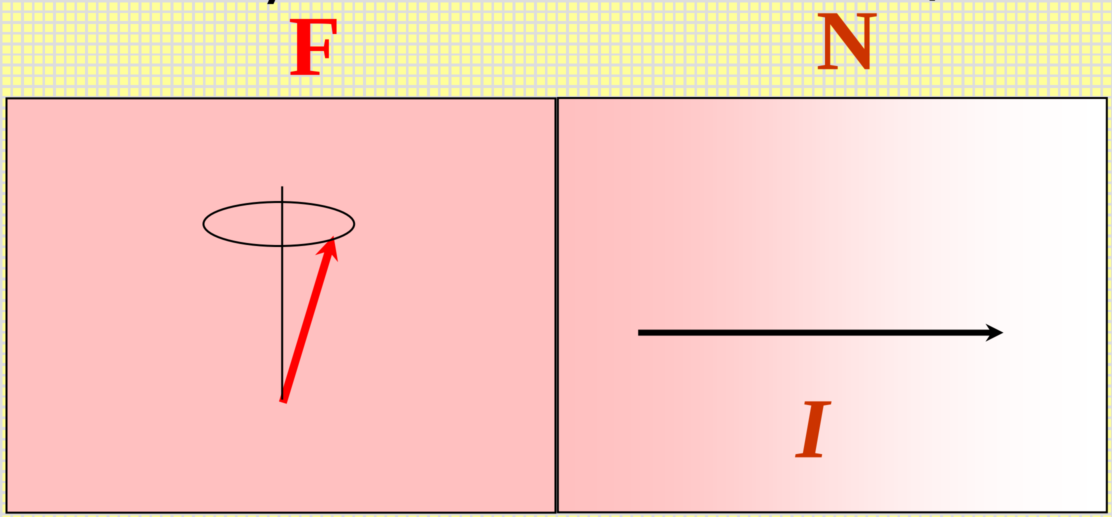

Ferromagnetic Resonance (FMR) described by

- Landau-Lifshitz-Gilbert

$$\dot{\mathbf{m}} = -\gamma \mathbf{m} \times \mathbf{H}_{\text{eff}} + \mathbf{m} \times \left(\tilde{\alpha} \dot{\mathbf{m}} \right)$$

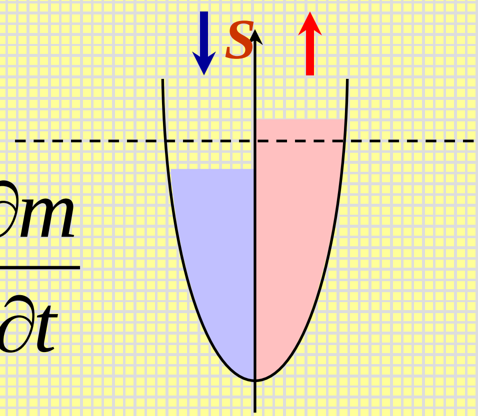

$$I_S^{pump} = \frac{\hbar}{4\pi} g_r^{\downarrow\uparrow} m \times \frac{\partial m}{\partial t}$$

In the FMR condition, the steady magnetization precession in a F is maintained by balancing the absorption of the applied microwave and the dissipation of the spin angular momentum --the transfer of angular momentum from the local spins to conduction electrons, which polarizes the conduction-electron spins.

Spin accumulation gives rise to spin current in neighboring normal metal

N-F: Reflection/Transmission

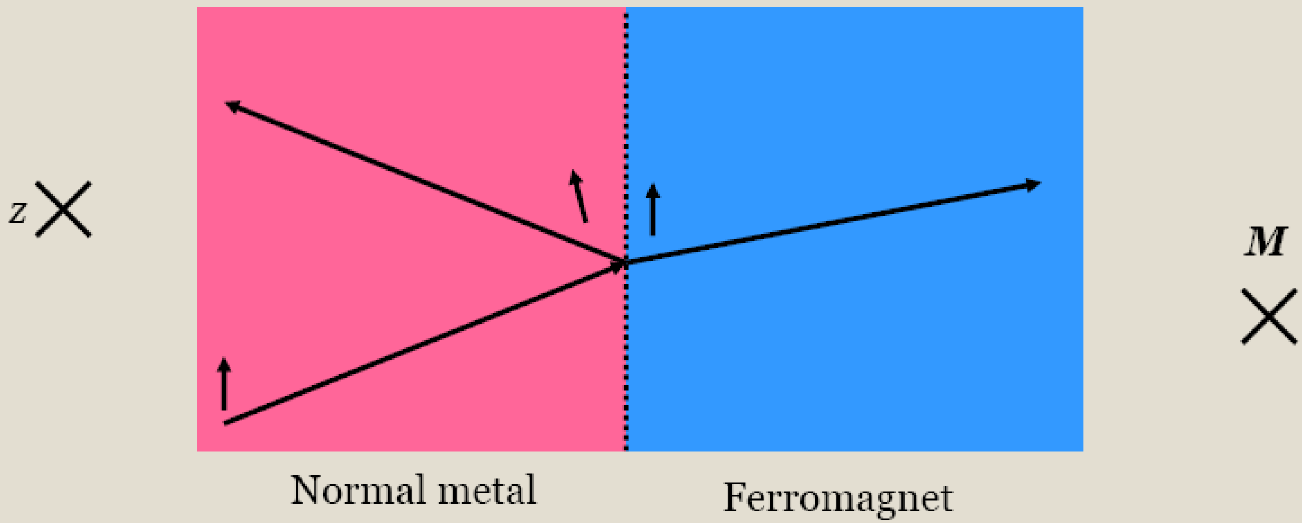

$$I_S^{pump} = \frac{\hbar}{4\pi} g_r^{\downarrow\uparrow} m \times \frac{\partial m}{\partial t}$$

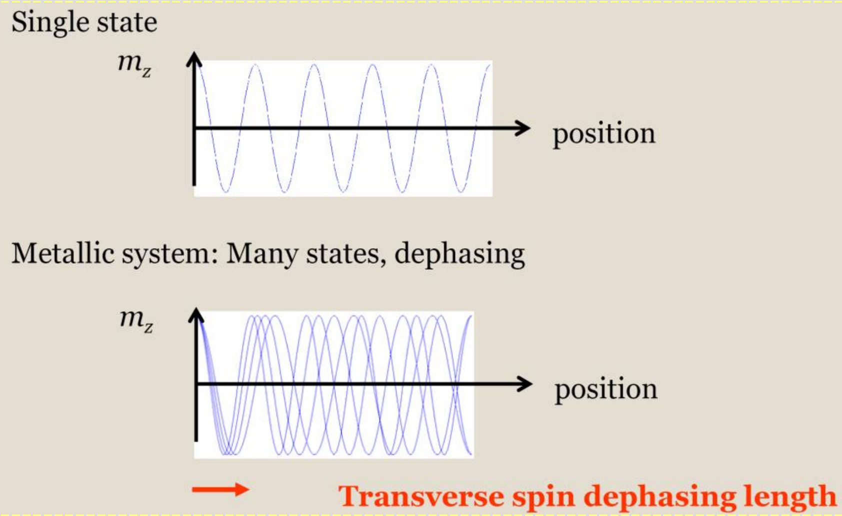

PRL 100, 067602 (2008) PHYSICAL REVIEW LETTERS week ending 15 FEBRUARY 2008

Tunnel Barrier Enhanced Voltage Signal Generated by Magnetization Precession of a Single Ferromagnetic Layer

T. Moriyama,[1] R. Cao,[1] X. Fan,[1] G. Xuan,[2] B. K. Nikolić,[1] Y. Tserkovnyak,[3] J. Kolodzey,[2] and John Q. Xiao[1]
[1]Department of Physics and Astronomy, University of Delaware, Newark, Delaware 19716, USA
[2]Department of Electrical and Computer Engineering, University of Delaware, Newark, Delaware 19716, USA
[3]Department of Physics and Astronomy, University of California, Los Angeles, California 90095, USA
(Received 27 September 2007; published 14 February 2008)

Incoming wave: Normal metal

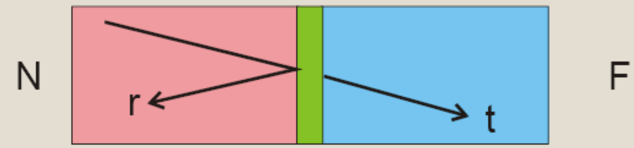

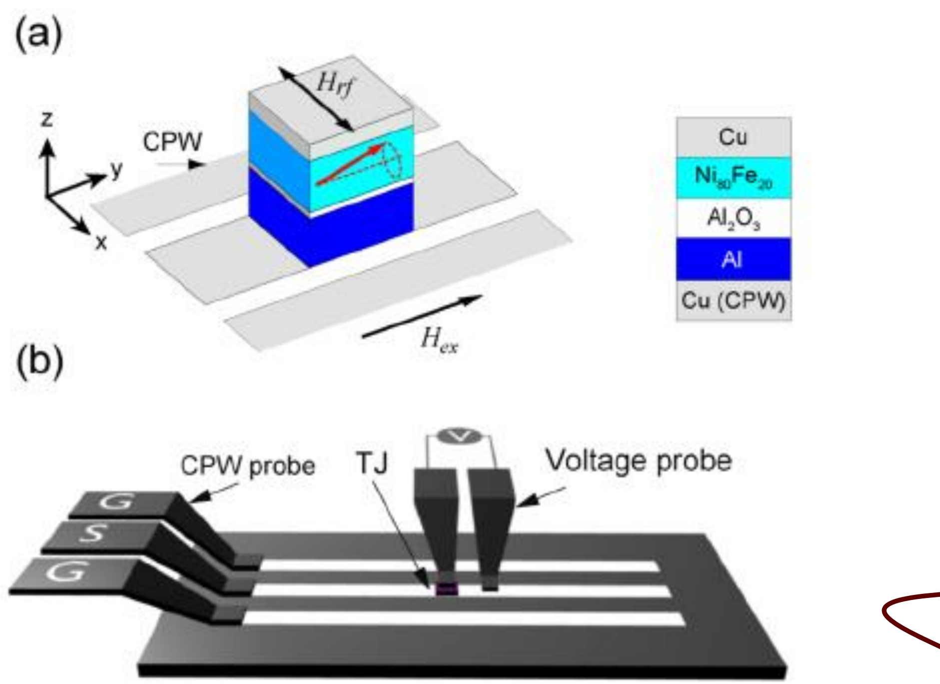

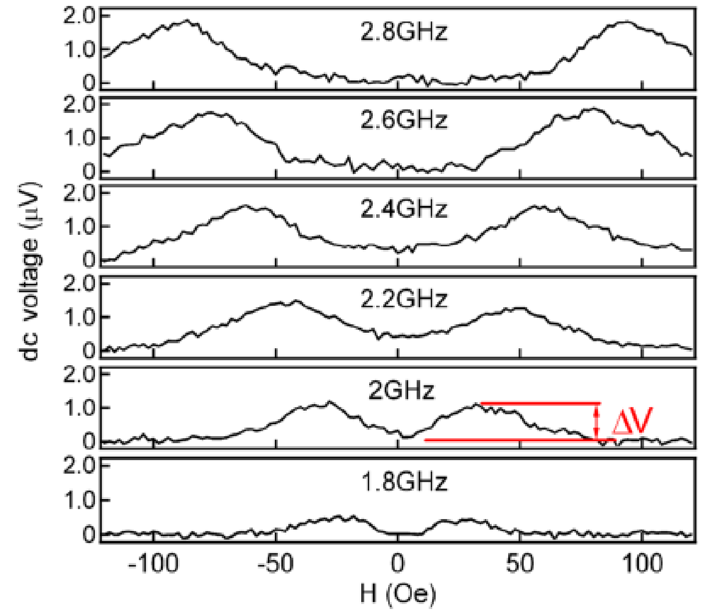

APPLIED PHYSICS LETTERS 96, 022502 (2010)

Suppression of spin-pumping by a MgO tunnel-barrier

O. Mosendz,[1,a)] J. E. Pearson,[1] F. Y. Fradin,[1] S. D. Bader,[1,2] and A. Hoffmann
[1]Materials Science Division, Argonne National Laboratory, Argonne, Illinois 60439, USA
[2]Center for Nanoscale Materials, Argonne National Laboratory, Argonne, Illinois 60439, USA

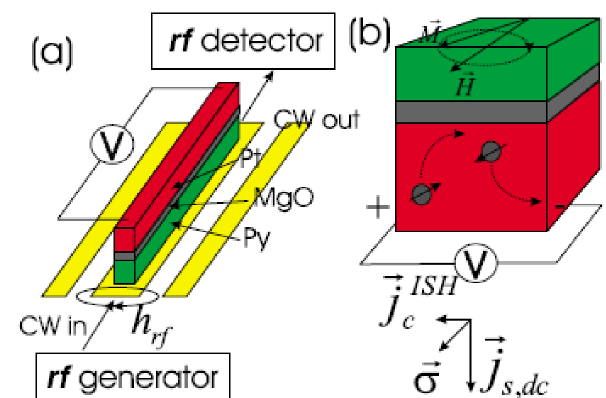

Spin Pumping

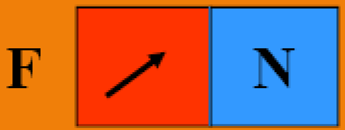

Magnetization precession emits spin-currents

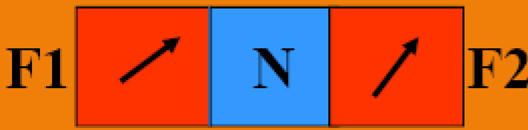

- No spin-dissipation in N
  - Spin-battery
    - PRB 66, 060404(R) (2002)
    - PRL 979, 2166702 (2006)
    - PRL 216603 (2006)
    - PRB, 064423 (2008)
- Spins relax in N
  - Enhanced Gilbert damping
    - PRL 88, 117601 (2002)
    - PRL 101, 037207 (2008)
- Spins relax in F2
  - Angular-dependent Gilbert damping
    - PRB 67, 140404(R) (2003)
- Spin transfer between F1 and F2
  - Acoustic and optical modes
    - PRL 90, 187601 (2003)
    - Phys. Rev. Lett. 99, 246603 (2007).

A real spin transistor?

Switch function – OK

Current amplification? No

Dissipationless spin current from a new material?

Topological insulator

- A **topological insulator** is a material conducting on its boundary but behaves as an insulator in its bulk.
- The conducting channel(s) are guaranteed by time-reversal symmetry, topologically protected, will not be affected by local impurities etc, and thus robust.

- Band insulator
- Mott insulator
- Kondo insulator
- Topological insulator

Why the word ‘topological’?

- Topological order:
  a pattern of long-range quantum entanglement in quantum states, can be described by a new set of quantum numbers, such as ground state degeneracy, quasiparticle fractional statistics, edge states, topological entropy, etc.

- **Landau symmetry breaking**

  describes classical orders in materials. But it failed to describe the chiral spin state, which was proposed (but failed) to explain HTS.

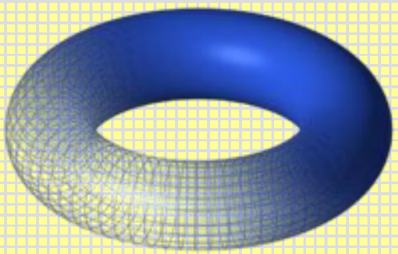

=

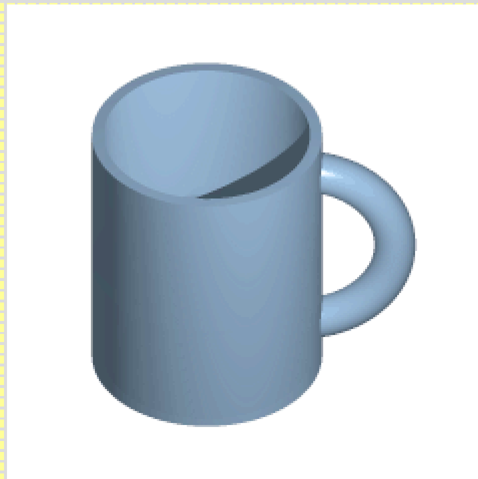

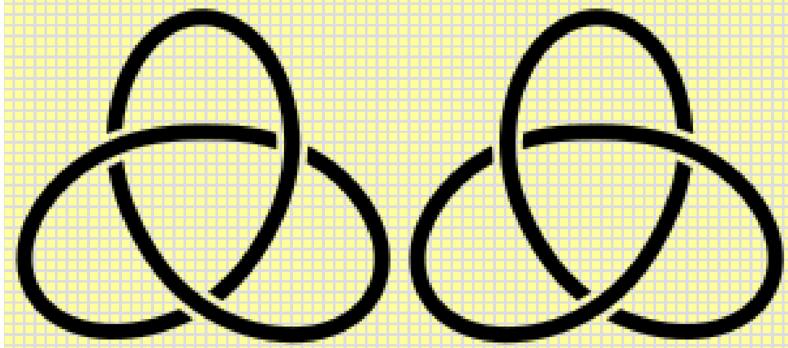

- Z_2 topological quantum number
- Chern numbers (陳省身) explains Quantum Hall Effect (from Foucault pendulum to Chern numbers)

$$1/2\pi \int_{S} K \, dA = 2\,(1 - g)$$

How to become a topological insulator?

Or, how to cross from an intrinsic insulator to a topological insulator?

Or, how to build the edge conducting states?

- Spin-orbit effect
- Lattice constant adjustment

To get inversion states and Dirac cone on the boundary.

- Carriers in these states have their spin locked at a right-angle to their momentum. At a given energy the only other available electronic states have opposite spin, so scattering is strongly suppressed and conduction on the surface is nearly dissipationless.

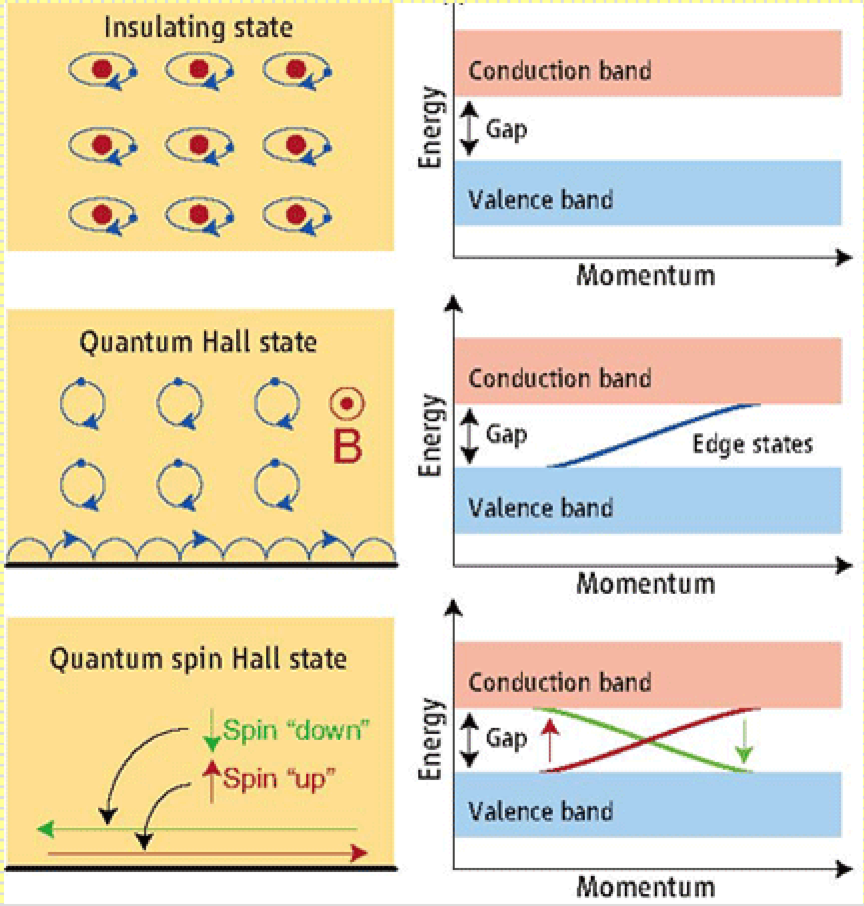

- States of matter. (**Top**) Electrons in an insulator are bound in localized orbitals (left) and have an energy gap (right) separating the occupied valence band from the empty conduction band. (**Middle**) A two-dimensional quantum Hall state in a strong magnetic field has a bulk energy gap like an insulator but permits electrical conduction in one-dimensional "one way" edge states along the sample boundary. (**Bottom**) The quantum spin Hall state at zero magnetic field also has a bulk energy gap but allows conduction in spin-filtered edge states.

A zoo of Hall effects

- Hall effect --- $B \perp I$, $V \perp I$ $R_H = \dfrac{-n\mu_e^2 + p\mu_h^2}{e(n\mu_e + p\mu_h)^2}$
- Anomalous (Extra-ordinary) Hall effect ---

  extra voltage proportional to magnetization
- Planar Hall effect --- in-plane field, $V \perp I$
- (Integer) Quantum Hall effect --- $\sigma = \nu\,\dfrac{e^2}{h},$

  $B \perp I$, $V \perp I$ in 2D electron gas
- Fractional Quantum Hall effect ---

  electrons bind magnetic flux lines
- Spin Hall effect --- B = 0, $V \perp I$
- Quantum Spin Hall effect --- 2D topological insulator

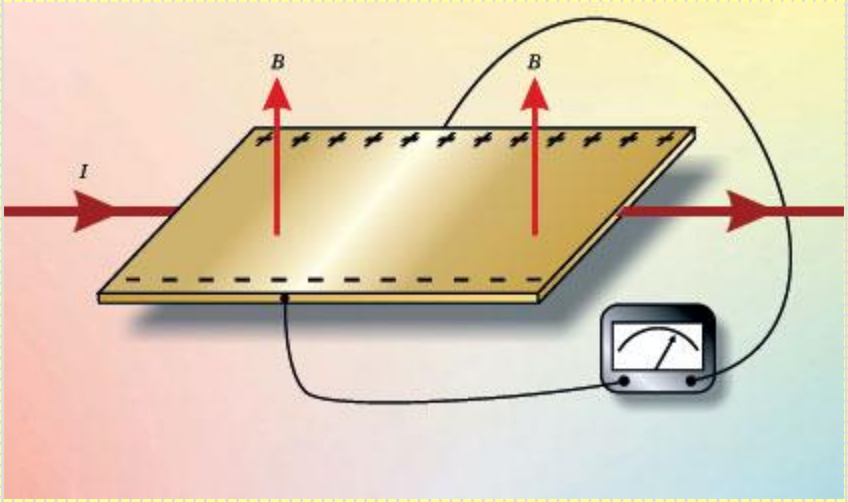

Edwin Hall's 1878 experiment was the first demonstration of the Hall effect. A magnetic field *B* normal to a gold leaf exerts a Lorentz force on a current *I* flowing longitudinally along the leaf. That force separates charges and builds up a transverse "Hall voltage" between the conductor's lateral edges. Hall detected this transverse voltage with a voltmeter that spanned the conductor's two edges.

PhysicsToday, Aug 2003, p38

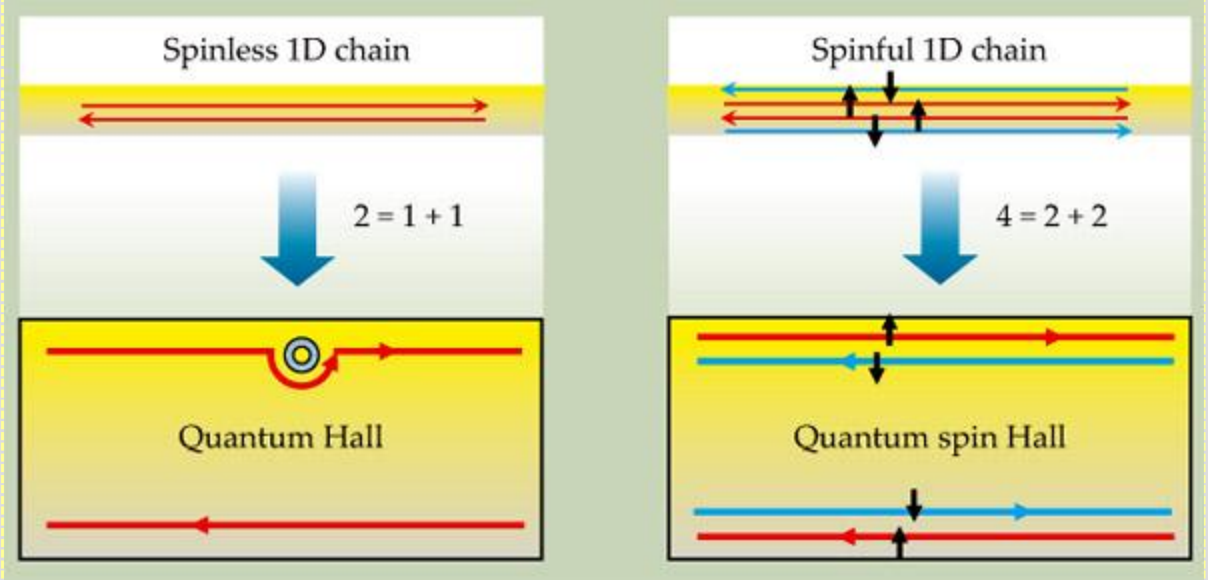

PhysicsToday, Jan 2010, p33

Figure 1. Spatial separation is at the heart of both the quantum Hall (QH) and the quantum spin Hall (QSH) effects. (a) A spinless one-dimensional system has both a forward and a backward mover. Those two basic degrees of freedom are spatially separated in a QH bar, as illustrated by the symbolic equation "2 = 1 + 1." The upper edge contains only a forward mover and the lower edge has only a backward mover. The states are robust: They will go around an impurity without scattering. (b) A spinful 1D system has four basic channels, which are spatially separated in a QSH bar: The upper edge contains a forward mover with up spin and a backward mover with down spin, and conversely for the lower edge. That separation is illustrated by the symbolic equation "4 = 2 + 2."

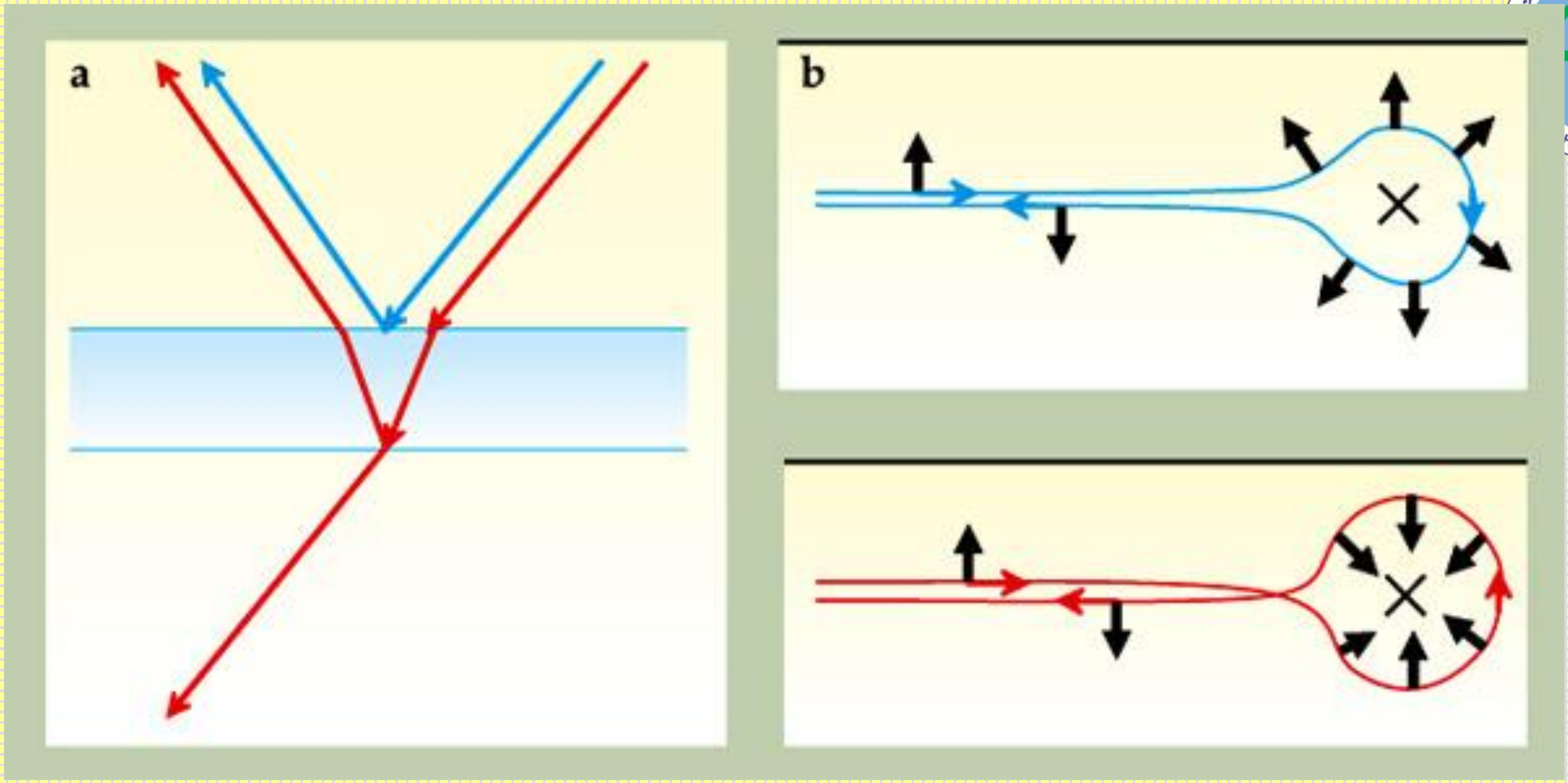

Figure 2. (a) On a lens with antireflection coating, light waves reflected by the top (blue line) and the bottom (red line) surfaces interfere destructively, which leads to suppressed reflection. (b)A quantum spin Hall edge state can be scattered in two directions by a nonmagnetic impurity. Going clockwise along the blue curve, the spin rotates by π; counterclockwise along the red curve, by $-\pi$. A quantum mechanical phase factor of -1 associated with that difference of 2π leads to destructive interference of the two paths—the backscattering of electrons is suppressed in a way similar to that of photons off the antireflection coating.

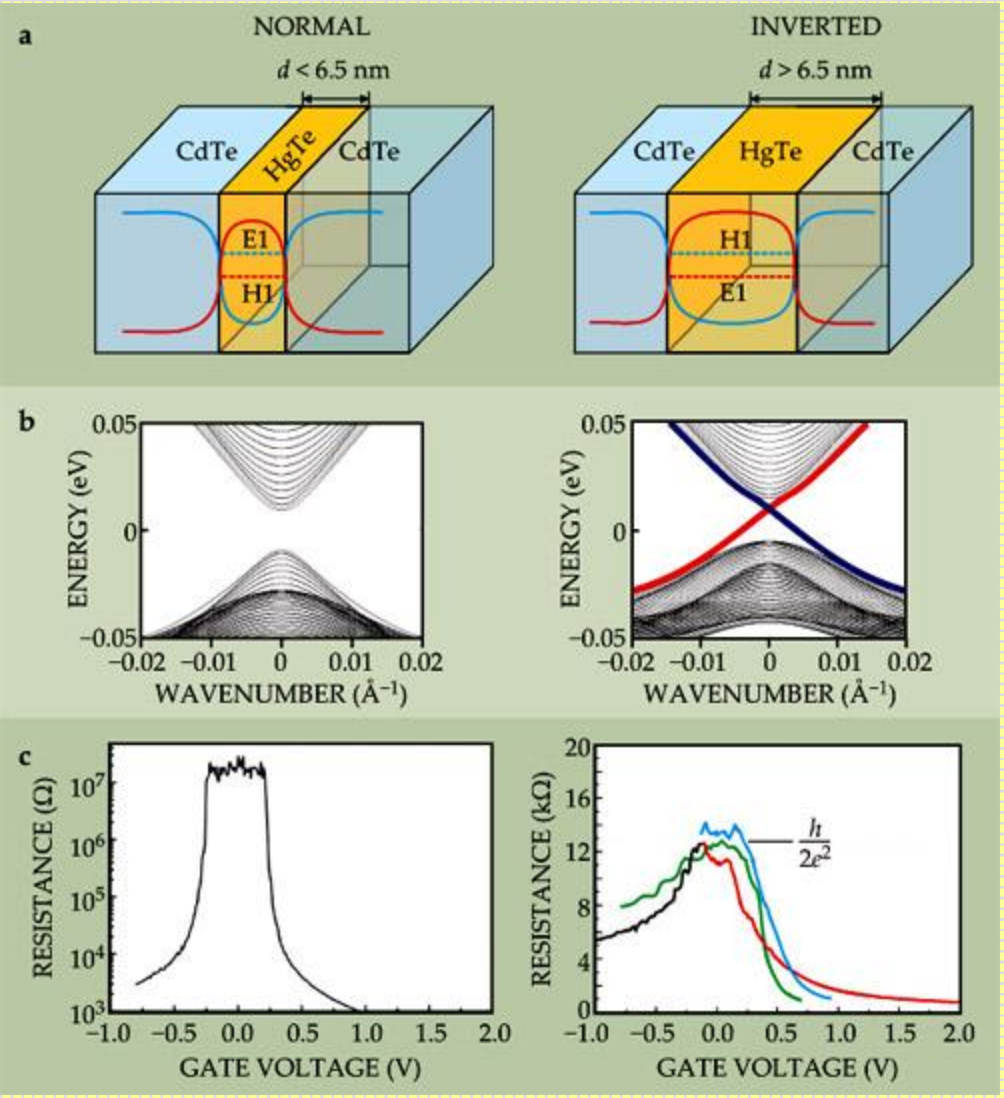

Figure 3. Mercury telluride quantum wells are two-dimensional topological insulators. (a) The behavior of a mercury telluride–cadmium telluride quantum well depends on the thickness *d* of the HgTe layer. Here the blue curve shows the potential-energy well experienced by electrons in the conduction band; the red curve is the barrier for holes in the valence band. Electrons and holes are trapped laterally by those potentials but are free in the other two dimensions. For quantum wells thinner than a critical thickness $d_c \simeq 6.5$ nm, the energy of the lowest-energy conduction subband, labeled E1, is higher than that of the highest-energy valence band, labeled H1. But for $d > d_c$, those electron and hole bands are inverted. (b) The energy spectra of the quantum wells. The thin quantum well has an insulating energy gap, but inside the gap in the thick quantum well are edge states, shown by red and blue lines. (c) Experimentally measured resistance of thin and thick quantum wells, plotted against the voltage applied to a gate electrode to change the chemical potential. The thin quantum well has a nearly infinite resistance within the gap, whereas the thick quantum well has a quantized resistance plateau at $R = h/2e^2$, due to the perfectly conducting edge states. Moreover, the resistance plateau is the same for samples with different widths, from 0.5 μm (red) to 1.0 μm (blue), proof that only the edges are conducting.

Fig. 1. Electronic band structure of undoped Bi_2Se_3 measured by ARPES. (**A**) The bulk conduction band (BCB), bulk valence band (BVB), and surface-state band (SSB) are indicated, along with the Fermi energy (E_F), the bottom of the BCB (E_B), and the Dirac point (E_D). (**B**) Constant-energy contours of the band structure show the SSB evolution from the Dirac point to a hexagonal shape (green dashed lines). (**C**) Band structure along the K-Γ-K direction, where Γ is the center of the hexagonal surface Brillouin zone (BZ), and the K and M points [see (D)] are the vertex and the midpoint of the side of the BZ, respectively (*14*). The BCB bottom is ~190 meV above E_D and 150 meV below E_F. (**D**) Photon energy–dependent FS maps (symmetrized according to the crystal symmetry). Blue dashed lines around the BCB FS pocket indicate their different shapes.

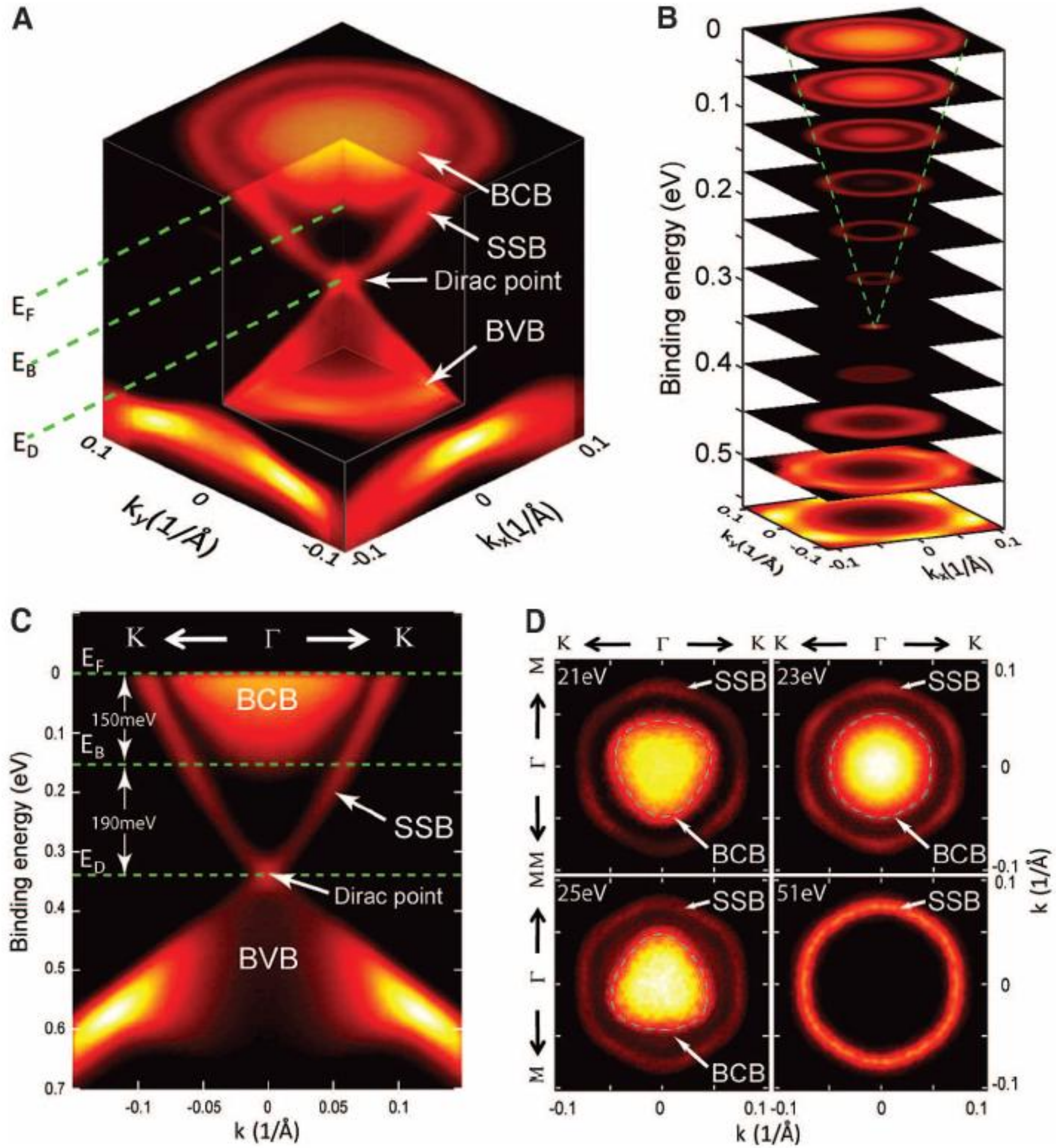

3 D topological insulators:
Bi_2Sb_3, Bi_2Se_3, Bi_2Te_3, Sb_2Te_3. There is optical proof of the Dirac cone, but no transport evidence.

SCIENCE 329, 659 (2010)

[M. Z. Hasan](), [C. L. Kane]()
[arXiv:1002.3895v2]()

Tunable multifunctional topological insulators in ternary Heusler compounds

Stanislav Chadov, Xiaoliang Qi, Jürgen Kübler, Gerhard H. Fecher, Claudia Felser, and Shou Cheng Zhang

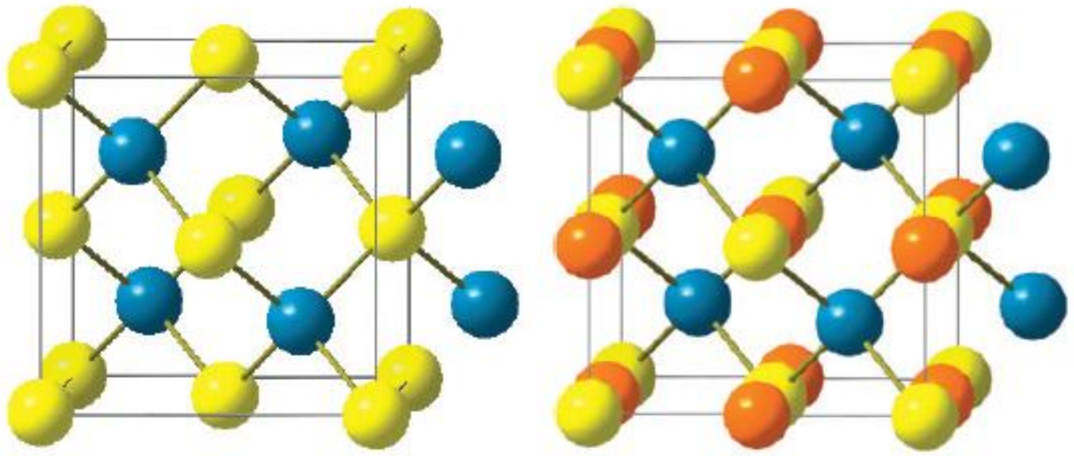

Figure 1 | Comparison of the zinc-blende and the $C1_b$ crystal structure. The zinc-blende (XY) structure is shown on the left, and the $C1_b$ (XYZ) on the right. Yellow and blue spheres correspond to the main-group (Z) and transition (Y) elements, respectively. The orange spheres in $C1_b$ stand for the additional stuffing (X) element.

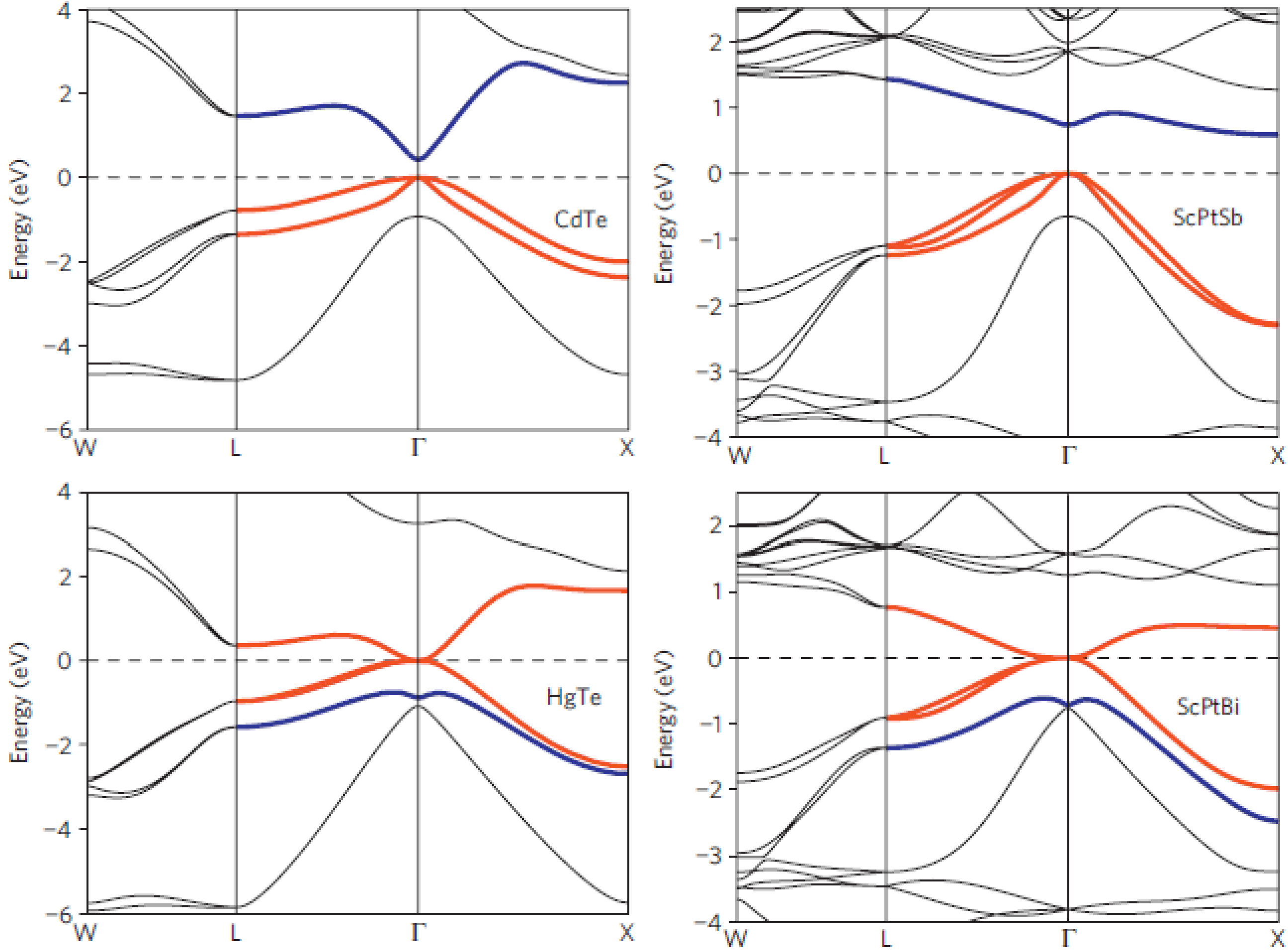

Figure 2 | Bandstructures of CdTe and HgTe compared with ScPtSb and ScPtBi Heuslers. Red colour marks the bands with Γ_8 symmetry, blue with Γ_6. Comparison reveals obvious similarity between binary systems and their ternary equivalents: both CdTe and ScPtSb are trivial semiconductors with Γ_6 situated above Γ_8, which sits at the Fermi energy (set to zero). Both HgTe and ScPtBi are topological with inverted band order; the band with Γ_6 symmetry is situated below Γ_8.

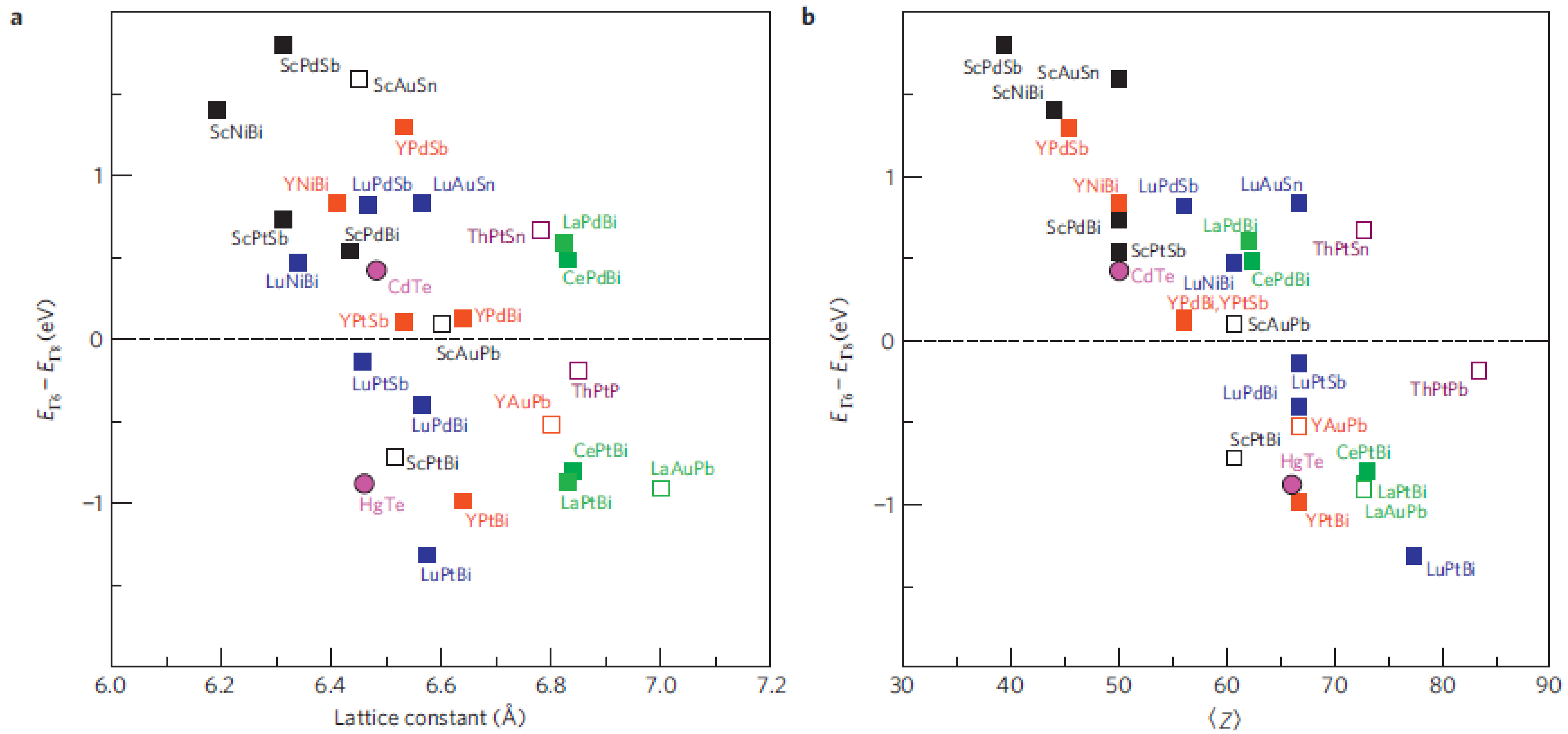

Figure 3 | $E_{\Gamma_6} - E_{\Gamma_8}$ difference calculated for various Heuslers at their experimental lattice constants. HgTe and CdTe binaries are shown for comparison. Open squares mark the systems not reported in the literature. **a**, $E_{\Gamma_6} - E_{\Gamma_8}$ difference as a function of the lattice constant. Pairs of materials with well-matching lattices for the QSH quantum wells can be easily picked up along the same vertical lines. The borderline compounds (between trivial and topological) insulators (YPtSb, YPdBi, ScAuPb) are situated closer to the zero horizontal line. **b**, $E_{\Gamma_6} - E_{\Gamma_8}$ difference as a function of the average spin–orbit coupling strength represented by the average nuclear charge $\langle Z \rangle = (1/N)\sum_{i=1}^{N} Z(X_i)$, where N is 3 for ternaries and 2 for binaries.

High energy physicist stretches their imagination

- Dyon: an image electric charge and image magnetic monopole above a 3D TI surface, which is a behave with any possible statistics
- Anyon
- Axions
- Skyrmions

- **Noether's theorem** symmetry implies conservation

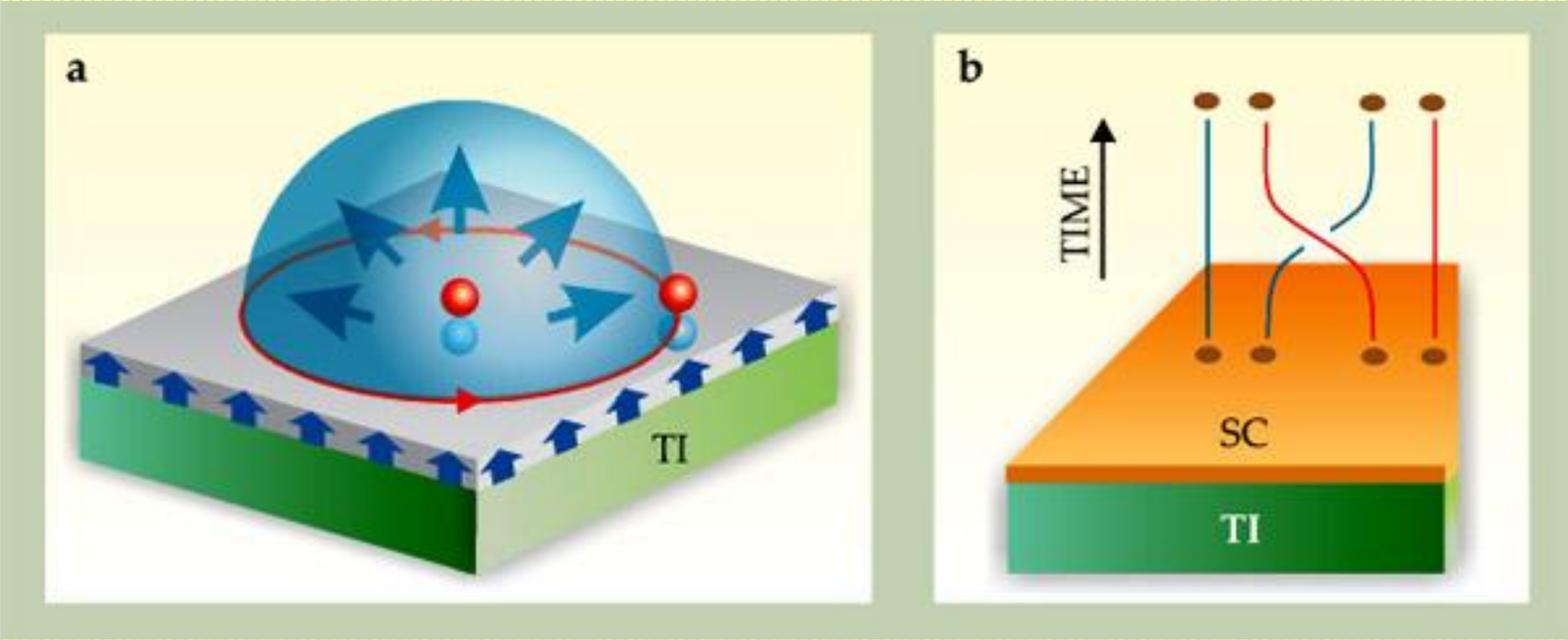

Figure 5. Novel behavior is predicted for topological insulators. (a) When a topological insulator (TI, green) is coated by a thin ferromagnetic layer (gray), each electron (red sphere) in the vicinity of the surface induces an image monopole (blue sphere) right beneath it.[12] When one electron winds around another (red circle), it will experience the magnetic flux (arrows in the blue dome) carried by the image monopole of the other, so that the electron–monopole composite, called a dyon, obeys fractional statistics. (b) When a TI is coated by an *s*-wave superconductor (SC), the superconducting vortices are Majorana fermions—they are their own antiparticles. Exchanging or braiding Majorana vortices, as sketched here, leads to non-abelian statistics.[17] Such behavior could form the basis for topological quantum computing.

Dynamical axion field in topological magnetic insulators

Suggest attenuated total reflection (ATR) measurements

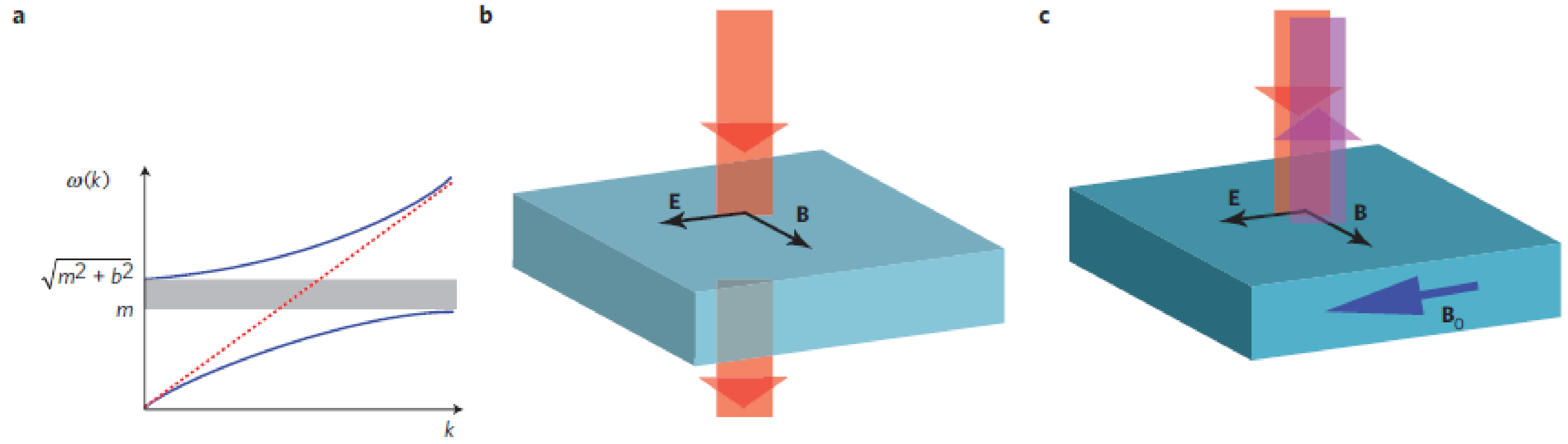

Figure 2 | Axionic polariton and ATR experiment. a, The dispersion of the axionic polariton. The grey area indicates the forbidden band between frequencies m and $\sqrt{m^2+b^2}$ (see text), within which light cannot propagate in the sample. The red dotted line shows the bare photon dispersion $\omega = c'k$. **b**, Set-up for the ATR experiment. Without an external magnetic field, the incident light can transmit through the sample. **c**, When an external magnetic field is applied parallel to the electric field of light, the incident light will be totally reflected if its frequency lies within the forbidden band.

NATURE PHYSICS 6, 284 (2010)

- Demonstration of TI
- On the surface of a 3D TI, induced magnetic gap leads to novel quantum Hall state --- topological magnetoelectric effect?
- Induced superconducting gap --- Majorana fermion states --- topological quantum computation?

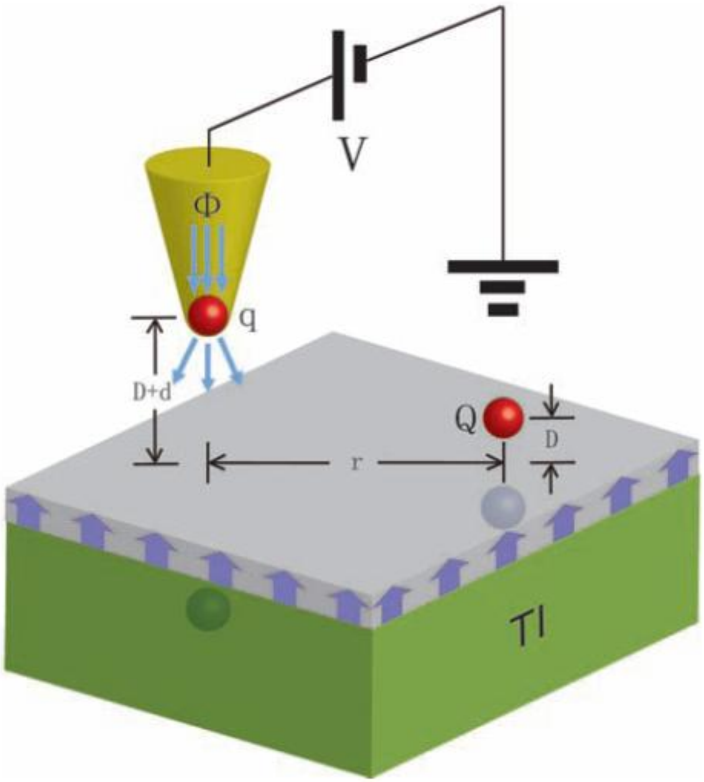

Fig. 2. Illustration of the experimental setup to measure the image monopole. A magnetic layer is deposited on the surface of the topological insulator, as indicated by the layer with blue arrows. (The same layer is drawn in Figs. 3 and 4.) A scanning MFM tip carries a magnetic flux ϕ and a charge q. A charged impurity is confined on the surface with charge Q and distance D out of the surface. By scanning over the voltage V and the distance r to the impurity, the effect of the image monopole magnetic field can be measured (see text).

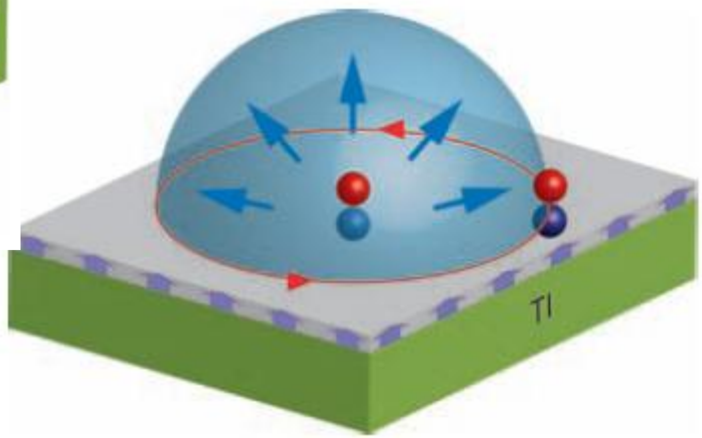

Fig. 3. Illustration of the fractional statistics induced by image monopole effect. Each electron forms a dyon with its image monopole. When two electrons are exchanged, an AB phase factor is obtained (which is determined by half of the image monopole flux) and leads to statistical transmutation.

SCIENCE 323, 1184 (2009)

Present and future impact of spintronics

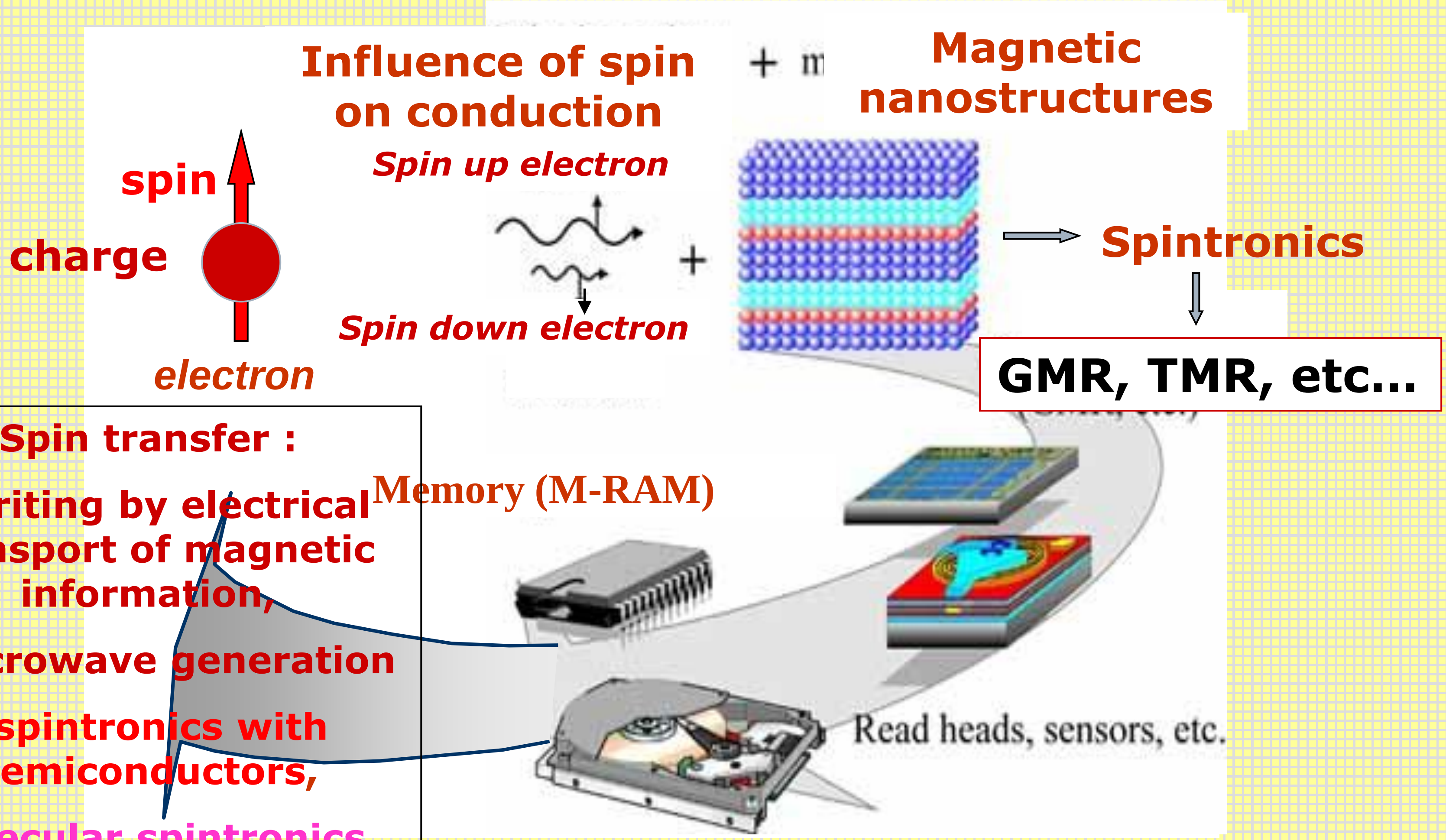

Spin transfer :

- writing by electrical transport of magnetic information,

- microwave generation

spintronics with semiconductors,

molecular spintronics,

Single-electron spintronics, etc

Summary

GMR effect – charge can be controlled
by magnetization (spin).

STT (spin transfer torque) effect
-- magnetization can be controlled by
spin polarized current.
-- New materials with high spin polarization,
low saturation moments,
high Curie temperature are needed.

Pure spin current – will it be realized in circuits?